Dehydration of hydrazine hydrate by pervaporation using commercially available polymer membranes

by

Pierru Petrus Paulus Roberts

Thesis presented in partial fulfilment
of the requirements for the Degree

of

MASTER OF ENGINEERING
(CHEMICAL ENGINEERING)

UNIVERSITEIT
iYUNIVESITHI
STELLENBOSCH
UNIVERSITY

in the Faculty of Engineering
at Stellenbosch University

Supervisor
Dr Percy van der Gryp

March 2018

DECLARATION

By submitting this thesis electronically, I declare that the entirety of the work contained therein is my own, original work, that I am the sole author thereof (save to the extent explicitly otherwise stated), that reproduction and publication thereof by Stellenbosch University will not infringe any third party rights and that I have not previously in its entirety or in part submitted it for obtaining any qualification.

Date: March 2018

ABSTRACT

Hydrazine (N_2H_4) is a valuable, commercial, inorganic compound that is characterised as a small, reactive molecule with good reducing properties. In its anhydrous form, hydrazine is used in the medical field and in space applications for the adjustment of altitude in orbital satellites (Schliebs, 1985). Commercially produced hydrazine hydrate solutions can be partially dehydrated by fractional distillation to provide a constant boiling mixture or azeotrope of about 71.5 wt. % hydrazine (Sunitha et al., 2011).

A possible alternative dehydration technique is the use of fractional distillation in combination with pervaporation (Dutta et al., 1996). Ravindra et al. (1999a) and Satyanarayana and Bhattacharya (2004) are among a limited number of authors that investigated pervaporation of hydrazine monohydrate systems. The main aim of these initial studies was to characterise the system and develop a laboratory synthesised membrane with optimal water selectivity and acceptable mass flux.

The main aim of this study was to investigate the dehydration of hydrazine monohydrate (36 wt. % water) by pervaporation using commercially available polymeric membranes. Three objectives were set in this study;

1. Screening of commercially available polymeric membranes for the hydrazine-water.
2. Characterising the best performing membrane (Pervap™ 4101) in terms of sorption and pervaporation performance at various concentration (36 to 100 wt. % water) and temperature ranging from 30 to 60 °C.
3. Modelling the separation performance of the best performing membrane (Pervap™ 4101) and comparing the performance with data from two literature sources namely: Ravindra et al. (1999c) and Sunitha et al. (2011).

A standard experimental procedure was used to select and screen eight commercial membranes (Pervap™ 4060, 4100, 4101, 4102, POL-AL-M2, POL-OL-M1 and PEBA and PDMS) through visual and mechanical stability tests, contact angle characterisation and pervaporation performance screening tests. A stable membrane that showed the highest pervaporation screening results (Pervap™ 4101) was

characterised in terms of sorption and pervaporation selectivity, membrane swelling and total flux.

Visual screening tests using hydrazine monohydrate at room temperature (25 °C) showed that the Pervap™ 4060, 4101 and 4102 membranes had no visual interaction with hydrazine. The visual observations were confirmed by mechanical stability tests that showed that Pervap™ 4101 and 4102 membranes had the smallest deviation in tensile strength after exposure to hydrazine. Commercial Pervap™ 4101 does, however, not compare to literature results obtained by Ravindra et al. (1999c) and Sunitha et al. (2011).

Satyanarayana and Bhattacharya (2004) state that any membrane with a water selectivity higher than 1.4 would be able to break the water-hydrazine azeotrope. Further pervaporation screening tests were conducted at 50 °C and 36 wt. % water which resulted in water selectivities as high as 1.6 for Pervap™ 4101 and 4102 membranes, with the former having the higher flux rate of 0.5 $kg \cdot m^{-2} \cdot h^{-1}$. Both membranes are theoretically able to successfully break the azeotrope, but the Pervap™ 4101 membrane was selected for further characterisation due to the higher flux and pervaporation performance index (PSI) obtained.

Sorption studies on Pervap™ 4101 membranes at 50 °C and feed concentrations between 36 and 100 wt. % water revealed that membrane swelling was as high as 80 %. Both the sorption and pervaporation mechanisms are water selective, but higher diffusion water selectivity's indicate that the separation process is diffusion controlled. Sorption tests further confirmed that the sorption process is independent of temperature.

An increase in pervaporation water feed concentration, from 36 wt. % water, decreased the experimental flux from 0.48 to 0.1 $kg \cdot m^{-2} \cdot h^{-1}$ and increased the water selectivity from 1.6 to 20, while an increase in temperature increased the flux and decreased the water selectivity.

The membrane transport was modelled in terms of the solution diffusion model with the sorption step described with the Flory-Huggins theory and the diffusion step with Fick's first law. A water-hydrazine interaction parameter of -2.05 was calculated for hydrazine monohydrate (36 wt. % water) and 50 °C that suggests a strong affinity between water and hydrazine. A concentration independent interaction parameter between hydrazine-polymer (3.68) that is lower than water-polymer (5.47) confirms the preferential hydrazine to water sorption results.

The concentration dependent interaction parameter as proposed by Long (1965) describe the experimental partial fluxes of this study well (R^2 > 0.9896). It also describes the reference pervaporation experimental data by Ravindra et al. (1999c) and Sunitha et al. (2011).

Keywords: Pervaporation, Hydrazine hydrate, Dehydration, Azeotrope

TABLE OF CONTENT

NOMENCLATURE

Symbols	Description	Unit
$A_{ij/ji}$	Two constant Margueles constant	-
A_m	membrane area	m^2
$c_{i/j}$	molar concentration of water or hydrazine	-
D	diffusion / diffusion coefficient	m^2/s
${D_{i/j}}^0$	limiting water or hydrazine diffusion coefficient	m^2/s
E	activation energy for permeation	
g_{ij}	concentration dependent interaction parameter between water and hydrazine	kJ/mol
$g_{ip/jp}$	concentration dependent interaction parameters between water or hydrazine and the polymer	-
J	total pervaporation flux	$g \cdot m^{-2} \cdot h^{-1}$ $kg \cdot m^{-2} \cdot h^{-1}$
$J_{i/j}$	partial water or hydrazine pervaporation flux	$g \cdot m^{-2} \cdot h^{-1}$ $kg \cdot m^{-2} \cdot h^{-1}$
J_0	Flux constant	-
$L_{i/j}$	coefficient of proportionality	-
$\overline{M_c}$	average molecular weight between polymer cross-links	-
M_s	mass swollen membrane	kg, g
M_d	mass dry membrane	kg, g
P	proportionality factor / permeance	-
P^{sat}	vapour pressure of the binary mixture	kPa
Q	mass permeate collected	kg
r	ratio of the hydrazine to water molar volumes	-
R	universal gas constant	$J \cdot mol^{-1} \cdot K^{-1}$
S	sorption / sorption coefficient / membrane swelling	-
T	temperature	K, °C
t	time	h
$u_{i/j}$	volume fraction of water and hydrazine in the polymer on a polymer free	-

Symbols	Description	Unit
$v_{i/j}$	volume fraction water or hydrazine in the binary feed	-
$V_{i/j}$	molar volume of water or hydrazine	$cm^3 \cdot mol^{-1}$
W_s	weight of wet membrane	g
W_d	weight of dry membrane	g
Y	permeate mole fraction	-
$X_{i/j}$	feed mole fraction	-
$x_{i/j}$	molar feed fractions for water and hydrazine	-
z	membrane thickness	µm
ΔG^E	excess free energy of mixing	$J \cdot mol^{-1}$

Greek symbols	Description	Units
α	activity	-
α	membrane selectivity	-
α_s	sorption selectivity	-
β	enrichment factor	-
$\beta_{i,j,ii,jj,ij,ji}$	plasticisation coefficient	-
$\varphi_{i,j}$	chemical potential of water or hydrazine	-
$\Phi_{i/j}$	volume fraction of either water of hydrazine in a ternary system	-
Φ_p	polymer fraction in the ternary system	-
µ	chemical potential	$J \cdot mol^{-1}$
μ_i^0	standard state chemical potential	-
γ	activity coefficient	-
ρ_m	polymer membrane density	$kg \cdot m^{-2} \cdot h^{-1}$
ρ_s	solvent density	$kg \cdot m^{-2} \cdot h^{-1}$
$\chi_{ip/jp}$	water-polymer and hydrazine-polymer binary interaction parameter	-
δ_p	polymer solubility parameter	-
$\delta_{i/j}$	water or hydrazine solubility parameter	-

Subscripts	Definition
i	water
j	hydrazine

Definitions and acronyms

EC	ethyl cellulose
ETBE	ethyl tert-butyl ether
FID	flame ionising detector
FTIR	fourier-transform infrared spectroscopy
GC	gas chromatogram
IEC	ion exchange capacity
MAPE	mean absolute percentage error
MMH	monomethyl hydrazine
PAN	polyacrylonitrile
PB	polybutadiene
PDMS	polydimethyl siloxane
PEBA	polyether block polymide
PEBAX®	tradename for polyether block polymide
PEI	polyethermide
PP	polypropylene
PSI	pervaporation performance index
PTFE	polytetrafluoro ethylene
PVA	polyvinyl alcohol
R^2	coefficient of determination
RMSE	root mean square error
TAME	tertiary-amyl methyl ether
THF	tetrahydrofuran
TMBE	methyl-tertiary butyl ether
UDMH	unsymmetrical dimethyl hydrazine
VLE	vapour-liquid equilibrium
VOC	volatile organic compounds

LIST OF FIGURES

LIST OF TABLES

CHAPTER ONE – RESEARCH OVERVIEW

Overview

The research overview chapter is divided into three sub-sections, starting with a brief background on hydrazine and hydrazine production, followed by a motivation for the current research (Section 1.1). The main aim and three objectives of this study is discussed in Section 1.2 with the scope of the investigation along with the outline of the study (Section 1.3).

1.1. Project introduction

Hydrazine (N_2H_4) is a commercially valuable inorganic compound that is characterised as a small, reactive molecule with good reducing properties. Great care needs to be taken when working with hydrazine, as it is considered a flammable, highly toxic and unstable molecule. (Schliebs, 1985)

The majority of the 120 000 tons of hydrazine produced globally on an annual basis is used as hydrazine hydrate, corresponding to 64 wt. % or less of hydrazine in water (Imam, 2016). In the diluted form, hydrazine hydrate finds applications as a foaming agent in polymer foams; as an oxygen scavenger in both coal fired and nuclear power plants and acts as a precursor in both polymerization catalysts and pharmaceuticals (Audrieth and Ogg, 1951). In its anhydrous form hydrazine is used to prepare the gas precursor used in airbags, as well as a hygroscopic rocket fuel to propel space shuttles and guided missiles. (Schliebs, 1985)

In this study the focus is on anhydrous hydrazine, specifically with purity levels acceptable for space propulsion. The purity of anhydrous hydrazine required for space propulsion as specified by Schliebs (1985) ranges between 98.5 wt. % to 99.5 wt.% hydrazine, with aniline concentration of 0.5 wt. % or less.

Small quantities of anhydrous hydrazine, mostly for laboratory use, have been prepared by various researchers like Watt and Chrisp (1955), Feher and Linke (1966) and Nicolaisen (1957) by the chemical reaction of dry hydrazinium salts with non-aqueous bases, or by thermolysis of readily dissociated hydrazinium salts as performed by Nachbaur and Leiseder (1971) and Stolle and Hofmann (1904). None of these laboratory synthesised methods are commercially viable.

Commercially, hydrazine hydrate is produced mainly by three methods: the Raschig process, the ketazine process, and the peroxide process. All three of these methods produce a highly diluted hydrazine product which needs to be partially dehydrated by fractional distillation where part of the water is removed to provide a constant boiling mixture or azeotrope of about 71.5 wt. % hydrazine.

Removal of additional water past the azeotropic point is currently done by chemical reaction by adding sodium hydroxide as patented by Penneman and Audrieth (1949), or alternatively by adding alternative binding chemicals (Bush and Sims, 1974, Hale and Shetterly, 1911, Bock, 1958). These methods have been thoroughly proven, but pose numerous safety risks due to the hazardous nature of sodium hydroxide. Aniline has been used during azeotropic distillation, but leaves aniline residue that needs to be removed to conform to the specification for use in space propulsion (Bircher Jr John, 1954, Nicolaisen, 1956, Nicolaisen and Smith, 1958, Wilson et al., 1955). Liquid-liquid extraction as proposed by Lewis (1957) and Dunlop (1967) has not been demonstrated on a large scale for the dehydration of hydrazine hydrate.

A possible alternative dehydration technique is to use fractional distillation in combination with pervaporation. Pervaporation is a membrane process in which a liquid feed mixture is in contact with a permselective membrane and one component is preferentially transported through the membrane. It evaporates on the permeate side of the membrane and can be condensed and collected (Feng and Huang, 1997). According to Wynn (2001), pervaporation occupies a special niche in the chemical industry since it is the only membrane process primarily used to purify chemicals that form azeotropes or have a high affinity between them. Dutta et al. (1996) patented a process for the separation of azeotropic mixtures by combining pervaporation and fractional distillation.

According to Ravindra et al. (1999a) and Satyanarayana and Bhattacharya (2004) pervaporation has the potential to overcome some of the most common problems associated with the current industrial processes for the dehydration of hydrazine hydrate mixtures for space propulsion purposes. Various researchers have already demonstrated that pervaporation has the potential to separate azeotropic mixtures of hydrazine monohydrate (Ravindra et al., 1997, Ravindra et al., 1999c, Ravindra et al., 2000, Dutta, 2004).

All the research is however focussed on laboratory synthesised membranes with the exception of Pervap™ 2200, 2201 and 2202 tested by Satyanarayana and Bhattacharya (2004). All pervaporation and sorption literature is limited to a single temperature and only two laboratory synthesised membranes were used to quantify

the effect of concentration on pervaporation performance (Ravindra et al., 1999c, Sunitha et al., 2011).

1.2. Objectives

The main aim of this study was to investigate the dehydration of hydrazine monohydrate by pervaporation using commercially available polymeric membranes.

The objectives of this study were:

1. Identification and screening of several commercially available polymeric membranes.
2. Characterise the best performing membrane in terms of sorption and pervaporation performance at various concentration and temperature ranges.
3. Describe and model the separation performance of the best performing membrane and pervaporation experimental data from two additional literature sources.

1.3. Scope of investigation

A basic schematic representation for the scope of this investigation is given in Figure 1.1, with the main objective as well as the chapter it is addressed listed.

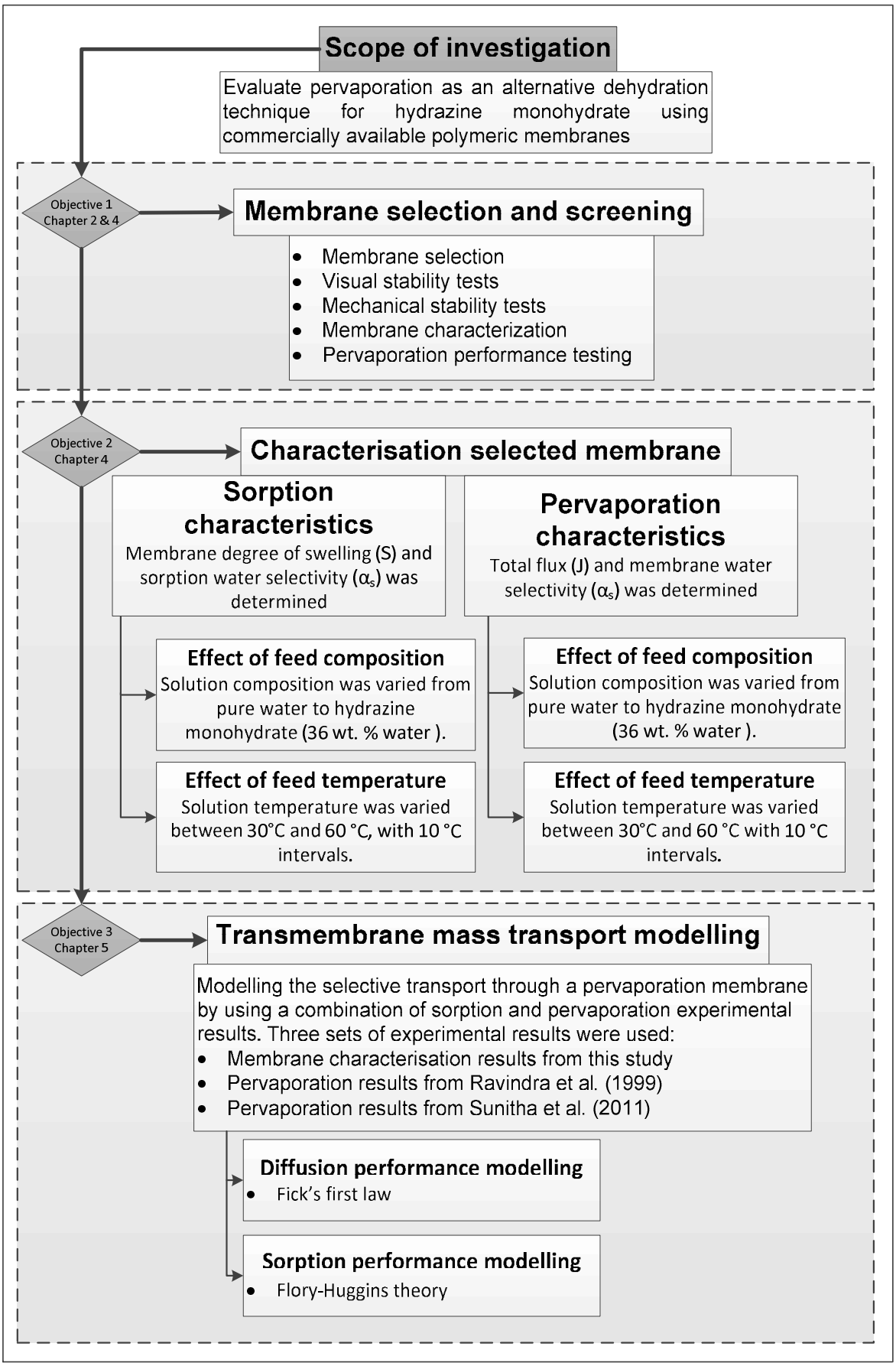

Figure 1.1: Schematic representation of the scope of this investigation

This study is subdivided into seven chapters consisting of the following that address the three main objectives of the study:

I. A background and literature review in Chapter 2 provides an overview of the definitions and terminology used as well as the performance parameters for membrane processes. A membrane and pervaporation module overview is provided that concludes with pervaporation literature specifically focussed on pervaporation literature specifically pertaining to hydrazine hydrate.

II. A detailed theoretical background on modelling the mass transfer over a polymeric membrane is provided in Chapter 3 with reference to a simplified solution-diffusion model. The focus of this chapter is to provide a detailed understanding of the transport mechanisms involved in pervaporation modelling, as well as the necessary assumptions and shortcomings in the selected modelling approach.

III. The experimental methods and analysis used in this study are discussed in Chapter 4. The chapter is sub-divided into two main objectives, with the first part of the chapter addressing the first objective of the study in screening commercially available polymeric membranes. The second part of the chapter is dedicated to the membrane performance of Pervap™ 4101 by means of the sorption and pervaporation characteristics of the membrane.

Sorption Characteristics

The focus of the sorption experiments was to determine the effect of the solution composition and operating temperature on the swelling and preferential sorption of the membrane. The experimental results were used as inputs parameter in the solution–diffusion model.

Pervaporation characteristics

The focus of the pervaporation experiments was to test the selective removal of water from the hydrazine-water binary system by means of pervaporation using Pervap™ 4101 membrane under various feed temperatures and solution compositions.

IV. The results from the screening tests as discussed in Chapter 4 are used to reduce the number of commercial polymeric membranes sourced from nine to a single membrane that has the highest likelihood of dehydrating a hydrazine monohydrate sample past the azeotropic point. Pervap™ 4101 was selected and the sorption and pervaporation results obtained were compared with ordinary distillation on a VLE curve.

V. The procedure for both sorption and mass transfer modelling is supplied in Chapter 6. The focus in this chapter is to describe a solution diffusion model and compare the results with the experimental results obtained in this study as well as the pervaporation data obtained by two literature sources.

VI. The main findings and conclusions of this study are summarized in Chapter 7. The chapter is concluded with recommendations and proposed future work.

CHAPTER TWO - BACKGROUND AND LITERATURE SURVEY

Overview

The background and literature survey chapter is sub-divided into nine sections starting with a general introduction to the chapter (Section 2.1), and a general membrane overview (Section 2.2). The types of membrane generally used in pervaporation are described in Section 2.3, followed by membrane characteristics including membrane contact angle (Section 2.4), and the various types of pervaporation processes (Section 2.5). The various types of pervaporation modules are described in (Section 2.6) and the factors affecting membrane performance (Section 2.7). This chapter also investigates integrated systems involving pervaporation and applications (Section 2.8) and lastly discusses pervaporation literature that is specifically focussed on the dehydration of hydrazine hydrate (Section 2.9).

2.1. Introduction

Membranes and membrane related technologies have been of great economic importance as a separating tool especially in the last few decades (Baker, 2000). Membrane applications are expanding from the traditional fields such as water desalination and purification to industries in the oil, petrochemical, pharmaceutical and energy sectors (Mohanty and Purkait, 2011). Membrane separation technology across all fields has become more important due to an increase in product purity requirements (Porter, 1989).

Pervaporation, as a concentration driven process, has become an important field of study due to its potential in applications relating to difficult separation problems (Flemming and Slater, 1992). The application of pervaporation has grown with the potential to complement or replace traditional distillation methods for the purification of industrial solvents. Pervaporation differs from the normal membrane applications in that it has a phase change across the membrane barrier (Hickey et al., 1992). Separation in pervaporation occurs due to membrane-compound interactions. Therefore, the chemical nature and the structure of the membrane are important when determining membrane performance (Basile et al., 2015).

Pervaporation has the potential to separate closely boiling compounds and azeotropic mixtures that are difficult to separate by ordinary distillation (Baker, 2000). This fact has been exploited by various researchers to break the azeotrope in hydrazine hydrate to obtain anhydrous hydrazine that can be used as a monospace propellant. Some of the published articles on hydrazine pervaporation include: Ravindra et al. (1997), Ravindra et al. (1999c), Ravindra et al. (2000), (Hoda et al. (2005)), Satyanarayana et al. (2006), Mandal et al. (2008) and Sunitha et al. (2011).

2.2. General overview of membranes

2.2.1. Definitions of membrane technology

Various first generation membrane processes like microfiltration, utrafiltration, nanofiltration, reverse osmosis, electrodialysis, as well as second generation membrane processes such as gas separation, vapour permeation, pervaporation and membrane distillation exist (Mulder, 2012). All of these membrane separation methods use different separation principles and mechanisms, but they all make use of a permselective barrier between two phases, called a membrane.

The principal purpose of membranes is to regulate the rate of permeation of the individual species within a multicomponent system. A potential gradient is generated by a chemical potential, a partial pressure or a concentration difference. The extent of the force is determined by the potential gradient over the membrane (Baker, 2000; 15).

Two main models of permeation have been proposed, one being the solution-diffusion model and the other the pore flow model. The mechanisms for molecular transport through membranes are shown in Figure 2.1.

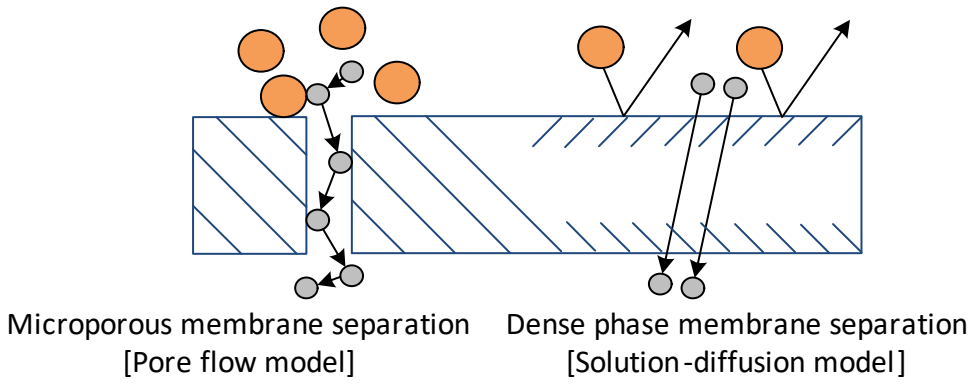

Figure 2.1: Molecular transport through membranes adapted from Baker (2000)

The solution-diffusion model stipulates that the permeate dissolves into the membrane material and thereafter diffuses through the membrane driven by a concentration gradient. Separation occurs due to the varying solubilities of the components and therefore varying rates of diffusion. The pore flow model stipulates that permeates are transported by pressure-driven convective flow through micropores. Separation

occurs due to the exclusion of certain permeates in selected pores, while other permeants pass through (Baker, 2000).

2.2.2. Performance parameters

Dutta et al. (1996), Baker (2000) and Mohanty and Purkait (2011) are among a number of authors that define the performance of a membrane as characterised by flux and selectivity (or in some cases the separation factor).

The permeation flux denotes the rate of permeation of a specific compound per unit surface area for a given membrane as:

$$J = \frac{Q}{A_m t} \tag{2-1}$$

where J ($kg \cdot m^{-2} \cdot h^{-1}$) is the membrane flux, Q (kg) the mass of permeate collected, A_m (m^2) the membrane effective area and t (h) the time.

The membrane selectivity (α) is calculated using the feed and permeate concentrations as shown below:

$$\alpha = \frac{X_i \,.\, Y_j}{X_j \,.\, Y_i} = \frac{Y_i \,/\, (1 - Y_i)}{X_i \,/\, (1 - X_i)} \tag{2-2}$$

where X refers to feed and Y to permeate mole fractions. The subscript i refers to the preferentially permeating species and j to the slower permeating species. A selectivity of unity indicates that no separation takes place while a value approaching infinity designates a membrane that becomes “semipermeable” (Mohanty and Purkait, 2011).

The enrichment factor (β) is the ratio of concentrations of the preferentially permeating species in the feed and permeate, calculated from:

$$\beta = \frac{Y_i}{X_i} \tag{2-3}$$

(Dutta et al., 1996)

2.2.3. Swelling and sorption

Membrane swelling can be attributed to large-scale polymer expansion due to the solvent diffusing into the polymer chains (Izák et al., 2007). Swelling drastically reduces the membrane selectivity and increases the overall flux. A trade-off between these two parameters is normally required. Swelling in composite membranes is reduced by various methods including cross-linking of the membrane monomers (Basile et al., 2015). Several studies such as Shao and Huang (2007) and Jiang et al. (2009) have shown how swelling affects the membrane performance. Based on this, it is important to quantify the membrane swelling. The degree of swelling can be calculated from.

$$\text{Degree of swelling} = \frac{M_s}{M_d} \tag{2-4}$$

The percentage sorption can be calculated by the following equation:

$$\%\ \text{sorption} = \frac{M_s - M_d}{M_d}.100\% \tag{2-5}$$

where M_s and M_d are the mass of swollen and dry material respectively.

Cross-linking a membrane makes the membrane insoluble in the feed mixture to decrease the swelling of the membrane. The reduced swelling enhances the membrane's selectivity towards the target compound. Most industrial membranes are cross-linked to various degrees. The degree of cross-linking can be altered by varying the reaction time, temperature, and reagent concentration during the manufacturing process. The degree of cross-linking can be estimated by the ion exchange capacity (IEC) (Mohanty and Purkait, 2011).

2.3. Membrane types

A membrane merely acts as a discreet thin interface that regulates the permeation of chemical solutions. A vast range of membranes has been synthesised on laboratory and industrial scale. Depending on the focus and application, different conventions are used to classify these membranes (Melin and Rautenbach, 2007). A summary table is supplied in Table 2.1.

Table 2.1: Membrane classifications

Structure	Porous	
	Dense	
Shape	Flat sheet	
	Tubular	
Morphology	Symmetric / isotropic	
	Asymmetric / anisotropic	
Primary mechanism	Hydrophilic	
	Hydrophobic	
	Organoselective	
Material	Organic	Polymer
	Inorganic	Silica
		Zeolite
	Mixed matrix membranes	

In pervaporation, the dense-phase, flat sheet polymers and porous, tubular and inorganic membranes are the most widely available. Asymmetric polymeric membranes are currently the most advanced membranes with a large range of target compounds. When considering the primary function or target compound of membrane separation, hydrophilic membranes have a high water selectivity. Hydrophobic membranes have a low selectivity towards water and tend to allow organic compounds to permeate with a higher selectivity. Organoselective membranes target specific organic compounds from a mixture of organic solvents. Pervaporation membranes can be classified according to the material of construction which includes polymers, inorganics and mixed matrices. (Bachmann et al., 2010, Shao and Huang, 2007)

Symmetric or isotropic membranes are normally prepared on laboratory scale due to the ease of preparation. Asymmetric or anisotropic membranes are manufactured on an industrial scale and offer enhanced pervaporation performance (Smitha et al., 2004).

2.3.1. Polymeric membranes

Polymeric membranes make up the bulk of the membranes currently used in pervaporation. The most widely commercialised hydrophilic membrane is a composite polyvinyl alcohol (PVA) cast on a polyacrylonitrile (PAN) ultraporous substrate. The most widely used hydrophobic membrane is polydimethyl siloxane (PDMS). (Mohanty and Purkait, 2011).

A commercial polymeric membrane (shown in Figure 2.2) consists of various layers, with the upper dense layer being the selective part of the membrane. The selective part has a thickness of approximately 1-2 µm to minimise transport resistance. This layer is cast on a porous asymmetric support layer of the same material with increased pore size. A fabric fleece support layer provides mechanical strength to the membrane.

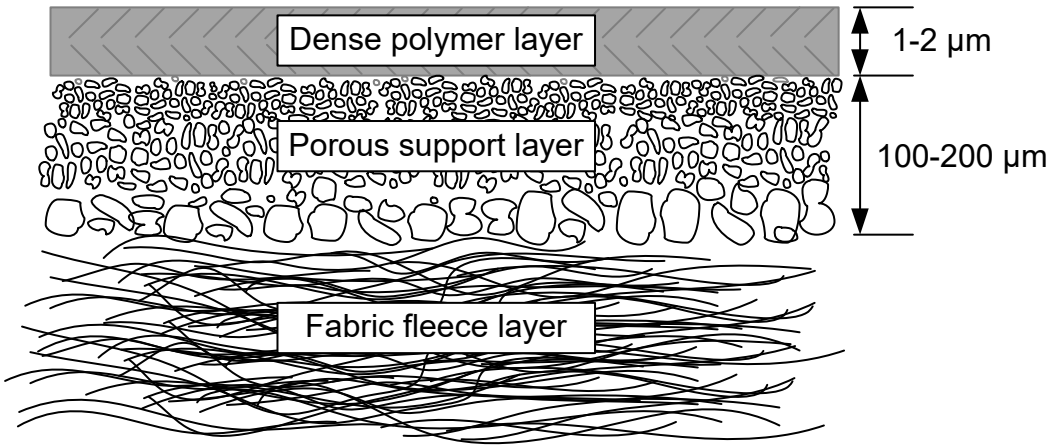

Figure 2.2: Principle structure of a polymeric composite membrane adapted from Mohanty and Purkait (2011) (Mohanty and Purkait, 2011)

2.3.2. Inorganic membranes

The most general inorganic membranes are ceramics, glass, metals and zeolites which are generally versatile in terms of application, temperature and pH ranges. They also tend to offer a low degree of swelling and better chemical- and temperature-resistance (Mohanty and Purkait, 2011). In contrast to polymeric membranes, inorganic membranes are more expensive and brittle (Basile et al., 2015; p 30).

The microporous support normally has very large pores and to prevent any defects in the active layer, multiple layers of the latter are coated on to the support tube (Nunes and Peinemann, 2001). The separation is governed by molecular sieving through the defined pores and adsorption of small molecules at the outer membrane and the inner pore surface of the active layer (Bowen et al., 2004).

Silica membranes coated on ceramic supports for dehydration applications up to 250 °C, are commercially produced by Pervatech BV, Netherlands and Sulzer Chemtech GmbH. NaA type zeolite membranes, fabricated commercially by Mitsui Engineering, Japan show enhanced thermal stability as well as increased mechanical strength.

2.3.3. Mixed matrix membranes

Inorganic materials, carbon nanotubes or carbon molecular sieves are normally integrated into polymeric membranes to enhance the pervaporation separation performance. Mass transport occurs through a combination of the solution-diffusion mechanism (polymer section) and molecular sieving (inorganic section) (Mohanty and Purkait, 2011).

2.4. Membrane characterisation

Due to the large number of membrane types, manufacturing methods and classification, characterisation is of fundamental importance to correlate membrane pervaporation performance with membrane properties. A shortened list of the most common characterisation methods relevant to this study is supplied below.

2.4.1. Contact angle

During contact angle measurements, the angle formed between a liquid droplet and the solid surface of the membrane is determined. The affinity between the fluid and the water determines the surface properties of the membrane and classifies the membrane as either hydrophilic (water contact angle < 90 °) or hydrophobic (water contact angle > 90 °) (Basile et al., 2015).

2.4.2. Further characterisation

Numerous additional characterisation methods are available, but mainly finds application in laboratory synthesised membranes. These techniques are described in full in the review article by Tylkowski and Tsibranska (2015) and in Mohanty and Purkait (2011). They include:

- Swelling and sorption
- Thermal gravimetric analysis
- Atomic force microscopy
- Surface analysis
- Positron annihilation lifetime spectroscopy
- Scanning electron microscopy
- Infrared spectroscopy
- Tensile strength

The present study focuses exclusively on commercialised membranes and the above mentioned techniques are therefore not discussed in further detail.

2.5. Pervaporation

Pervaporation is a membrane separation process where a component of a volatile liquid transports through a dense membrane (Figure 2.3) and emerges as a vapour. Pervaporation is a unique membrane process where the feed components undergo a phase change (Huang, 1991). Kober (1917) first introduced the term “pervaporation” by combining the words “permeation” and “evaporation” in his publication.

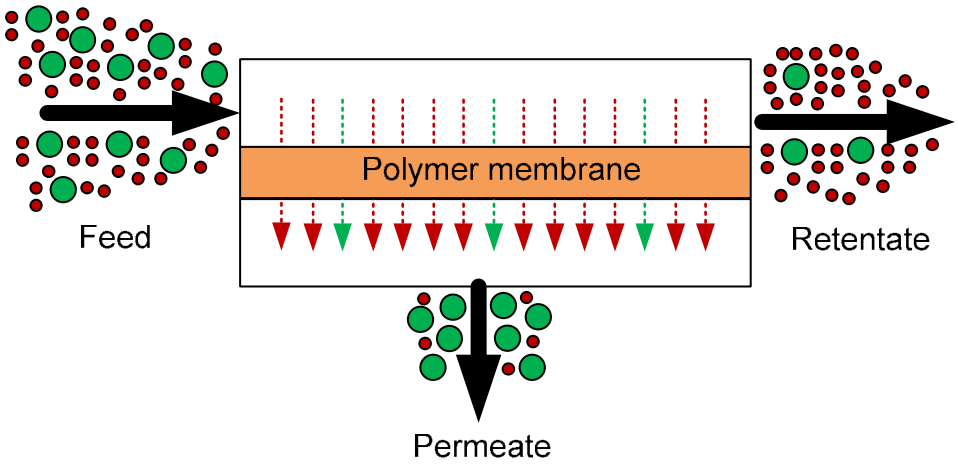

Figure 2.3: Pervaporation schematic adapted from by Mohanty and Purkait (2011)

Liquid feed flows along the membrane and selective components preferentially permeate through the membrane, emerging as a vapour. The permeate is swept from the membrane surface under vacuum conditions or by adding a sweep gas and is collected in a condenser (Feng and Huang, 1997).

The driving force of pervaporation is the gradient of chemical potential of a selected component within a multi-component system. Baker (2000) states that the performance of pervaporation is directly dependent on membrane and solvent interactions and properties, feed composition and operating temperature.

According to Mohanty and Purkait (2011) pervaporation adds numerous benefits to conventional distillation including:

- Reduced energy demand as only the permeate is vaporised.
- Absorbent free operation.
- No emissions to the environment.
- It is not limited to azeotropic compositions.
- It is considered a safer alternative to distillation.
- It is able to operate using a modular design.
- It can be used to successfully separate hazardous or heat sensitive components.

Much of the attention has now faded, and the number of companies involved in developing pervaporation technology has decreased significantly. The oil companies

like British Petroleum, Exxon and Texaco seem to have abandoned pervaporation research. The key problem seems to be economic viability.

Pervaporation seems to be more competitive on smaller scale applications, but current membranes and modules are unable to compete economically with distillation, solvent extraction, steam stripping, or in larger plants (Baker, 2000).

On the basis of the target compound to be removed from the feed solution, pervaporation is classified as:

(i) hydrophilic pervaporation,
(ii) hydrophobic pervaporation/ and
(iii) organoselective pervaporation.

2.5.1. Hydrophilic pervaporation

The target compound of hydrophilic pervaporation is water, which is normally present in azeotropic mixtures or close boiling point mixtures of organic solvents like alcohols, acetic acid, tetrahydrofuran (THF) and acetone. These dehydrations normally find great economic importance especially in the chemical manufacturing industry.

Membranes generally include polyvinyl alcohol (PVA), PAN, polyethermide (PEI), chitosan and cellulose derivatives.

Mohanty and Purkait (2011) state that hydrophilic pervaporation can also be used for the dehydration of hazardous hygroscopic compounds like hydrazine, monomethyl hydrazine (MMH) and unsymmetrical dimethyl hydrazine (UDMH).

2.5.2. Hydrophobic pervaporation

The target compound is normally a single volatile organic compound to be removed in small quantities from aqueous solutions. Hydrophobic pervaporation normally finds application in the following industries: pharmaceuticals, removal of aromas in heat-sensitive applications and treatment of wastewater by removal of volatile organic compounds (VOCs) (Mulder, 2012).

Membranes generally include polydimethyl siloxane (PDMS), polyether block polymide (PEBA), polytetrafluoro ethylene (PTFE), polypropylene (PP) and polybutadiene (PB).

Sunitha et al. (2011) used a laboratory synthesised PEBA membrane with an active thickness of 10 µm for the dehydration of hydrazine hydrate. They reported a maximum flux of 52 $g \cdot m^{-2} \cdot h^{-1}$ and a selectivity of 107 (the highest reported selectivity among literature sources).

Blending two or more non-covalently bonded polymers is a technique used to combine properties from various polymers into one membrane. Varying amounts of hydrophilic and hydrophobic membrane are blended together in an aim to increase the membrane permeability and selectivity as exemplified by work performed by Park et al. (1994) and George et al. (1999).

2.5.3. Organophilic pervaporation

The target organic compound is exclusively separated from an organic-organic mixture by preferential sorption through the membrane. Mohanty and Purkait (2011) report that organophilc separations are normally the most difficult of all pervaporation types. Separations include: separating methanol from methyl-tertiary butyl ether TMBE or toluene, ethanol from ethyl tert-butyl ether (ETBE) or benzene and benzene from cyclohexane.

2.6. Factors affecting membrane performance

For a given membrane the effect of various parameters mentioned below need to be investigated to ensure optimal operating conditions are attained on commercial scale (Mohanty and Purkait, 2011).

2.6.1. Feed composition / concentration

Mohanty and Purkait (2011) state that as a general rule, the selectivity increases as the preferentially permeating component concentration decreases due to lower membrane swelling.

2.6.2. Feed temperature

It is generally accepted that temperature has an Arrhenius type effect on the permeability of pervaporation membranes as described by the equation:

$$J = J_0 \exp\left(\frac{E}{RT}\right) \tag{2-6}$$

where J is the flux through the membrane, J_0 is a constant, E is the activation energy for the permeation, R is the universal gas constant and T is the absolute temperature of the feed solution.

From Equation (2-6) it can be seen that pervaporation flux is directly proportional to the feed temperature and Mohanty and Purkait (2011) state that this phenomenon is due to an increase in activation energy. An increase in flux will result in a decrease in membrane selectivity and vice versa as selectivity is inversely proportional to flux.

2.6.3. Permeate pressure

The overall membrane flux increases with an increasing vacuum (decreased permeate pressure) (Mohanty and Purkait, 2011). Permeation of the more volatile component should be lower with a decrease in vacuum (increased permeate pressure) and therefore the selectivity.

2.6.4. Feed flow rate

Depletion of the target solute near the membrane surface leads to a reduction of the driving force, a phenomenon called concentration polarisation. Optimization of the fluid dynamics reduces concentration polarisation and can potentially lead to an increase in flux, but on a commercial scale can require additional energy input (Basile et al., 2015).

2.6.5. Membrane properties

2.6.5.1. Thickness of membrane

Mohanty and Purkait (2011) state that only the flux is affected with membrane thickness and that selectivity is therefore independent of thickness. An increase in membrane thickness will lead to a decrease in permeate flow through the membrane and therefore a decrease in flux.

2.6.5.2. Membrane pre-treatment

Dutta et al. (1996) confirmed that pre-treating a membrane only improves the initial membrane performance and untreated membranes catch up in performance over time.

2.7. Pervaporation focused on hydrazine

Ravindra et al. (1997) investigated interactions of hydrazine, water and hydrazine hydrate with ethyl cellulose (EC) polymeric membranes, focussing on Fourier-transform infrared spectroscopy (FTIR), diffusivity and aging studies. From the results they reported that hydrazine hydrate in EC showed less interaction than both pure water and anhydrous hydrazine and described it being possible due to higher interaction between water and hydrazine when compared to either pure components with the EC polymer. By using reduced sorption curves, they further found that the diffusion coefficient is a function of feed concentration and that the EC membrane is more selective towards water. FTIR, mechanical strength and accelerated aging tests indicated that, even after a period of six months, the membranes showed no signs of membrane degradation or loss of mechanical properties.

Ravindra et al. (1999c) reviewed the dehydration of hydrazine hydrate with EC polymeric membrane by using pervaporation. Their work focused on the effect of membrane thickness, concentration polarization, and feed concentration on partial component flux and membrane water selectivity. The authors made use of Flory–Huggins interaction parameters and Hansen solubility parameters, as well as chemical

tolerance to select the EC polymeric membrane. From the pervaporation results, water selectivities as high as 6.1 were obtained with a total flux of 0.03 $kg \cdot m^{-2} \cdot h^{-1}$.

Ravindra et al. (1999b) studies the state of water, hydrazine and hydrazine hydrate by using EC polymeric membranes and various compositions of solvents by using differential scanning calorimetry (d.s.c.). From the d.s.c spectra results for the solvent membrane system, the authors found that the binding capacity of hydrazine with the functional groups in EC is far greater than with water that hinders free diffusion of the water molecules and rendering good membrane selectivity towards water.

Pervaporation investigations using EC polymeric membranes were further enhanced by using both hydrazine and MMH as solvents. The investigation included an extensive study of the overall mass transfer resistance over the membrane. The study found that diffusion through the membrane and desorption resistance of the liquid solvents are significant contributors in membrane selectivity. (Ravindra et al., 2000)

According to Satyanarayana and Bhattacharya (2004) pervaporation may act as an alternative process for dehydrating hydrazine hydrate to produce anhydrous hydrazine for space propulsion purposes. Because of the highly alkaline nature of hydrazine the proper selection of polymers for the pervaporation-membrane plays a vital role and they therefore investigated the separation characteristics of several polymeric membranes. The hydrophilic/hydrophobic behaviour of the membranes was tested by contact angle measurements. The pervaporation studies on the selected polymers revealed that selective diffusion of water played a greater role compared to sorption. They further found that apolar materials exhibited higher separation factors than polar materials. They reported that their results were encouraging for some modified polymeric membranes such as EC and acrylonitrile-butadiene-styrene (ABS).

Hoda et al. (2005) reported a mathematical model to simulate the performance of a hollow fibre, EC polymeric membrane for the pervaporative separation of a binary hydrazine hydrate liquid mixture. The model is based on the solution-diffusion mechanism for the hydrazine-water system. The property variation of feed and permeate streams along the axial side was studied as well as the influence of operating parameters on flux and selectivity. It was found that separation was better

with feed flow on the tube side compared to the feed flow on the shell side of the membrane module.

LI et al. (2009) reviewed the development of the dehydration of hydrazine fuels by pervaporation. From their results, they report that pervaporation can overcome the shortcomings such as low efficiency and processing safety of the traditional dehydration methods of hydrazine fuels. Due to the properties of hydrazine fuels various membrane materials such as chitosan, ceramic and zeolite are suitable for dehydration of hydrazine fuels by pervaporation. They found that multiple pervaporation modules connected in series can improve the dehydration efficiency. They also report that the key applications regarding the dehydration of hydrazine fuels by pervaporation include:

- recovery of hydrazine fuels from diluted aqueous solutions
- dehydration of high concentration hydrazine fuels.

This literature survey reveals that among the various polymeric membranes studied for hydrazine dehydration, the PEBAX®-2533 membrane exhibited the highest selectivity with reasonably high flux. The membranes have shown adequate mechanical strength and chemical stability (Sunitha et al., 2011).

A detailed summary of the available hydrazine related pervaporation research is given in Table 2.2, with an overall summary and major contribution followed by the main pervaporation related results.

Table 2.2: Summary of hydrazine related pervaporation research

Reference	Summary	Major contribution	Main Results
Ravindra et al. (1997)	• Specific interaction sites of EC with water, hydrazine and hydrazine hydrate by FTIR spectra • Measure diffusion and sorption coefficients to determine overall selectivity • Determine effect of membrane aging on physico-chemical and mechanical properties by FTIR and mechanical tests	• EC membranes can be used to separate hydrazine-water mixtures • EC membranes can be used for extended periods of time	Diffusion coefficient (D [cm^2/s]) • Water = 2.57 x 10^{-8} • Hydrazine = 0.28 x 10^{-8} • Hydrazine hydrate = 0.19 x 10^{-4} Equilibrium percentage sorption [%] • Water = 3.4 • Hydrazine = 7.6 • Hydrazine hydrate = 4.86 Overall selectivity • water/hydrazine = 2.1657
Ravindra et al. (1999b)	• Studies on the energetic state of various concentrations of hydrazine-water mixtures using differential scanning calorimetry (d.s.c.)	• Four or five distinct energetic states of the hydrazine-water solvents in EC membrane have been observed • A new peak of enthalpy of mixing was observed at a higher temperature	Overall selectivity water/hydrazine = 3.94
Ravindra et al. (1999c)	• Separation of hydrazine hydrate solutions with lab synthesised EC membranes by using pervaporation • Effect of input parameters on flux and selectivity - Membrane thickness - Concentration polarization - Feed concentration	• Proposed a separation mechanism based on sorption measurements, diffusion coefficient, Flory-Huggins interaction parameters and Hansen's solubility parameters • Published a flux and selectivity curve for various hydrazine-water concentrations	Thickness μm / Flux $kg \cdot m^{-2} \cdot h^{-1}$ / α 25 / 0.0412 / 2.435 45 / 0.0285 / 3.74 65 / 0.027 / 2.827 85 / 0.0189 / 3.489 120 / 0.0169 / 3.55 45 / 0.03 / 6.1

Table 2.2 (cont.): Detailed summary of hydrazine related pervaporation research

<table>
<tr><th>Reference</th><th>Summary</th><th>Major contribution</th><th>Main Results</th></tr>
<tr><td>Ravindra et al. (2000)</td><td>• Study of the overall mass transfer resistance through a lab synthesised EC membrane by pervaporation
• The resistance values were estimated by varying the membrane thickness</td><td>• Pervaporation selectivity results for hydrazine monohydrate feed mixtures were obtained
• Higher sorption of hydrazine did not result in preferential separation
• Desorption resistance and diffusivity were predominant when compared to the separate solubilities</td><td>Desorption resistance [$mol^2N^{-1}m^{-3}s^{-1}$]
• Water = 1.493 x 10^{12}
• Hydrazine = 1.242 x 10^{14}
Membrane resistance [$mol^2N^{-1}m^{-3}s^{-1}$]
• Water = 0.588 x 10^3
• Hydrazine = 0.180 x 10^3</td></tr>
<tr><td>Dutta (2004)</td><td>• Pervaporation studies on hydrazine hydrate using blended polymers with the aim to modify membrane characteristics and improve the separation performance
• Pervaporation and equilibrium sorption tests were used to quantify lab synthesised membrane performance</td><td>• Acrylo-nitrile butadiene styrene (ABS) and EC membranes were blended in various compositions as well as sulphated polystyrene membranes during this study</td><td><table><tr><th>Mem</th><th>Thick. µm</th><th>Flux $kg·m^{-2}·h^{-1}$</th><th>α</th></tr><tr><td>EC</td><td>60</td><td>8.042</td><td>1.71</td></tr><tr><td>BABS1</td><td>80</td><td>9.571</td><td>2.45</td></tr><tr><td>BABS2</td><td>40</td><td>16.928</td><td>1.45</td></tr><tr><td>BABS3</td><td>70</td><td>9.956</td><td>1.97</td></tr><tr><td>BABS4</td><td>110</td><td>1.967</td><td>5.21</td></tr><tr><td>BABS5</td><td>60</td><td>2.274</td><td>13.23</td></tr><tr><td>ABS</td><td>75</td><td>5.763</td><td>4.59</td></tr></table></td></tr>
<tr><td>Satyanarayana et al. (2006)</td><td>• Using positron annihilation to study effect of free volume in dense phase membranes in separation of hydrazine hydrate by pervaporation
• Study includes both commercial and lab synthesised polymeric membranes</td><td>• Proved that positron annihilation lifetime spectroscopy can be used to estimate free volume size in pervaporation membranes
• Free volume parameters can be used in future transport modelling</td><td><table><tr><th>Mem</th><th>Flux $g·m^{-2}·h^{-1}$</th><th>α</th></tr><tr><td>EC</td><td>9.65</td><td>1.72</td></tr><tr><td>ECNC01</td><td>9.35</td><td>1.87</td></tr><tr><td>ABS</td><td>7.81</td><td>5.07</td></tr></table></td></tr>
</table>

Table 2.2 (cont.): Detailed summary of hydrazine related pervaporation research

Reference	Summary	Major contribution	Main Results
Satyanarayana and Bhattacharya (2004)	Pervaporation of hydrazine monohydrate, investigating the effect of hydrophilic to hydrophobic membranes on separation characteristics for both lab synthesised and commercial membranes	• Pervaporation of hydrazine experiments provided encouraging results, with water selectivity higher than 1.4 in all experiments (except Pervap™ 2200). • Apolar membranes have higher separation factors when compared to polar membranes • Described an exponential relationship between process selectivity and ratio of contact angles	Sorption characteristics (50 °C) Membrane: α EC: 0.681 MEC1: 0.667 MEC2: 0.665 MEC3: 0.570 MEC4: 0.533 PS: 0.390 ABS: 0.482 Pervaporation performance Mem: Flux[1] g·m^{-2}·h^{-1}: α Pervap 2200: 122.4: 133.4 Pervap 2201: 4.0: 14.32 Pervap 2202: 31.4: 60.6 EC: 96.5: 166 MEC 4: 81.8: 262.4 PS: 11.5: 62.6 ABS: 78.1: 395.9 [1] Normalised flux to 5 µm
Hoda et al. (2005)	Mathematical model was expressed to simulate the pervaporation performance of a hollow fibre module based on the experimental results from Ravindra et al. (1999c)	• First mathematical model to simulate pervaporation model for hydrazine hydrate separation • A better separation was achieved for feed flow in the tube side when compared to shell side	• Margules constant for hydrazine-water = 5606.6 J/mol • Water-hydrazine interaction parameter = -2.265 • Water-polymer interaction parameter = 2.5 • hydrazine-polymer interaction parameter = 1.8

Table 2.2 (cont.): Detailed summary of hydrazine related pervaporation research

<table>
<tr><th>Reference</th><th>Summary</th><th>Major contribution</th><th>Main Results</th></tr>
<tr><td>Mandal et al. (2008)</td><td>• Pervaporation studies on hydrazine hydrate using blended polymers with the aim to modify membrane characteristics and improve the separation performance.
• Characterization of blended polymeric membranes</td><td>• Blended polymers could be could be useful in developing new membranes with improved pervaporation performance
• Sorption and diffusion selectivity values were obtained by the Flory-Huggins theory
• Preferential hydrazine sorption when compared to water</td><td>Sorption results
<table><tr><th>Mem</th><th>% Sorption H_2O g/g</th><th>% Sorption N_2H_4 g/g</th></tr><tr><td>EC</td><td>4.12</td><td>5.23</td></tr><tr><td>BM20</td><td>2.67</td><td>4.81</td></tr><tr><td>BM30</td><td>2.20</td><td>4.56</td></tr><tr><td>BM40</td><td>1.31</td><td>3.53</td></tr><tr><td>BM70</td><td>1.12</td><td>2.21</td></tr><tr><td>ABS</td><td>0.31</td><td>0.50</td></tr></table>Pervaporation results
<table><tr><th>Mem</th><th>Thick. [µm]</th><th>Flux[1] $g/m^2.h$</th><th>α</th></tr><tr><td>EC</td><td>60</td><td>4.825</td><td>1.710</td></tr><tr><td>BM20</td><td>80</td><td>7.657</td><td>2.049</td></tr><tr><td>BM30</td><td>40</td><td>6.771</td><td>2.350</td></tr><tr><td>BM40</td><td>70</td><td>6.6972</td><td>2.500</td></tr><tr><td>BM70</td><td>110</td><td>2.717</td><td>5.947</td></tr><tr><td>ABS</td><td>75</td><td>4.322</td><td>4.587</td></tr></table>[1] Normalised flux to 5 µm</td></tr>
<tr><td>LI et al. (2009)</td><td>• Pervaporation studies on dehydration of hydrazine</td><td colspan="2">• They found that multiple pervaporation modules connected in series can improve the dehydration efficiency.
• Chitosan, ceramic and zeolite are possible to dehydrate hydrazine</td></tr>
<tr><td>Sunitha et al. (2011)</td><td>• Pervaporation studies on dehydration of hydrazine using a laboratory synthesised PEBAX®-2533 membrane</td><td>• Published a flux and selectivity curve for various hydrazine-water concentrations
• Reported a reduction in water selectivity with an increase in water feed is due to enhanced sorption of water leading to swelling of the membrane</td><td>PEBAX®-2533 on PPSU (10 µm)
• Flux = 51.95 $g/m^2.h$
• Water selectivity = 107.109</td></tr>
</table>

From the literature review on pervaporation related experiments on hydrazine-water system, it is became evident that the majority of the research was focussed on laboratory synthesised EC polymeric membranes, either in pure form or blended with components like acrylo-nitrile butadiene or sulphated polystyrene to various degrees (Ravindra et al., 1997, Ravindra et al., 1999c, Ravindra et al., 1999b, Ravindra et al., 1999a, Ravindra et al., 2000, Satyanarayana and Bhattacharya, 2004, Dutta, 2004, Mandal et al., 2008). The only documented pervaporation related experiments performed on commercial polymer membranes were on Pervap™ 2200, Pervap™ 2201 and Pervap™ 2202 and no sorption tests were performed. It was therefore the first objective of this study to identify and screen all commercially available polymeric membranes from various international supplies.

Characterisation of pervaporation membranes over a spectrum of concentrations and temperatures are very limited. Ravindra et al. (1999c) investigated the effect of concentration on both sorption selectivity and pervaporation flux and selection by using an EC polymeric membrane. The same experiments were repeated by Sunitha et al. (2011) using a PEBAX®-2533 membrane. Both experiments were limited to a fixed temperature and the effects of activation energy was therefore not taken into account. It was therefore the second objective of this study to determine the effects of both concentration and temperature on commercially available membranes for both sorption and pervaporation experiments.

Ravindra et al. (1999c) proposed a separation mechanism based on their sorption and pervaporation experimental results. Hoda et al. (2005) reported the first mathematical model to simulate pervaporation model for hydrazine hydrate separation. The limited work therefore created the third objective of this study to create a mass transfer model over the membrane to simulate the pervaporation performance over the membrane.

CHAPTER THREE - MODELLING OF MASS TRANSFER OVER A POLYMERIC PERVAPORATION MEMBRANE

Overview

Pervaporation involves both mass and heat transfer over the membrane and differs from other membrane processes by having a change of state from a liquid to a vapour solution. Cunha et al. (2002) explained that mass transport in pervaporation is more complex that other membrane process due to the swelling in the polymer matrix. Several pervaporation models have been developed in literature with the aim to describe and predict the mass transport through both organic and inorganic membranes. This chapter aims to introduce the modelling approach and equations used for the dehydration of hydrazine hydrate by using the solution-diffusion model as first described by Binning (Binning et al., 1961).

The chapter is divided into four main sections, starting with an introduction in Section 3.1, followed by a general description of mass transfer over a polymeric membrane (Section 3.2). The solution-diffusion model is discussed in Section 3.3, along with the most common assumptions. Section 3.3 further describes the sorption equilibria that is based on the Flory-Huggins sorption theory. The Flory-Huggins theory makes use of interaction parameters and the diffusion equilibria. In this chapter the ideal and non-ideal mixtures are considered to obtain the interaction parameters to calculate the component flux by making use of various diffusion coefficients. Section 3.4 describes the mass transfer component by diffusion making use Fick's law and diffusion coefficients.

3.1. Introduction and background

Pervaporation involves mass and heat transfer over the membrane. The change of state, from a liquid solution to a vapour mixture, leads to a resulting enthalpy of evaporation. Therefore energy needs to be continuously added to the inlet stream for the inlet stream to remain isothermal (Basile et al., 2015). The driving force for pervaporation is the gradient in chemical potential of the most selective component in the mixture with units ($J \cdot mol^{-1}$), which describes the general energetic state of said component in its environment. (Basile et al., 2015)

The membrane material plays an integral part in the mass transfer through the membrane and for modelling purposes can be divided into organic (polymer), inorganic (ceramics, zeolites, glass and metal) and hybrid (combination of organic /and inorganic) membranes (Kujawski, 2000). The most important difference between organic and inorganic membranes is that organic membranes are normally dense phase membranes prone to membrane swelling, while inorganic membranes are made from inert porous material.

A strict distinction should therefore be made between models used for organic, inorganic and hybrid membranes. The solution-diffusion model has been the most accepted model used to describe the diffusion through a dense polymeric membrane, while the pore flow model, which provides for microscopic transport regions, is used for porous inorganic membranes (Wijmans and Baker, 1995). According to Basile et al. (2015) both these models have been demonstrated to give good approximation of mass transfer when binary mixtures are used, while for more complex multi-component mixtures the Maxwell-Stefan theory can be used to describe the interaction between components.

This chapter will only focus on the modelling aspects of polymeric membranes. Several factors influence the mass transport mechanism through polymeric membranes, including: the polymer type and molar mass, plasticisers used in membrane manufacturing, nature, degree and density of cross-links, and operating temperature. The characteristics of the membrane itself will determine the mass transport (George and Thomas, 2001).

There is no universal model capable of predicting the behaviour of the pervaporation process for any component. Thus particular considerations have to be taken into account to adequately represent the process for each different mixture, yielding as many models as there are mixtures to separate (Lone et al., 2015). Lipnizki and Trägårdh (2001) published a review of the literature models with regard to their application, range and mathematical description.

Since the work done by Binning et al. (1961) various researchers have published variations from the initial model, especially in the way non-idealities are taken into account (Mulder, 2012). The majority of these models vary in the description of the variation of the diffusion coefficient across the membrane (Jonquieres et al., 1996).

Lee (1975) used a solution-diffusion model that included a concentration independent diffusion coefficient, therefore it did not take account any potential coupling effects in the partial fluxes of binary mixtures and the membrane.

Long (1965) proposed an exponential model to simulate the diffusivity of a pure component permeate as a function of its own concentration in the membrane (Brun et al., 1985). Greenlaw et al. (1977a) proposed a model that describes the effect of pressure, which is valid for ideal systems such as mixtures of hydrocarbons and polyethylene films. The same model was later used by Rautenbach and Albrecht (1980) to describe the results obtained with benzene-cyclohexane-polyethylene system. The “Greenlaw”-model was later improved by Shelden and Thompson (1984) for computer simulations of non-ideal systems.

Mulder and Smolders (1984) also proposed an exponential relationship between the diffusion coefficient for a water-ethanol system through a cellulose acetate membrane. Except for concentration, two other variables have been included in the model to determine the diffusion coefficient. In the case of liquid mixtures, a combined plasticising action was assumed.

A more complex, six-coefficient exponential model, was proposed by Brun et al. (1985). This model was used for the non-ideal water-chloroform system and water-benzene mixtures with elastomer membranes. Trong (1987) added simplifying

assumptions to the Brun et al. (1985) model. Among the assumptions Trong (1987), assumed that only one component swells the cellulosic membrane and therefore affects the mobility of both permeates. The model Trong (1987) proposed is only a specific variation of the model proposed by Brun et al. (1985).

Hoda et al. (2005) modelled a hydrazine hydrate system using an EC polymeric membrane. In their model they used the diffusion coefficient model as described by Brun et al. (1985): thus the model assumes that the diffusion coefficient varies exponentially with the volume fraction of the components. They selected the strong-cross dependence to account for the strong coupling effect as is the case in hydrazine-water systems (Hoda et al., 2005).

3.2. Mass transfer through a polymeric membrane

The movement of permeate through all membranes can mathematically be described by a gradient in chemical potential, in the direction of decreasing chemical potential (Mulder et al., 1985). The chemical potential gradient takes the interrelation between the individual driving forces of pressure, temperature, concentration and electromotive forces into account. The partial flux (J_i) of component i can be described by the following equation:

$$J_i = -L_i \frac{d\mu_i}{dz} \tag{3-1}$$

where $\frac{d\mu_i}{dz}$ is the chemical potential gradient of component i and L_i is the coefficient of proportionality that links the above mentioned chemical potential driving force to flux (Wijmans and Baker, 1995). The above-mentioned approach is applied so successfully due to the fact that multiple driving forces can be taken into account as is the case for instance in reverse osmosis that makes use of pressure and concentration gradients.

A simplistic way to illustrate Equation (3-1) is to show that there is a proportionality relationship between the flux and the driving force (chemical potential gradient):

$$\text{Flux } (J_i) = \text{Proportionality factor } (P) \times \text{Driving force} \quad (3\text{-}2)$$

The proportionality factor or permeability is a measure of how fast the component is transported through the membrane when a give force is applied (Mulder, 2012). The solution diffusion model states that the permeability (P) is a combination between sorption (S) and diffusivity (D), assuming a negligible effect of desorption:

$$\text{Permeability } (P) = \text{Sorption } (S) \times \text{Diffusion } (D) \quad (3\text{-}3)$$

Sorption is a thermodynamic parameter that indicates the amount of penetrant sorbed into the membrane under equilibrium conditions (Mulder, 2012). Diffusion is a kinetic parameter, resulting from a random movement of molecules that is dependent on size and geometry of the permeating species as well as the nature of the membrane or permeating media (Meuleman et al., 2001).

3.3. Solution-diffusion model

A solution-diffusion model was first described by Binning et al. (1961) for permeation through a dense phase polymeric membrane. Generally the solution-diffusion model used for pervaporation assumes that the transport mechanism through the dense phase membrane can be divided into three stages: the components are first adsorbed into the membrane, then diffuse through the membrane and lastly desorb at the opposite end of the membrane (Lone et al., 2015, George and Thomas, 2001, Baker, 2000). The last desorption step is normally neglected as it is fast in comparison to the sorption and diffusion steps (Shieh and Huang, 1998a, Shieh and Huang, 1998b). The solution-diffusion mechanism with the effect of chemical potential, pressure and solvent activity is shown in Figure 3.1.

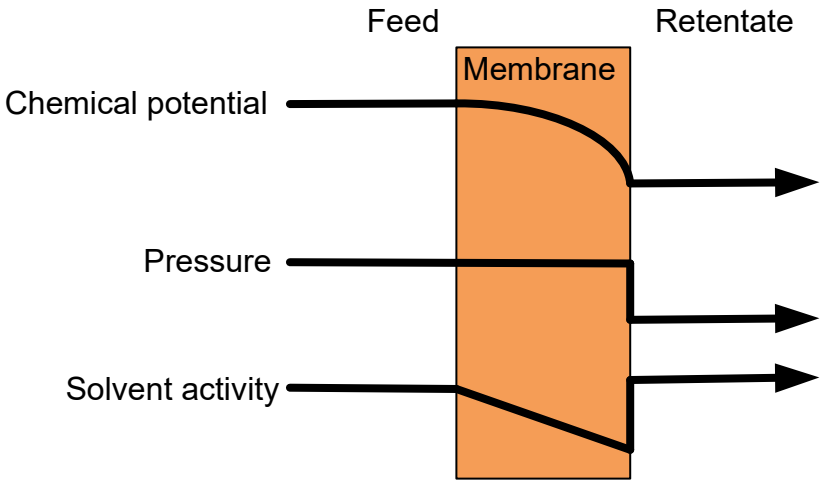

Figure 3.1: Schematic solution-diffusion model representation adapted from Wijmans and Baker (1995)

The most common assumptions made in the application of the solution-diffusion model were described by Basile et al. (2015) as the following:

- The membrane is treated as a homogeneous medium and is restricted to the top active layer.
- The system is treated as an isothermal system with no heat gain or loss over the module.
- The module functions under steady-state.
- No convection is assumed and therefore Fick's first law is valid.
- No coupling mass transport effects are taken into account.
- All membrane interfaces are in equilibria, i.e. the feed / membrane interface is at the same pressure and the chemical potential downstream of the membrane is the same as at the membrane / downstream interface of the membrane.
- The pressure within a membrane is uniform and therefore the chemical potential gradient is only expressed as a concentration gradient.
- The chemical potential or activity of a compound in the polymeric membrane can be obtained by using Flory-Huggins thermodynamics (Mulder, 2012).

3.3.1. Sorption equilibria

The sorption coefficient in the membrane, S_i [dimensionless] is obtained by assuming at the chemical potential of the feed liquid is in equilibrium with the chemical potential in the membrane at the same pressure (Wijmans and Baker, 1995):

$$\mu_{i,f} = \mu_{i,m} \tag{3-4}$$

where $\mu_{i,f}$ is the chemical potential of the feed solution and $\mu_{i,m}$ is the chemical potential of the membrane. The chemical potential can therefore be written as:

$$\mu_i{}^0 + RT.ln(\Upsilon_{i,f}.c_{i,f}) + V_{i,f}.(p_0 - p_{i_{sat}}) = \mu_i{}^0 + RT.ln(\Upsilon_{i0,m}.c_{i,m}) + V_i.(p_0 - p_{i_{sat}}) \tag{3-5}$$

where $\mu_i{}^0$ is the standard state chemical potential of component i, $\Upsilon_{i,f}$ is the activity coefficient of component i in the feed, $c_{i,f}$ and $c_{i,m}$ are the molar concentration of component i in the feed and membrane respectively, $V_{i,f}$ is the molar volume in the feed, p_0 is the pressure of the fluids at the feed-permeate interfaces, $p_{vi,f}$ and $p_{i_{sat}}$ is the saturation partial pressure of component i. Rearranging this equation leads to an expression for the concentration at the liquid solution / membrane feed-side interface:

$$c_{i,m} = \frac{\gamma_{i,f} c_{i,f}}{\gamma_{i,m}} = S_i.c_{i,f} \tag{3-6}$$

where S_i is the liquid-phase sorption coefficient. The sorption selectivity is an important factor in understanding the selective transport in pervaporation and selecting the most suitable polymer for this process. For systems that assume ideal sorption, the liquid phase sorption coefficient is assumed to be unity and therefore the concentration inside the membrane is assumed to be the same as the feed concentration. Diffusion therefore dominates pervaporation selectivity.

Preferential or selective sorption is obtained due to a difference in composition of the binary liquid mixture inside the polymeric membrane and the liquid feed mixture. Experimental sorption data can be used to test pervaporation models that are sorption dominated and to calculate the interaction parameters that is required for thermodynamic modelling.

Various thermodynamic models and theories have been developed and applied to interpret the sorption equilibria in polymeric pervaporation systems (Basile et al., 2015). Flory-Huggins thermodynamics (Flory, 1953) have been the most widely used to calculate the chemical potentials for sorption equilibria in pervaporation systems (Mulder et al., 1985, Yang et al., 1998, Hoda et al., 2005).

The full derivation was performed by (Mulder et al., 1985) and given a volumetric fraction of a component in the feed, the theoretical values of the preferential sorption can therefore be calculated by Equation (3-7) if the interaction parameters, the ratio of molar volumes and the volume fraction of the polymer are known.

$$\begin{aligned} ln\left(\frac{\Phi_i}{\Phi_j}\right) - ln\left(\frac{v_i}{v_j}\right) \\ = (r-1)ln\left(\frac{\Phi_i}{v_j}\right) - g_{ij}(u_j)(\Phi_j - \Phi_i) - g_{ij}(v_j)(v_i - v_j) \\ - \Phi_p(g_{ip} - r g_{jp}) + u_i\Phi_j\frac{\partial g_{ij}}{\partial u_j} - v_i v_j\frac{\partial g_{ij}}{\partial v_j} + \Phi_p u_i\frac{\partial g_{ip}}{\partial u_j} \\ - \frac{V_i}{V_j}u_j\Phi_p\frac{\partial g_{jp}}{\partial u_i} \end{aligned} \tag{3-7}$$

where Φ_i is the volume fraction of component "i" in a ternary system, v_i is the volume fraction of component "i" in a binary system, r is the ratio of molar volumes (V_i/V_j), g_{ij} is the concentration dependent interaction parameter between component "i" and "j", u_j is the volume fraction confined to the non-solvent part of the ternary phase.

3.3.1.1. Interaction parameters

Before the preferential sorption in Equation (3-7) can be solved, the concentration dependent binary interactions between water and hydrazine (g_{ij}), the water-polymer (g_{ip}) and hydrazine-polymer (g_{jp}) must be solved.

Binary interaction parameter (g_{ij})

Several methods for calculating the concentration dependent binary interaction parameter (g_{ij}) between water and hydrazine has been proposed and used in literature (Yang et al., 1998, Mulder and Smolders, 1984, Cao and Henson, 2002)

Yang et al. (1998) calculated the activity (α_i) from the Flory-Huggins thermodynamics for a binary system according to the Flory-Huggins (Flory, 1953) in their method as shown in Equation (3-8).

$$\ln \alpha_i = lnv_i + \left(1 - \frac{V_i}{V_j}\right) v_2 + g_{ij} {v_j}^2 \tag{3-8}$$

where the activity of component "i" (α_i) can be determined by using a relevant chemical modelling software package in ChemCad® or Aspen Plus® with the relevant thermodynamic model. Yang et al. (1998) further states that the dependence of the concentration dependent binary interaction parameter (g_{ij}) on the molar volume (v_2) can be expressed as a fourth order polynomial.

Mulder and Smolders (1984) states that the binary interaction parameter (g_{ij}) is strongly concentration dependent and is a free energy parameter that can be calculated from the excess free energy of mixing data (ΔG^E) by using Flory-Huggins thermodynamics.

$$g_{ij} = \frac{1}{x_i v_j}\left[x_i ln\frac{x_i}{v_i} + x_j ln\frac{x_j}{v_j} + \frac{\Delta G^E}{RT}\right] \tag{3-9}$$

The dependence of the binary interaction parameter (g_{ij}) can be calculated as a function of volume fraction ($v_{i,j}$). This method has also been successfully used by Aminabhavi and Munk (1979) as well as Altena and Smolders (1982). The excess free energy of mixing (ΔG^E) data was calculated with Equation (3-10) .

$$\frac{\Delta G^E}{RT} = x_i x_j \left(A_{ji} x_1 + A_{ij} x_2\right) \tag{3-10}$$

Cao and Henson (2002), as well as Hoda et al. (2005) used a slight variation, shown in Equation (3-11), by making use of one Margules constant (A) to calculate the binary interaction parameter (g_{ij}). This method is suggested when the excess free energy of mixing data (ΔG^E) is not readily available.

$$g_{ij} = \frac{1}{x_i v_j}\left[x_i ln\frac{x_i}{v_i} + x_j ln\frac{x_j}{v_j} + \frac{A x_i x_j}{RT}\right] \tag{3-11}$$

Cao and Henson (2002) calculated the Margules constant (A) with vapor-liquid equilibrium data. The relationship between Margules constant (A) and the vapor-liquid equilibrium data are shown in Equation (3-12).

$$P^{sat} = x_i {P_i}^{sat} \exp\left[\frac{A}{RT}{x_j}^2\right] + x_j {P_j}^{sat} \exp\left[\frac{A}{RT}{x_i}^2\right] \tag{3-12}$$

where P^{sat} is the vapour pressure of the binary mixture and P_i^{sat} is the temperature dependent vapor pressure of pure component i.

Hoda et al. (2005) calculated the Margules constant (A) for a hydrazine-water system by minimising the least square error using the vapor-liquid equilibrium data provided by Wilson et al. (1955).

Dondos et al. (1970) proposed an alternative equation for calculating the binary interaction parameter (g_{ij}) and the excess free energy of mixing (ΔG^E) data.

$$g_{ij} = \frac{\Delta G^E}{R\ T\ x_i\ x_j} \tag{3-13}$$

Equation (3-13) becomes Equation (3-9) if the molar volumes of the binary components are the same.

Binary parameter (g_{ip} and g_{jp})

Mulder and Smolders (1984) reports that the two most widely used methods used to determine the binary interaction parameters of the polymer and a penetrant are inverse gas chromatography and equilibrium swelling experiments. The equilibrium swelling experiments can easily be done at any required temperature.

Polymers that are used in experimental procedures like pervaporation are normally homogeneous dense phase membranes with only a small quantity of penetrant. The membrane can therefore be considered as a swollen gel or a crosslink network. (Mulder and Smolders, 1984). The swelling behaviour of such networks can be expressed by making use of the Flory-Reihner theory (Flory, 1953). The free energy change, ΔG can be obtained by Equation (3-14).

$$\Delta G = \Delta G_m + \Delta G_{el} \tag{3-14}$$

where ΔG_m is the free energy of mixing and ΔG_{el} is the elastic free energy. At swelling equilibrium ΔG = 0 and Mulder and Smolders (1984) proposes the following equation to determine the interaction of a pure component and a membrane:

$$ln(1 - v_p) + v_p + \chi {v_p}^2 + \frac{V_1}{\bar{M}_c \bar{v}_p}\left({v_p}^{1/3} - 0.5 v_p\right) \tag{3-15}$$

where $\bar{M}_c$ can be taken as the average molecular weight between two cross links and v_p as the molar fraction of the polymer in the penetrant-membrane binary system. v_p is the difference between one and the penetrant volume fraction. In case of polymer-non-solvent systems with a small amount of non-solvent in the polymer, the interaction parameters can be considered concentration independent and Equation (3-15) reduces to Equation (3-16) (Krigbaum and Carpenter, 1954, Scott, 1949).

$$\chi = -\frac{\left[ln(1 - v_p) + v_p\right]}{{v_p}^2} \tag{3-16}$$

To take into account second order ternary concentration dependent effects, g_{ip} and g_{jp} need to be calculated in terms of volume fraction confined to the non-solvent part in the ternary phase for hydrazine (u_j), water (u_i) and volume fraction in polymer (v_p).

$$g_{ip} = g_{ip}(u_j \to 0) + au_2 + b[v_p - v_p(u_j \to 0)] \tag{3-17}$$

$$g_{jp} = g_{jp}(u_i \to 0) + ac + d[v_p - v_p(u_i \to 0)] \tag{3-18}$$

for the limiting case where $(u_i \to 0)$ and $(u_j \to 0)$ from Equations (3-17) and (3-18) $g_{ip}(u_j \to 0) = \chi_{ip}$ and $g_{jp}(u_i \to 0) = \chi_{jp}$ that are equal to the concentration independent interaction variables. χ_{ip} and χ_{ip} can be calculated from Equation (3-16), while $v_p(u_i \to 0)$ is obtained from the equilibrium sorption testing results.

3.3.2. Diffusion equilibria

It is widely accepted that both kinetic and equilibrium properties of the permeants are equally involved in the pervaporation process according to the solution-diffusion model. Various researchers have however, found that diffusive properties play a larger role than selectivity when reviewing their dependencies on concentration (VASSE, 1974, Larchet et al., 1983, Cabasso, 1983, Paul, 1976).

Fick's first law can be used to describe the relation between diffusive flux of component i in a dense phase polymeric membrane with the driving force under the assumption of steady state and one spatial dimension (Dutta et al., 1996):

$$J_i = -D_i \frac{d\varphi_i}{dz} \tag{3-19}$$

where J_i is the molar diffusion flux with units $mol \cdot (m^{-2} \cdot s^{-1})$, D_i is the diffusion coefficient with units $(m^2 \cdot s^{-1})$, and φ_i is the chemical potential that for ideal mixtures is the molar concentration $(mol \cdot m^{-3})$.

3.3.2.1. Ideal mixtures

For ideal mixtures, the molar diffusion flux can therefore be written as:

$$J_i = -D_i \frac{dc_i}{dz} \tag{3-20}$$

When the primary variable is mass fraction, $x\ kg_i/kg_T$, the concentration, c_i can be expressed as:

$$c_i = \rho_i \cdot x_i \tag{3-21}$$

When the primary variable is mass fraction feed, x_i (kg_i/kg_T) the mass concentration, c_i can be expressed as:

$$c_i = \rho_T \cdot y_i \quad \left[\frac{\mathrm{kg_i}}{\mathrm{m_s}^3} = \frac{\mathrm{kg_s}}{\mathrm{m_s}^3} \cdot \frac{\mathrm{kg_i}}{\mathrm{kg_s}}\right] \tag{3-22}$$

where ρ_T is the combined fluid density $(kg \cdot m^{-3})$ of the binary mixture. The diffusion mass flux for one dimensional ideal liquids can therefore be written as:

$$J_i = -\rho . D_i \frac{dx_i}{dz} \tag{3-23}$$

where the units for diffusional mass flux (D_i) changes to $(kg \cdot m^{-2} \cdot s^{-1})$.

Penetrant diffusion into polymeric membranes are strongly dependent on the permeate concentration in the materials. The relationships that describe the variation of diffusion coefficients as a function of concentration are therefore required for a complete characterization of the pervaporation mass transfer (Jonquieres et al., 1996).

Greenlaw et al. (1977a) proposed that the concentration dependence of the diffusion coefficient is partially due to the plasticising effect of the permeate and the polymer. It was further proposed that each of the two components diffusing through the membrane should contribute to the plasticising action.

$$D_i = D_i^0\left(c_i + \beta_{ji}c_j\right) \tag{3-24}$$

$$D_j = D_j^0\left(c_j + \beta_{ij}c_i\right) \tag{3-25}$$

were D_i^0 is the rate limiting diffusion coefficient of component "i", β_{ij} is the plastisisation exerted component "j" on component "i" and c_i and c_j are the concentration of components i and j inside the membrane respectively.

Converting the concentration of the components inside the membrane to mass fraction; the diffusion coefficient can be written as:

$$D_i = \rho_T . D_i^0\left(x_i + \beta_{ji}x_j\right) \tag{3-26}$$

$$D_j = \rho_T . D_j^0\left(x_j + \beta_{ij}x_i\right) \tag{3-27}$$

Greenlaw et al. (1977a) successfully used this method in the modelling of the binary pervaporation mixture of hexane-heptane. Later the same method was used by Rautenbach and Albrecht (1980) to describe aromatic-alkene separation through polyethylene membranes. These models are however limited to systems where the diffusivity variations in the material are not important and large plasticizing effects often lead to large deviations from linearity (Jonquieres et al., 1996).

Mulder (1991) proposed an exponential relationship for the concentration dependent diffusion coefficient for a water-ethanol system. This relationship accounted for the interaction between the permeating species and the membrane by making use of the plasticising coefficient.

$$D_i = D_{0,i}\, e^{\tau_i c_i} \tag{3-28}$$

$$D_j = D_{0,j}\, e^{\tau_j c_j} \tag{3-29}$$

where τ_i is the plasticizing coefficient and $D_{0,i}$ is the Fickian diffusion coefficient at infinite dilution.

A linear concentration dependence for diffusivity cannot take into account the large plasticising effects associated with the majority of pervaporation systems. If the logarithm of the diffusivity of a pure component permeate is calculated as a function of its own concentration in the membrane leads to the “long model” formulations. (Brun et al., 1985).

$$D_i = D_i^0 \exp(\beta_i \cdot c_i) \tag{3-30}$$

$$D_j = D_j^0 \exp(\beta_j \cdot c_j) \tag{3-31}$$

Brun et al. (1985) proposed a six-coefficient exponential model in which the exponential depends separately on the local concentrations:

$$D_i = D_i^0 \exp(\beta_{ii} c_i + \beta_{ij} c_j) \tag{3-32}$$

$$D_j = D_j^0 \exp(\beta_{jj}.c_j + \beta_{ji} c_i) \tag{3-33}$$

3.3.2.2. Non-ideal mixtures

In all other cases that contain non-ideal mixtures, Fick’s law for the driving force for diffusion of each species uses the gradient of the chemical potential of the species and can be written as:

$$J_i = -\frac{D_i^0 c_i}{RT} \frac{\partial \mu_i}{\partial z} \tag{3-34}$$

The driving force of pervaporation is the gradient in chemical potential of compound "i", namely μ_i $[J/mol]$, describing the general energetic state of a compound within its environment described as follows (considering no electric field) (Basile et al., 2015).

$$d\mu_i = RT.d\ ln(a_i) + V_i.dp - S_i.dT \tag{3-35}$$

$$d\mu_i = RT.d\ ln(\gamma_i.c_i) + V_i.dp - S_i.dT \tag{3-36}$$

where R is the ideal gas constant $8.314\,J/mol.K$, c_i [-] is the molar fraction of compound i, a_i is the activity of compound i, γ_i [-] the activity coefficient of component i, V_i $[m^3/mol]$ is the molar volume of component, p $[Pa]$ is the pressure, S_i $[J/mol \cdot K]$ is the molar entropy of compound i and T $[K]$ is the temperature.

The gradient in chemical potential in the case of no electrical field and of pervaporation at a constant pressure inside a membrane is simplified to:

$$d\mu_i = RT.d\ ln(\gamma_i.c_i) \tag{3-37}$$

Basile et al. (2015) states that with incompressible phases, such as a liquid or a solid membrane, the volume does not change with pressure. Integrating with respect to concentration yields:

$$\mu_i = {\mu_i}^0 + RT.ln(\gamma_i.c_i) + V_i.(p_0 - p_{vi}) \tag{3-38}$$

$$\mu_i = {\mu_i}^0 + RT.ln(\gamma_i.c_i) + V_i.(p_0 - p_{i_{sat}}) \tag{3-39}$$

With compressible gasses, the molar volume changes with pressure. Using ideal gas laws to integrate results in:

$$\mu_i = {\mu_i}^0 + RT.ln(\gamma_i.c_i) + RT.ln\frac{p}{{p_i}^0} \tag{3-40}$$

$$\mu_i = {\mu_i}^0 + RT.ln(\gamma_i.c_i) + RT.ln\frac{p}{p_{i_{sat}}} \tag{3-41}$$

To ensure reference chemical potential μ_i^0 is the same for Equation (3-38) and (3-40), the reference pressure p_i^0 is defined as the saturation vapor pressure of "i" $(p_{i_{sat}})$ giving Equations (3-39) and (3-41).

Assuming there are no pressure differences, Equations (3-39) and (3-41) simplify to:

$$\mu_i = \mu_i{}^0 + RT.ln(\gamma_i.c_i) \tag{3-42}$$

Substituting the chemical potential (μ_i) into Equation (3-34) gives:

$$J_i = -D_i{}^T c_i \frac{ln\, a_i}{dz} \leftrightarrow J_i = -D_i \frac{d\, c_i}{d \ln a_i}.\frac{d \ln a_i}{dz} \tag{3-43}$$

From Equation (3-43) the relationship between the diffusion coefficient (D_i) and thermodynamic diffusion coefficient ($D_i{}^T$) is obtained.

$$D_i{}^T c_i = D_i \frac{d\, c_i}{d\, ln\, a_i} \leftrightarrow D_i = D_i{}^T \frac{d\, ln\, a_i}{d\, c_i} \tag{3-44}$$

The partial flux for a non-ideal system can therefore be calculated by making use of the solution-diffusion model:

$$J_i = \frac{\rho_i}{l}\int_0^{\Phi_{io}} D_i\, d\Phi_i = \frac{\rho_i}{l}\int_0^{\Phi_{io}} (D_T)_i \frac{\partial ln\, a_i}{\partial \ln \Phi_i} d\Phi_i \tag{3-45}$$

where the volume fraction under isothermal conditions (Φ_i) are obtained by dividing the component concentration with the component density ($\Phi_i = {}^{c_i}/_{\rho_i}$).

To calculate the component flux (J_i) using the chemical potential model from Equation (3-45) the values of $\frac{\partial ln\, a_i}{\partial \ln \Phi_i}$ and $(D_T)_i$ need to be calculated. The gradient of the activity coefficient with concentration may be obtained by differentiating the activity with respects to $\ln \Phi_i$.(Yang et al., 1998, Mulder, 1991)

$$\frac{\partial \ln a_i}{\partial \ln \Phi_i} = \Phi_i \left\{ \frac{1}{\Phi_i} - \left(1 - \frac{V_i}{V_p}\right) - g_{ij}\Phi_j + \frac{V_i}{V_j}\Phi_j\chi_{jp} - \chi_{ip}(2 - 2\Phi_i - \Phi_j) \right. \\ \left. - \frac{{\Phi_j}^2(1-\Phi_i)}{(1-\Phi_p)^2}\frac{\partial g_{ij}}{\partial u_j} + {u_j}^2(1-2u_j)\frac{\partial g_{ij}}{\partial u_j} + {u_j}^3(1-u_j)\frac{\partial^2 g_{ij}}{\partial {u_j}^2} \right\} \tag{3-46}$$

$$\frac{\partial \ln a_j}{\partial \ln \Phi_j} = \Phi_2 \left\{ \frac{1}{\Phi_j} - \left(1 - \frac{V_j}{V_p}\right) - \frac{V_j}{V_p} g_{ij} \Phi_i + \frac{V_j}{V_i} v_{ip} \Phi_i - v_{jp}\left(2\Phi_j + \Phi_i - 2\right) \right.$$
$$+ \frac{V_j}{V_i}\left(1 - \Phi_j\right) \frac{{\Phi_i}^2}{\left(1 - \Phi_p\right)^2} \frac{\partial g_{ij}}{\partial u_j} + \frac{V_j}{V_i} {u_i}^2 \left(1 - 2u_j\right) \frac{\partial g_{ij}}{\partial u_j} \qquad 3\text{-}47$$
$$\left. + \frac{V_j}{V_i} {u_i}^3 (1 - u_i) \frac{\partial^2 g_{ij}}{\partial {u_j}^2} \right\}$$

where g_{ij} is the binary interaction parameter between component i and j, χ_{ip} and χ_{jp} are the interaction parameters between components i and j with the polymer.

The thermodynamic diffusion coefficient of both binary components, D_T can be considered a function of Φ_i and Φ_j at constant temperature and therefore (Yang et al., 1998):

$$(D_T)_i = {D_i}^0 f\left(\Phi_i, \Phi_j\right) \qquad (3\text{-}48)$$

$$(D_T)_j = {D_j}^0 g\left(\Phi_i, \Phi_j\right) \qquad (3\text{-}49)$$

where D_0 is the diffusion coefficient at zero concentration, while f and g are functional forms representing the plasticizing effects of penetrants on D_T.

CHAPTER FOUR - EXPERIMENTAL METHODS AND ANALYSIS

Overview

The main purpose of the experimental work performed in this chapter is to screen and identify a potential commercially-available polymeric membrane that is able to dehydrate a hydrazine monohydrate mixture past the azeotropic composition. The performance parameters for said membranes are also evaluated for changes in feed conditions. The chapter is subdivided into seven sections, with the materials (membranes and chemicals) used for the various experiments discussed in Section 4.1. The membrane stability tests (visual and mechanical) are discussed in Section 4.2, followed by contact angle measurements that forms part of characterising the polymeric membranes in Section 4.3. The sorption and swelling experiments are discussed in Section 4.4 and the pervaporation experiments are described in Section 4.5. The analytical equipment used in all experiments is described in Section 4.6, while the reproducibility and experimental error for all experiments are described in Section 4.7.

4.1. Materials

4.1.1. Membranes

This study solely focussed on commercially available polymeric membranes. All the membranes were organic, flat sheet, polymeric membrane and sourced from different suppliers, namely: DeltaMem AG in Switzerland (a company previously registered as the membrane business Sulzer Chemtech), PolyAn GmbH in Germany and Pervatech BV in the Netherlands. General membrane information obtained from the suppliers is summarised in Table 4.1, with detailed information supplied in Appendix A.

Table 4.1: Membrane selection and properties

Membrane	Supplier	Active layer	Main application
Pervap™ 4060	DeltaMem AG	PDMS	Organophilic PDMS membrane to remove trace organics from aqueous solutions.
Pervap™ 4100	DeltaMem AG	PVA	Standard PVA membrane used for dehydration of VOC mixtures.
Pervap™ 4101	DeltaMem AG	PVA	Highly cross-linked PVA membrane for dehydration of reaction mixtures.
Pervap™ 4102	DeltaMem AG	PVA	Modified and highly cross-linked membrane used for the dehydration of VOC mixtures.
POL-AL-M2	PolyAn GmbH	PVA	Organophilic pervaporation membranes for the separation of aromatics, alcohols as well as the separation of polar from non-polar components.
POL-OL-M1	PolyAn GmbH	PVA	Organophilic pervaporation membranes for the separation of aromatics, alcohols as well as the separation of polar from non-polar components.
PEBA	Pervatech BV	PEBA	PEBA membranes have hydrophobic/organophilic characteristics, targeting the organic constituent of the feed.
PDMS	Pervatech BV	PEBA	PDMS membranes have hydrophobic/organophilic characteristics, targeting the organic constituent of the feed.

4.1.2. Chemicals

The process chemical used in this study was hydrazine monohydrate, 98+% purity supplied by Alfa Aesar. Demineralised water, obtained from Waterlabs (Pty) Ltd South Africa, was used for rinsing and diluting the hydrazine monohydrate to the required concentrations. Analysis grade acetone obtained from Merck (Pty) Ltd was used for the derivatisation of the hydrazine containing sample. Analysis grade dimethyl chloride and sodium hydroxide, supplied by Merck (Pty) Ltd, were used in GC sample preparation by removing the hydrazine derivative from the aqueous phase.

All chemicals were used in the state received without any further purification. Details of the chemicals used during this study are summarised in Table 4.2.

Table 4.2: Chemicals used for experimental work

Chemical	Supplier	Purity	Experiment
Hydrazine monohydrate	Alfa Aesar	98+ wt. %	Pervaporation Sorption Visual stability Mechanical stability Contact angle
Demineralised water	Waterlabs (Pty) Ltd	-	Dilution of hydrazine monohydrate
Acetone	Merck (Pty) Ltd	Analysis grade	GC analysis
Dimethyl chloride	Merck (Pty) Ltd	Analysis grade	GC analysis
Sodium hydroxide	Merck (Pty) Ltd	Analysis grade	GC analysis

4.2. Stability tests

A combination of both visual and mechanical stability tests were performed on all membranes to identify potentially stable membranes in hydrazine-water systems.

4.2.1. Membrane visual stability test

A standard membrane visual stability test set-up was used and is well described in literature, see for example (Van der Gryp, 2008, Meintjes, 2011).

A 50 mm glass Petri dish with a closed lid was filled with a hydrazine monohydrate solution as shown in Figure 4.1. A membrane strip (30 × 15 mm) was placed inside the petri dish at ambient temperature (25 °C) and allowed to soak for a period of seven days, with daily inspections.

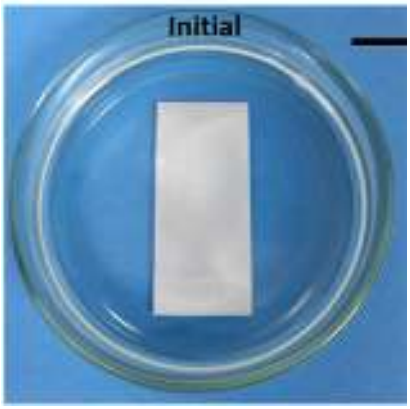

Figure 4.1: Typical experimental setup for membrane visual stability tests

The purpose of the visual stability tests was to investigate the effect of hydrazine monohydrate on the visual stability of each of the commercial membranes. A stable membrane should show no visible signs of deterioration, especially on the active layer and membranes were classified as either membranes with no interactions, slight interaction or severe interaction.

4.2.2. Membrane mechanical stability test

A standard test method for tensile properties of thin plastic sheeting (ASTM D 882) was used and is also well described in literature (Ravindra et al., 1997, Mandal et al., 2008, Chadehumbe, 2008).

An Instron tensile tester (Model 4444), fitted with a 0.2 kN self-calibrating load cell was used. The tensile load and amount of separation between the grips are digitally recorded at 50 ± 1 mm. The rate of separation of the grips was set at 25 ± 0.025 mm/min. The operating conditions were in a temperature and humidity controlled laboratory with an ambient temperature of 23 ± 0.5 °C and a relative humidity of 47 ± 5 % with a typical experimental setup shown in Figure 4.2.

Figure 4.2: Typical experimental setup for to measure membrane mechanical strength

The polymeric membrane sheets were cut into strips measuring 100 × 25 ± 0.2 mm. A membrane strip was exposed to hydrazine monohydrate for a period of two days in an accelerated aging test with a bath temperature of 60 ± 2 °C to be comparable with similar experiments done by Mandal et al. (2008). The membrane strips were then removed from the hydrazine monohydrate with the excess solution wiped from the membrane using a paper towel and air dried in a fume cupboard for a period of three days before analysis. Each tests was repeated three times and each membrane was analysed before and after exposure, with change in tensile strength indicating mechanical strength.

The membrane tensile stress was calculated by dividing the load at failure with the membrane cross-sectional area of failure, with units in megapascals (MPa).

$$\text{tensile strength} = \frac{\text{Load at break (kN)}}{\text{original width (mm) x original thickness (mm)}} \quad (4\text{-}1)$$

The experimental error for the mechanical strength tests were calculated at 7 % for the tensile strength, with details supplied in Appendix G.

4.3. Contact angle measurement

Equilibrium contact angles of either demineralised water or hydrazine hydrate with membranes were measured using the standard sessile drop method as used by various researchers (Mandal et al., 2008, Satyanarayana and Bhattacharya, 2004).

The contact angle between the liquid droplet and the solid surface of the membrane was determined by placing a droplet (100 µL) on the membranes strips. The droplet was dropped onto the membrane using an SGE eVol micro syringe.

The 100 µL sample in the syringe was placed onto the pre-cut 30 × 30 mm membrane strips. The drops remained in contact for at least 5 minutes before evaluation. Several digital photographs were taken of each sample and imported into the image processing package, Fiji™, with open source software plugin called Contact_Angle.jar. The software was used to first modify the digital image, then determine the contact angles of the droplets on the membranes samples. The software automatically computed both the left and right angles, with an example of the left angle shown in Figure 4.3.

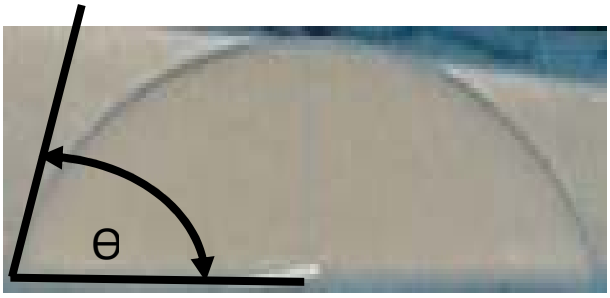

Figure 4.3: Illustration of the contact angles on a droplet

The purpose of the contact angle measurements was to investigate the superficial contact angle of each membrane and thereby determining whether the membrane will act hydrophilic or hydrophobic towards the hydrazine hydrate solution.

A traditional experimental design was followed, where the membranes and feed concentration were varied. The concentration was varied from hydrazine monohydrate (36 wt. % water) to pure water, with three concentrations in between.

The average of the left and right angles were used to calculate the equilibrium contact for each sample. Each analysis was repeated five times with an experimental error of 11 %, with detailed calculations supplied in Appendix G.

4.4. Sorption experiments

The standard method for sorption determination, including the standard equipment required is well described in literature (Aminabhavi et al., 1998, Van der Gryp, 2003, Ravindra et al., 1999c).

Dry membrane strips (15 mm x 15 mm) were weighed and immersed in various concentrations of hydrazine hydrate. The temperatures were controlled using a water bath between for 30, 40 and 50 ± 2 °C. The membranes were removed from the hydrazine hydrate solutions at fixed time intervals. The excess solution was wiped from the membrane using a paper towel, weighed and immediately returned to the solution. The procedure was repeated until no mass increase was observed, which indicated that the sorption equilibrium was reached.

The composition of the liquid mixture that sorbed into the polymeric membrane was determined using the method described by Yoshikawa et al. (1994) and used by Van der Gryp (2003) in separation studies of methanol from tertiary-amyl methyl ether (TAME). A diagram of the apparatus is shown in Figure 4.4.

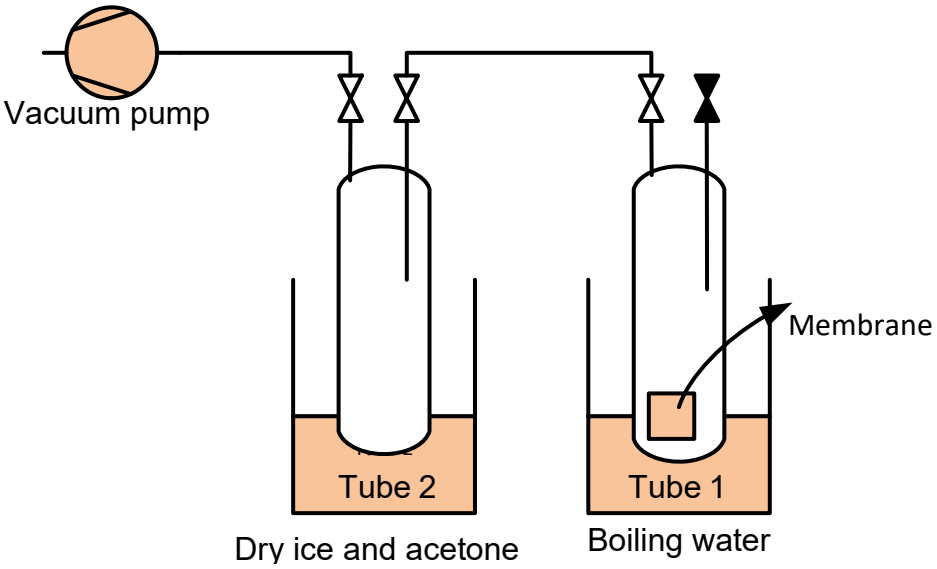

Figure 4.4: Schematic diagram of the apparatus used to determine the composition of the sorbed solution

After sorption equilibrium has been established, the membrane strip is again wiped with paper towel and placed into Tube 1 (on the right in Figure 4.4). Tube 1 is closed at both the inlet and outlet valve and immersed in a dry ice acetone mixture for a period of 5 minutes, while the vacuum pump brings the rest of a system to a downstream pressure of less than 100 Pa. The valve to the vacuum pump is then closed and Tube 1 is heated with boiling water to purge the solution from the membrane, which is then condensed within Tube 2 (on the left in Figure 4.4) for 10 minutes. The experiment was repeated five times before removing the sample for analysis. This was done to ensure adequate sample volume for GC analysis.

The purpose of the sorption experiments was to investigate the effect of concentration and temperature on the preferential sorption in terms of degree of swelling and sorption selectivity.

A traditional experimental design was followed. Sorption experiments were done on various membranes by varying the concentrations ranging between 36 to 100 wt. %, and keeping the temperature constant at 50 °C. The temperature was selected to increase the sorption rate and thereby generate adequate sample for analysis, but to remain below the vapour pressure that causes excessive fumes in an open experimental setup. The effect of temperature was quantified by varying the solution

temperatures from 30 to 60 ± 2 °C with 10 °C increments and keeping the solution constant at 36 wt. % water (hydrazine hydrate concentration).

The degree of swelling (S) of the membrane was calculated according to:

$$S = \frac{W_s - W_d}{W_d} \text{ x } 100\% \tag{4-2}$$

where W_s is the weight of the wet membrane and W_d the weight of the dry membrane. The sorption water selectivity (α_s) for a binary mixture can be calculated using:

$$\alpha_s = \frac{X_i \,.\, Y_j}{X_j \,.\, Y_i} = \frac{Y_{water} \,/\, (1 - Y_{water})}{X_{water} \,/\, (1 - X_{water})} \tag{4-3}$$

where Y_{water} and X_{water} are the mass fractions water in the permeate and feed respectively.

The sorption experimental error was calculated as 8 % for membrane swelling and 24 % for sorption composition with details in Appendix G.

4.5. Pervaporation experiment

The pervaporation experiments were carried out on a purposely designed laboratory scale pervaporation unit. The standard pervaporation setup is well described in literature (Mohanty and Purkait, 2011, Xie, 2012, Dutta, 2004). A schematic diagram of the experimental apparatus and instrumentation used in this study is shown in Figure 4.5.

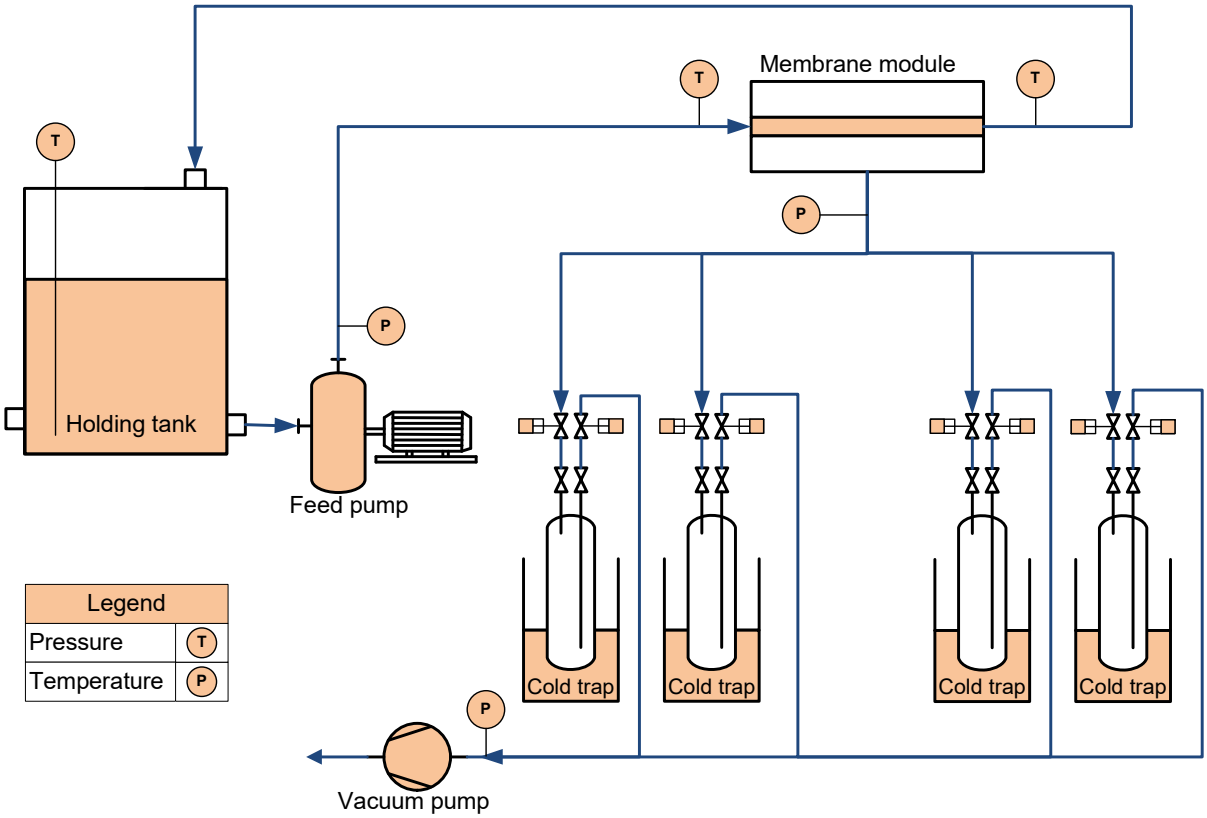

Figure 4.5: Schematic diagram of the pervaporation unit

The flat sheet polymeric membrane was placed in the middle of a round pervaporation module with a membrane surface area of 54 cm^2. Hydrazine hydrate solution from a 2 L heated stainless steel holding tank was circulated through the membrane module using a chemical resistant centrifugal feed pump. The temperature in the holding tank, and the membrane module inlet and outlet temperatures were measured. The outlet pressure on the feed pump was also monitored and used to determine the volumetric flow rate through the membrane module.

The permeate side of the membrane module was kept at a constant vacuum pressure of less than 100 Pa using a vacuum pump, while the vapour permeate was collected in four separate dry ice and acetone cold traps operated one at a time. The cold trap was selected by using electrically actuated solenoid valves. The vacuum pressure was measured at the vacuum pump inlet as well as the permeate side outlet. The sample solution in the cold traps were weighed, derivatised with acetone and analysed by GC.

The pervaporation system was enclosed and fitted with continuous air extraction due to the hazardous and toxic nature of hydrazine. To prevent the natural degradation of hydrazine through the oxygen in air, a nitrogen blanket was used in the holding vessel as well as during the sampling process. The measurements were taken after the system has come to a pseudo steady state (negligible removal of permeate in comparison to the feed volume) and the tank volume was continuously monitored to confirm this assumption. Detail is shown of the experimental equipment used during the pervaporation experiments are shown in Table 4.3.

Table 4.3: Pervaporation system equipment specifications

Equipment	Type	Supplier	Operating conditions
Feed vessel	2 L Stainless steel tank	Universal Fans	Filled with 2L solution
Feed pump	Magnetic drive chemical resistant pump	Prochem pumps	50 L/min
Vacuum pump	D2A double stage vacuum pump	Leybold-Heraeus	2 m^3/h, highest vacuum 1x10^{-3} Pa
Solenoid valves	Stainless coupled diaphragm system	Bürkert	Vacuum less than 100 Pa

A circular flat sheet module obtained from the Process Engineering Department at Stellenbosch University with an effective membrane diameter of 83 mm and a surface area of 54 cm^2 was used in combination with various commercially available flat sheet membranes. A photo of the membrane module unit is shown in Figure 4.6.

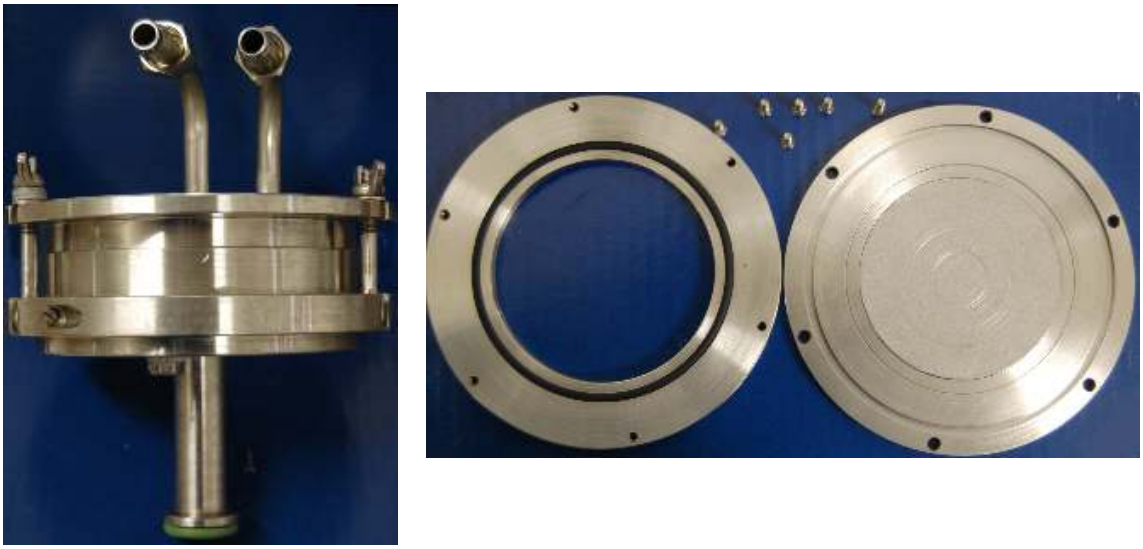

Figure 4.6: Circular flat sheet membrane module used in pervaporation experiments

Screening pervaporation experiments were used to determine the most suitable commercially available polymeric membrane for the dehydration of hydrazine monohydrate. Hydrazine monohydrate was used as feed at a temperature of 50 ±1 °C, with a vacuum pressure of less than 100 Pa. The total flux and membrane selectivity were calculated for each membrane.

A traditional experimental design was followed for the pervaporation characterisation experiments. The feed composition was varied between 36 and 70 wt. % water. The upper water concentration limit was selected to be close to the maximum allowable water content as reported by the membrane manufacturers. The lower water concentration limit was selected as the highest commercially available hydrazine monohydrate concentration. The temperature was varied between 30 and 60 ± 2 °C, with 10 °C intervals. The lower limit was selected to eliminate the need for cooling the hydrazine hydrate solution, while the upper limit was a physical constraint on the system operating at close to atmospheric pressure taking into account the system vapour pressure and the accelerated decomposition rate of hydrazine at elevated temperatures.

The permeation flux denotes the rate of permeation of a specific compound per unit surface area for a given membrane as:

$$J = \frac{Q}{A_m t} \tag{4-4}$$

where J ($kg \cdot m^{-2} \cdot h^{-1}$) is the membrane flux, Q (kg) the mass of permeate collected, A_m (m^2) the membrane effective area and t (h) the time.

The membrane selectivity (α) is calculated using the feed and permeate concentrations as shown below:

$$\alpha = \frac{X_i \,.\, Y_j}{X_j \,.\, Y_i} = \frac{Y_i \,/\, (1 - Y_i)}{X_i \,/\, (1 - X_i)} \tag{4-5}$$

where X refers to feed and Y to permeate mole fractions. The subscript i refers to the preferentially permeating species and j to the slower permeating species.

The reproducibility of the pervaporation experiment using water as simulation fluid was calculated at 11 %, while the experimental error in pervaporation experiments using hydrazine hydrate as feed was calculated as 11 % for total mass flux through membrane and 5 % for permeate water fraction, with details supplied in Appendix G.

4.6. Analytical equipment

A Scion 436-GC with a flame ionising detector (FID) was used to analyse the samples' concentrations. The gas chromatograph (GC) was fitted with a 30 m GsBP-5™ capillary column from GS-Tek. The column has an internal diameter of 0.32 mm and film thickness of 1 µm. The injector, detector and oven temperatures were set at 200 °C, 300 °C and ramping from 75 °C to 220 °C respectivly for a total analysis time of 5 minutes. Hydrogen was used as carrier gas, synthetic air as the combustion gas and nitrogen as make-up gas. The hydrogen, combustion gas and nitrogen were fed at 3 mL/min, 300 mL/min and 25 mL/min respectively. The split ratio was set at 220. The observed retention times at these conditions was 1.6 minutes for the acetone peak and for 3.1 minutes for the acetone azine peak. Calibration curves and sample preparation are supplied in Appendix F. The GC analysis was found to have an experimental error of less than 3 %, with details in Appendix G.

CHAPTER FIVE - EXPERIMENTAL RESULTS AND DISCUSSION

OVERVIEW

The main aim of this chapter is to address the first- (membrane screening) and second- (characterisation of selected membrane) objective of this study. This chapter is subdivided into three sections and starts with the results from the membrane screening, selection and contact angle characterisation (Section 5.1), followed by the performance characterisation of Pervap™ 4101 that includes sorption and pervaporation experiments varying both concentration and temperature (Section 5.2). The concluding remarks on all experimental work are in Section 5.3.

5.1. Membrane selection, screening and contact angle characterisation

In this section the first objective of this study (Objective 1: Membrane selection and screening) is addressed. From the information in the literature review performed in Chapter 2, as well as consultation with various international suppliers, eight commercial polymeric flat sheet membranes were procured. The eight membranes included: Pervap™ 4060, 4100, 4101 and 4102 from DeltaMem AG, POL-AL-M2, POL-OL-M1 from PolyAn GmbH and a PEBA and PDMS membrane from Pervtech BV. Membrane screening was done by means of visual stability tests, mechanical stability tests, membrane characterisation, followed by pervaporation performance tests.

5.1.1. Stability screening tests

Membrane stability tests were used to evaluate both the visual and mechanical stability tests of each of the eight commercial polymeric flat sheet membranes with the aim of eliminating unsuitable membranes form the evaluation process.

5.1.1.1. Visual stability tests

The stability of all eight commercial polymer membranes was tested visually according to the standard visual stability test as described in Section 4.2.1. A membrane strip (30 mm × 10 mm) was placed in an enclosed 50 mm Petri dish and submerged with a hydrazine monohydrate solution for a period of seven days at room temperature (25 °C). A sample results of the visual stability tests for each stability classification is given in Figure 5.1, with further details of the individual tests supplied in Appendix C.

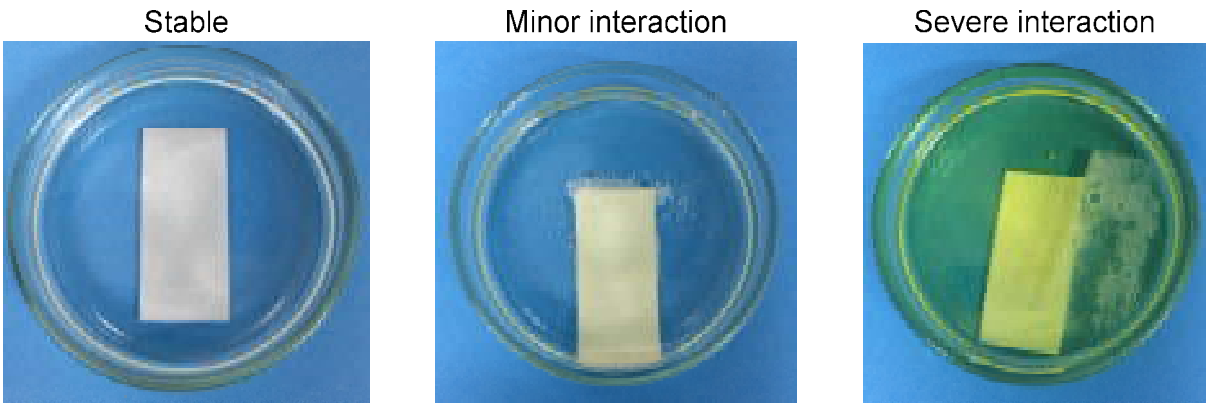

Figure 5.1: Example of visual stability results for each classifications

From Figure 5.1 it can be seen that a stable membrane (left) did not show any visual interaction with the hydrazine monohydrate solution after a period of seven days. Membranes with minor interactions (middle) were observed, especially on the support layer of the membrane where bubbles continuously formed on the edges of the membrane. Lastly membranes were classified as severe interaction (right) when the active and support layer noticeably separated from each other.

A summary of observations for the visual stability test of the eight polymeric membranes with hydrazine monohydrate at room temperature (25 °C) is given in Table 5.1.

Table 5.1: Polymer membranes visual stability result

Name	Supplier	Degree of interaction
Pervap™ 4101	DeltaMem AG	No visual interaction
Pervap™ 4102	DeltaMem AG	No visual interaction
Pervap™ 4060	DeltaMem AG	No visual interaction
Pervap™ 4100	DeltaMem AG	Slight interaction (membrane support layer)
POL-Al-M2	PolyAn GmbH	Slight interaction (membrane support layer)
POL-OL-M1	PolyAn GmbH	Slight interaction (membrane support layer)
PEBA	Pervatech BV	Severe interaction
PDMS	Pervatech BV	Severe interaction

From Table 5.1 it can be seen that all membranes supplied by DeltaMem AG (apart from Pervap™ 4100) remained stable for the duration of the tests and showed no visual signs of interaction. Pervap™ 4100 showed slight interaction of the active layer and continued to form bubbles on the edges of the membrane strip, with no visible interaction of the active layer.

It can be further seen that both membranes supplied by PolyAn GmbH showed slight interaction on the support layer and continued to form bubbles on the side of the membrane strip, but no visible interaction were observed on the active layer.

Both membranes supplied by Pervatech BV (PEBA and PDMS active layers) showed almost instantaneous interaction with the hydrazine monohydrate, with complete separation of the active layer from the support within minutes of commencing the test. The Pervatech BV PEBA and PDMS membranes were therefore not suitable nor recommended for further hydrazine hydrate dehydration tests by pervaporation.

The PEBA membrane supplied by Pervatech BV was further examined under a microscope with the resulting image shown in Figure 5.2. The active layer on the PEBA membrane showed no interaction and although it separated from the support layer it appeared to remain intact and stable.

Figure 5.2: Typical microscopic image of membrane with severe interaction

The high level of interaction between the commercial polymeric membranes and hydrazine monohydrate solution can be attributed to the high pH (>12) of the hydrazine monohydrate solution. An environment with a high basicity can be highly corrosive and only a few polymers are able to withstand such a high alkalinity (Mandal et al., 2008). Although none of the eight polymer membranes are recommended for alkaline operation above a pH of 10 (as noted in manufacturer datasheets supplied in Appendix A), the Pervap™ 4060, 4101 and 4102 showed no visible signs of interactions and therefore indicate that the suppliers might have provided a conservative stability recommendation.

All three visually stable membranes (Pervap™ 4060, 4101 and 4102) were therefore recommended for further analysis. The three membranes that showed slight visual interaction, only indicated interaction on the support layer and may still be able to yield meaningful pervaporation results and were therefore also recommended for further analysis.

5.1.1.2. Mechanical stability tests

A standard tensile strength test method as described in Section 4.2.2 was used to determine the mechanical strength of all suitable commercial polymeric membranes. The aim of the tests was to determine if a change in mechanical stability could be quantified after the polymeric membrane had been exposed to a hydrazine monohydrate solution. An accelerated aging method as described by Ravindra et al. (1997), was used by heating the hydrazine monohydrate solution to 60 ± 2 °C and exposing the membrane strip for a period of two days. The tests were performed with a 7 % experimental error with details given in Appendix G. The mechanical stability testing results are shown in Figure 5.3.

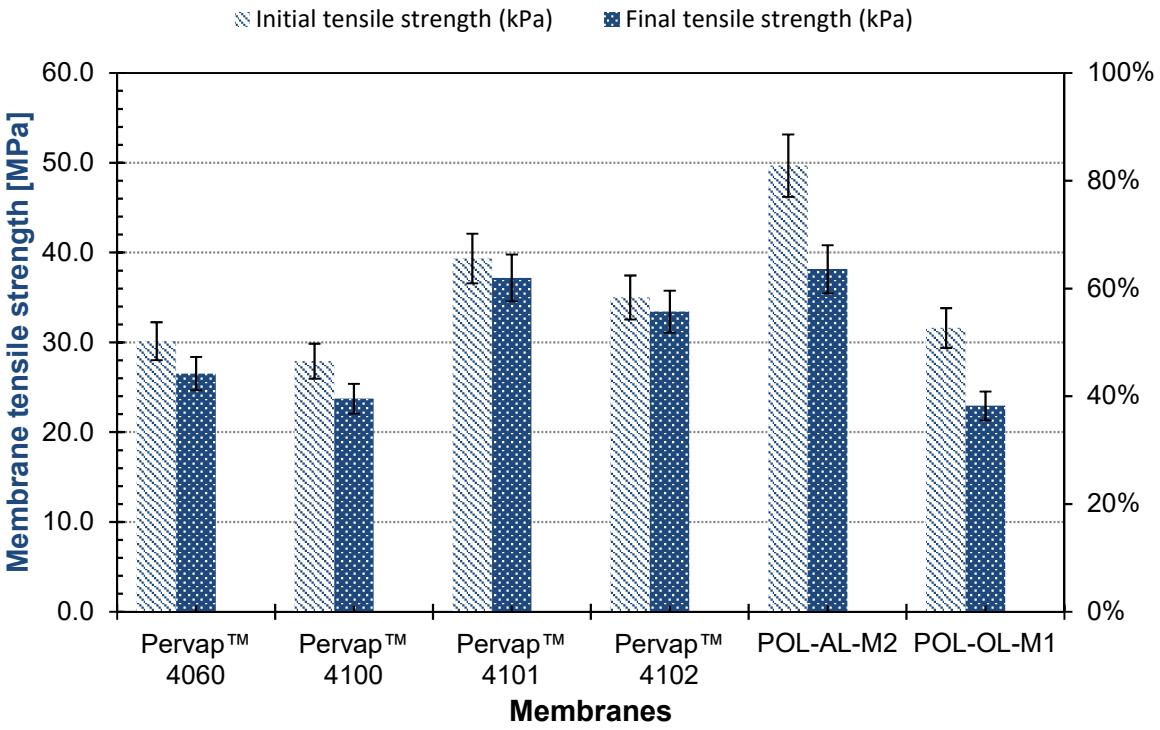

Figure 5.3: Membrane mechanical stability test results

From the test results in Figure 5.3 it can be seen that Pervap™ 4101 and 4102 membranes showed almost no signs of mechanical deterioration after exposure to hydrazine monohydrate, while the highest interaction was observed on the POL-AL-M2 and POL-OL-M1 membranes. Pervap™ 4101 and 4102 are highly crosslinked membranes, which may attribute to the higher stability noted.

Ravindra et al. (1997) and Mandal et al. (2008) performed similar mechanic strength experiment on ethyl cellulose membranes and reported that once the soaked membranes dried, they did not show any loss in original strength. Mandal et al. (2008) reported initial strengths in the order of 44 MPa, that is between the results obtained in this study for the Pervap™ range and lower than the POL-OL-M1 membrane.

5.1.2. Pervaporation screening performance

Pervaporation screening experiments as described in Section 4.5 were performed on the six polymeric membranes that showed acceptable visual and mechanical stability during the stability tests. The six polymeric membranes were screened using a pervaporation feed concentration of 36 wt. % water and inlet temperature of both 30

and 50 ±1 °C. Three performance parameters were evaluated, namely water selectivity, total flux ($kg \cdot m^{-2} \cdot h^{-1}$) and separation index (PSI). The results obtained are given in Figure 5.4. Detail calculations are supplied in Appendix F.

Satyanarayana and Bhattacharya (2004) state that for pervaporation to be considered a viable dehydration alternative and to successfully separate the hydrazine water azeotrope, the selectivity needs to be higher than the 1.4 obtained by conventional distillation. The selectivity of 1.4 assumes a 36 wt. % water feed composition and a final composition of 28 wt. % water and is represented by the dashed horizontal line in Figure 5.4.

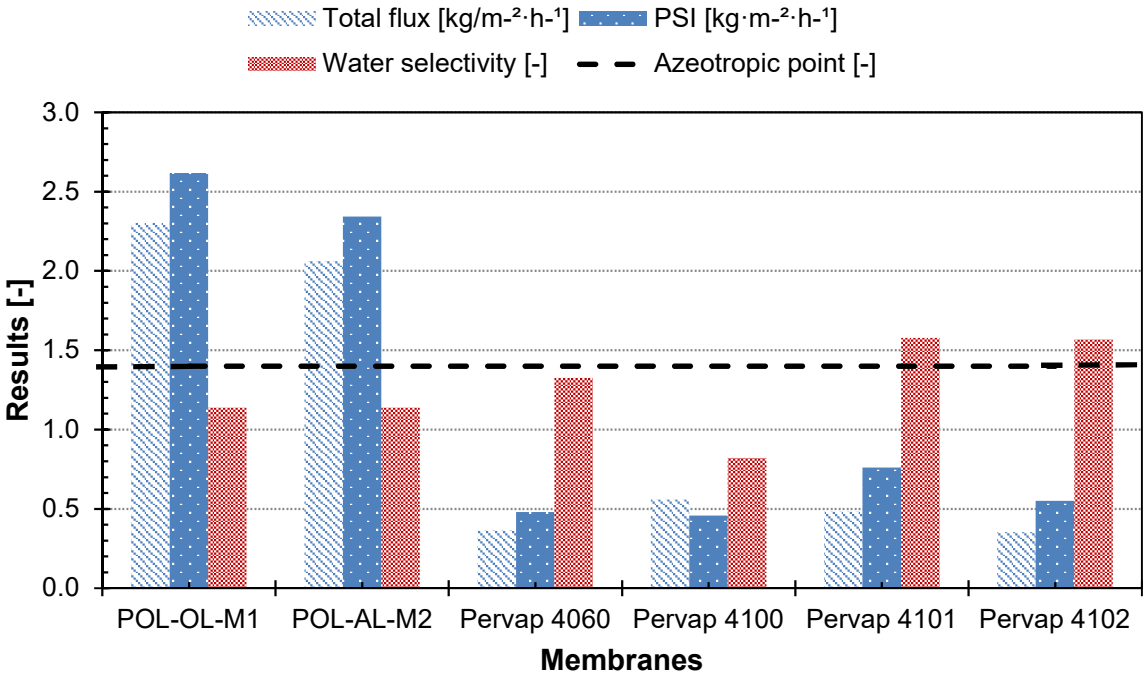

Figure 5.4: Comparison of the membrane selectivity at hydrazine monohydrate concentration for various pervaporation membranes

From Figure 5.4 it can be seen that of the six commercial polymeric membranes performance tested (POL-OL-M1, POL-AL-M2, Pervap™ 4060, 4100, 4101 and 4102), only Pervap™ 4101 and 4102 enhanced the separation with respects to the thermodynamic limit of distillation by achieving a water selectivity higher than 1.4.

Satyanarayana and Bhattacharya (2004) using similar operating conditions obtained selectivities on the Pervap two series membranes ranging between 1.09 and 3.58. The

results using commercial membranes, either from this study or from Satyanarayana and Bhattacharya (2004), still fall short of the results obtained by the laboratory synthesised membranes tested by Mandal et al. (2008) and Sunitha et al. (2011) that obtained a water selectivity of 10.6 and 20.0 respectively.

From Figure 5.4 it can further be seen that the two membranes supplied by PolyAn GmbH (POL-OL-M1 and POL-AL-M2) measured the highest total flux around 2.60 $kg \cdot m^{-2} \cdot h^{-1}$ for POL-OL-M1 and 2.3 $kg \cdot m^{-2} \cdot h^{-1}$ for POL-AL-M2, while all the Pervap™ membranes measured a flux of around 0.5 $kg \cdot m^{-2} \cdot h^{-1}$ and less.

Satyanarayana and Bhattacharya (2004) investigated the performance of Pervap™ 2200, 2201 and 2202 at similar operating conditions and reported flux values ranging from 0.306 $kg \cdot m^{-2} \cdot h^{-1}$ for Pervap™ 2200 to as low as 0.01 $kg \cdot m^{-2} \cdot h^{-1}$ for Pervap™ 2201. The Pervap™ 2200 value relates well to the 0.36, 0.56, 0.48 and 0.35 $kg \cdot m^{-2} \cdot h^{-1}$ measured for Pervap™ 4060, 4100, 4101 and 4102 in this study.

Pervap™4101 and 4102 are the only membranes that, at the testing conditions (50 °C) showed potential to dehydrate hydrazine monohydrate (36 wt. % water) past the azeotropic point. Pervap™ 4101 was selected for further characterisation as it achieved the desired selectivity with a higher flux 0.48 $kg \cdot m^{-2} \cdot h^{-1}$ and consequent higher PSI of 0.76 $kg \cdot m^{-2} \cdot h^{-1}$.

5.1.3. Membrane contact angle characterisation

Membrane properties, such as hydrophilicity and hydrophobicity, can be measured using contact angle. Contact angles of water and hydrazine monohydrate were measured on six polymer membranes. The results are given in Table 5.2, with details given in Appendix C. A standard contact angle experimental procedure was done as described in Section 4.3 with an experimental error of 11 % and details supplied in Appendix G.

Basile et al. (2015) states that membranes with a water contact angle smaller than 90 ° are considered hydrophilic (Figure 5.5), a statement shared by Satyanarayana and Bhattacharya (2004) in their analysis of the Pervap™ membranes.

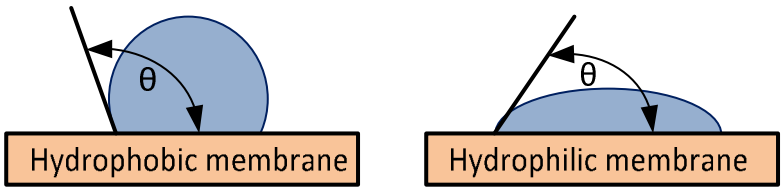

Figure 5.5: Processed droplet on contact angle tests

Table 5.2: Polymer membranes contact angle results

Membrane	Contact angle [°]		
	100 wt. % water	36 wt.% water	$\frac{\text{100 wt.\% water}}{\text{36 wt.\% water}}$
Pervap™ 4100	51.4	32.2	1.60
Pervap™ 4101	71.9	37.0	1.94
Pervap™ 4102	60.9	37.2	1.64
Pervap™ 4060	73.7	39.4	1.94
POL-AI-M2	71.4	58.0	1.23
POL-OL-M1	56.5	38.6	1.46
Pervap™ 2200 Note 1	65.2	30.7	2.12
Pervap™ 2201 Note 1	30.5	23.4	1.30
Pervap™ 2202 Note 1	51.3	30.0	1.71

Note 1: Extracted from worked performed by Satyanarayana and Bhattacharya (2004)

All six polymers tested in this study showed a water contact angle smaller than 90 ° and can therefore be concluded that all membranes tested in this study are hydrophilic. The contact angle is in all cases higher when using pure water when compared with hydrazine monohydrate. This enforces the fact that the membranes are hydrophilic, but also indicates that the membranes have an even higher affinity for water hydrazine mixtures. The same observation was noted by Satyanarayana and Bhattacharya (2004) in their analysis of the Pervap™ 2200, 2201 and 2202 membranes.

Mandal et al. (2008) and Satyanarayana and Bhattacharya (2004) both proposed a correlation between the membrane contact angle (either pure water of hydrazine hydrate) and pervaporation selectivity.

Mandal et al. (2008) found that hydrophilic membranes with a larger contact angle (more hydrophobic) yields improved pervaporation water selectivity. Using this reasoning and the data from Table 5.2 it can be seen that of the Pervap™ membranes, Pervap™ 4101 and Pervap™ 4060 have the highest water and water to hydrazine contact angle and therefore the highest theoretical water selectivity.

The membrane contact angle versus water concentration in hydrazine-water system was plotted in Figure 5.6 for the various polymeric membranes. The sample concentration varied from 36 to 100 wt. % water.

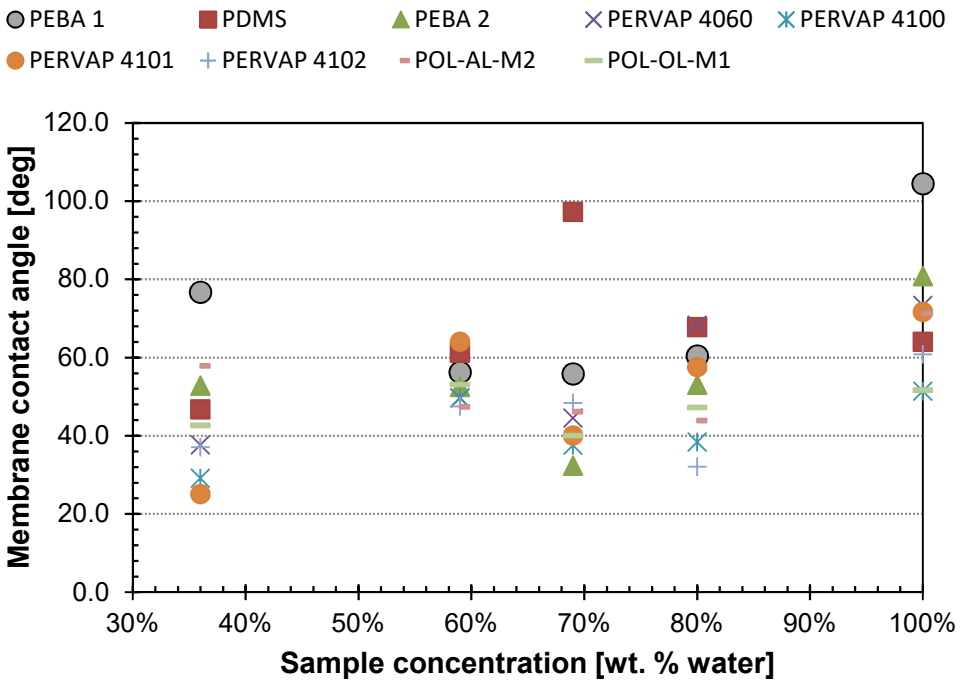

Figure 5.6: Membrane contact angle versus water concentration for various polymeric membranes

From Figure 5.6 that the membrane contact angle increases when sample water concentration increases. An increase in contact angle (although still smaller than 90 ° and therefore hydrophilic) indicates that the membrane becomes more hydrophobic and could indicate a higher water selectivity due to the decrease in hydrazine selectivity reported earlier.

5.1.4. Summary of membrane screening and characterisation

Eight commercial polymeric membranes (Pervap™ 4060, 4100, 4101, 4102, POL-AL-M2, POL-OL-M1 and PEBA and PDMS) were identified and screened for chemical compatibility, where after the relative pervaporation performance indexes was tested using hydrazine hydrate solutions.

Visual screening showed that Pervap™ 4060, 4101 and 4102 showed no visual interaction, while PEBA and PDMS supplied by Pervatech BV showed severe interaction. The mechanical stability tests confirmed these results with the exception of Pervap™ 4060 that showed slightly reduced mechanical properties after exposure to hydrazine hydrate.

From the pervaporation screening tests is was evident that only Pervap™ 4101 and Pervap™ 4102 with water selectivities of 1.6 showed potential to dehydrate hydrazine monohydrate past the required azeotropic point, with Pervap™ 4101 achieving it with a higher total flux of 0.48 $kg \cdot m^{-2} \cdot h^{-1}$ and PSI of 0.76 $kg \cdot m^{-2} \cdot h^{-1}$. Pervap™ 4101 was therefore selected for further characterisation tests.

Contact angle measurements indicates that Pervap™ 4101 and 4060 might have the best water selectivity. The membrane contact angle of all membranes increases as the water content increase, indicating a higher water selectivity due to the decrease in hydrazine selectivity reported earlier.

5.2. Characterisation of Pervap™ 4101 membrane

The performance characterisation of the selected membrane (Objective 2) is addressed by using Pervap™ 4101 membrane.

5.2.1. Sorption performance testing

The sorption characteristics for Pervap™ 4101 membrane with water-hydrazine mixtures was determined by using a standard sorption experimental setup as described in Section 4.4. Two performance parameters were addressed: firstly, the degree of swelling and secondly, the sorption water selectivity of the membrane. The dependence of the two performance parameters on both the feed water concentration

in the binary mixture and the feed temperature were evaluated. The calculated experimental error of the degree of swelling was 8 % and sorption selectivity 15 % with details supplied in Appendix G.

5.2.1.1. Influence of feed concentration

The influence of the feed water concentration on the sorption performance characteristics of the water-hydrazine binary mixture using the Pervap™ 4101 membrane was investigated by varying the mass fraction water in the feed at a constant temperature of 50 °C. The degree of swelling as a function of feed water concentration at a constant temperature of 50 °C is shown in Figure 5.7. Calculation details for the degree of swelling are given in Appendix E.

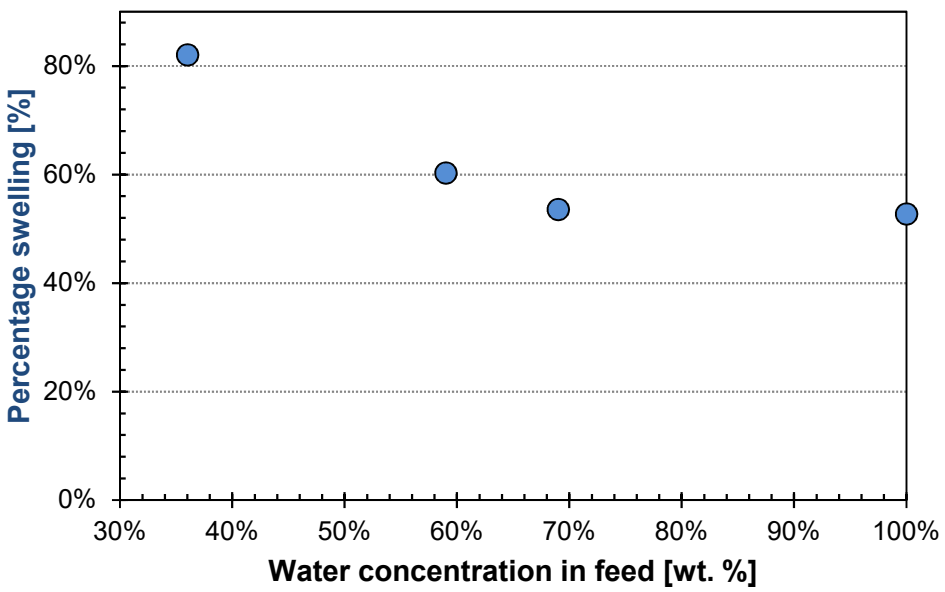

Figure 5.7: Degree of swelling for various concentrations at 50 °C feed temperature

From Figure 5.7 it can be seen that Pervap™ 4101 in hydrazine hydrate has a percentage swelling as high as 82 % with feed concentration of 36 wt. % water and steadily decreasing to 53 % with 100 wt. % water feed. Mulder (2012) recommend that membranes used in pervaporation should range between 5 and 25 % to ensure the membrane operates in the optimal selectivity range. The higher the membrane swelling the lower the overall water selectivity and the lower the membrane swelling the lower the flux (Basile et al., 2015).

The relationship between the equilibrium water mass fraction in the bulk feed with that in the membrane in terms of membrane selectivity, as well as the total liquid uptake in the membrane (g/g polymer) are shown in Figure 5.8 at a constant feed temperature of 50 °C.

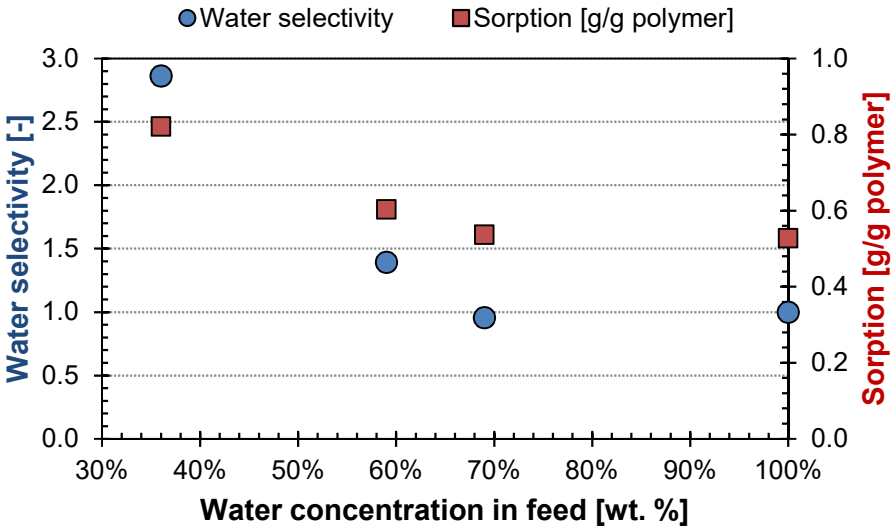

Figure 5.8: Polymer-liquid mixture equilibrium curve at 50°C

It can be seen from Figure 5.8 that the sorption is lowest with pure water at 0.53 g/g polymer and then increases to 0.82 as the feed water concentration decreases. The same observation was noted by both Mandal et al. (2008) and Satyanarayana and Bhattacharya (2004). Mandal et al. (2008) performed equilibrium sorption experiments using hydrazine monohydrate also at 50 °C and reported 0.31 g water / g polymer and 0.50 g hydrazine hydrate / g water for acrylonitrile butadiene styrene and as high as 4.12 and 5.23 for ethyl cellulose membranes. The sorption composition was not measured in either of the above-mentioned studies. The authors concluded that the higher sorption rates measured with hydrazine hydrate is an indication that the membranes in a hydrazine-water solution is hydrazine selective during the sorption step.

From Figure 5.8 it can be further seen, that the sorption water selectivity decreases from 2.9 to 1.0, with an increase in feed water concentration. The sorption step in hydrazine-water mixtures are therefore clearly water selective. A possible explanation

for the higher sorption measured with hydrazine hydrate when compared to water is that the presence of hydrazine enhances the water sorption rate.

5.2.1.2. Influence of feed temperature

The influence of the sorption feed temperature on the sorption performance characteristics of the water-hydrazine binary mixture using the Pervap™ 4101 membrane was investigated by varying the temperature between 30 °C and 50 °C with a constant feed of 36 wt. % water with the results shown in Figure 5.9.

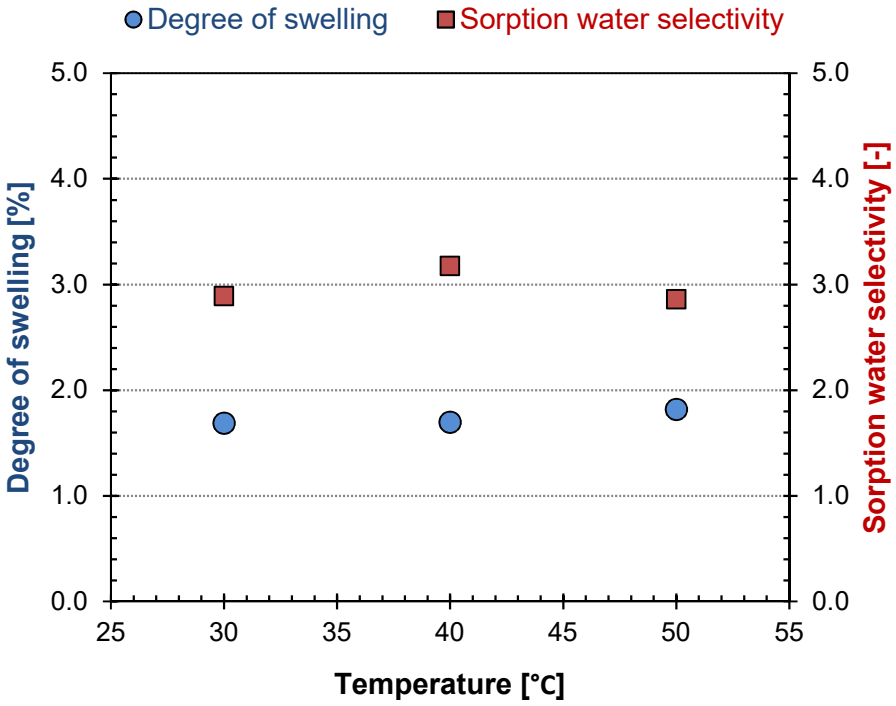

Figure 5.9: Degree of swelling and sorption water selectivity for 36 wt. % water at various temperatures

It can be seen from Figure 5.9 that the degree of swelling increases slightly from 1.7 at a feed water temperature of 30 °C to 1.8 at a feed water temperature of 50 °C. The sorption water selectivity varies between 3.1 at both 30 °C and 50 °C, with a maximum of 2.9 at 40 °C. With such a small variation in both degree of swelling and sorption water selectivity, both sorption performance parameters (for all practical purposes, especially considering the experimental error of 8 % for the membrane swelling and 24 % for membrane composition) can be seen as a temperature independent. The effect of temperature on sorption has not been reported for hydrazine water systems,

but Van der Gryp (2003) also reported that sorption of methanol and TAME was independent of temperature.

From the sorption experimental data, it can be concluded that Pervap™ 4101 is water selective and the water selectivity decreases as the water content increases. Sorption selectivity can be used to describe selective transport of water over hydrazine through the Pervap™ 4101 membrane.

5.2.2. Pervaporation performance

The pervaporation characteristics for Pervap™ 4101 membrane with hydrazine hydrate feed will be discussed in this section according to the experimental procedure described in Section 4.5. Two performance parameters were used namely membrane flux (both total flux and partial component fluxes) and the pervaporation water selectivity of the membrane. The dependence of the two performance parameters on both the feed water concentration in the binary mixture and the feed temperature was evaluated. The experimental error for measuring the membrane flux was calculated at 14 % and at 5% for measuring the permeate composition. Those details supplied in Appendix G.

5.2.2.1. Influence of feed composition

The effect of feed composition on the performance of Pervap™ 4101 membrane was investigated by varying the feed concentration from 36 to 80 wt. % water, while keeping the feed temperature constant at 50 ±1 °C and absolue vacuum less than 100 Pa.

The total membrane flux for the various feed water concentrations are given in Figure 5.10, while the membrane water selectivities over the same feed range are given in Figure 5.11 with details of the calculations supplied in Appendix D.

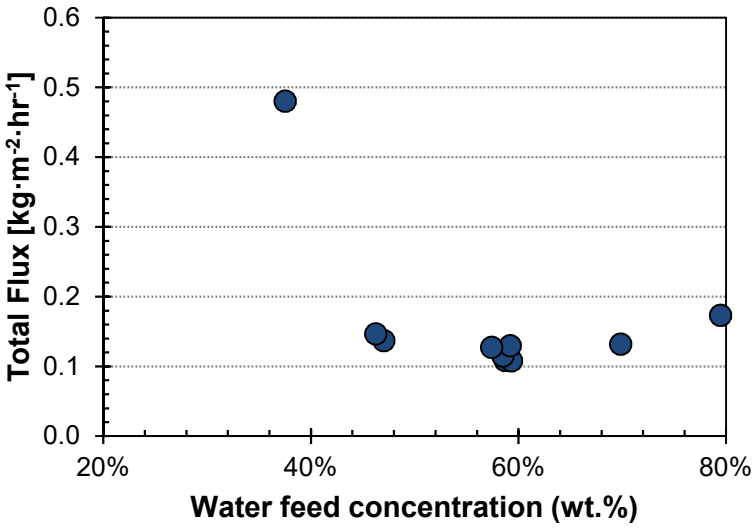

Figure 5.10: Influence of feed composition on the total membrane flux at a constant temperature of 50 °C for Pervap™ 4101

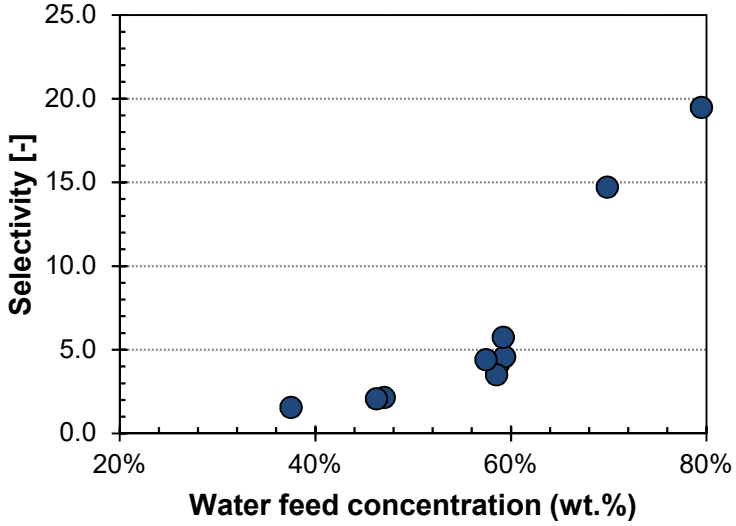

Figure 5.11: Influence of feed composition on the membrane selectivity at a constant temperature of 50 °C for Pervap™ 4101

From Figure 5.10 it can be seen that the total flux sharply decreases from 0.48 to 0.15 $kg \cdot m^{-2} \cdot h^{-1}$ when the feed water concentration increases higher than the azeotropic point (36 wt. % water) and then remains relatively concentration independent with a slight increase up to around 80 wt.% feed water concentration. The membrane water selectivity (Figure 5.11) increases from 1.56 at the azeotropic composition (36 wt. % water) to a maximum of 20 at 80 wt. % water.

Ravindra et al. (1999c) investigated the effect of hydrazine concentration on a laboratory synthesised EC polymeric membranes and obtained fluxes ranging from 0.02 $kg \cdot m^{-2} \cdot h^{-1}$ at 36 wt. % water to 0.17 $kg \cdot m^{-2} \cdot h^{-1}$ at 80 wt.% water. It is noticeable that the flux approximately doubled when the hydrazine concentration was reduced from 36 to 60 wt. % water.

The selectivity in the Ravindra et al. (1999c) experiments ranged from around 2.0 for concentrations at 36 wt.% water and higher to around 250 for water concentrations of 80 wt.%. In both the selectivity and flux results, only one local minima was obtained at 36 wt.% water with both selectivity and flux increasing towards the higher water concentration (range 36 to 80 wt. %) when compared to the lower water range (15 to 36 wt. %).

Sunitha et al. (2011) investigated the effect of hydrazine concentration on a laboratory synthesised PEBAX®-2533 on PPSU membrane in the water concentration range of 36 vol. % to 58 vol. % water. Similar to the work done by Ravindra et al. (1999c) they observed an increase in flux with a decrease in hydrazine concentration with values ranging from 0.052 $kg \cdot m^{-2} \cdot h^{-1}$.

In contrast to the results obtained by Ravindra et al. (1999c), the selectivity found by Sunitha et al. (2011) increased with an increase in feed hydrazine concentration. Mohanty and Purkait (2011) state that in the case of dehydration through a hydrophilic membrane, flux increases with the feed water concentration. Furthermore the selectivity generally increases with a decrease in the concentration of the preferentially permeating component (in this case water) due to lower swelling. The measured partial fluxes for both water and hydrazine are shown in Figure 5.12.

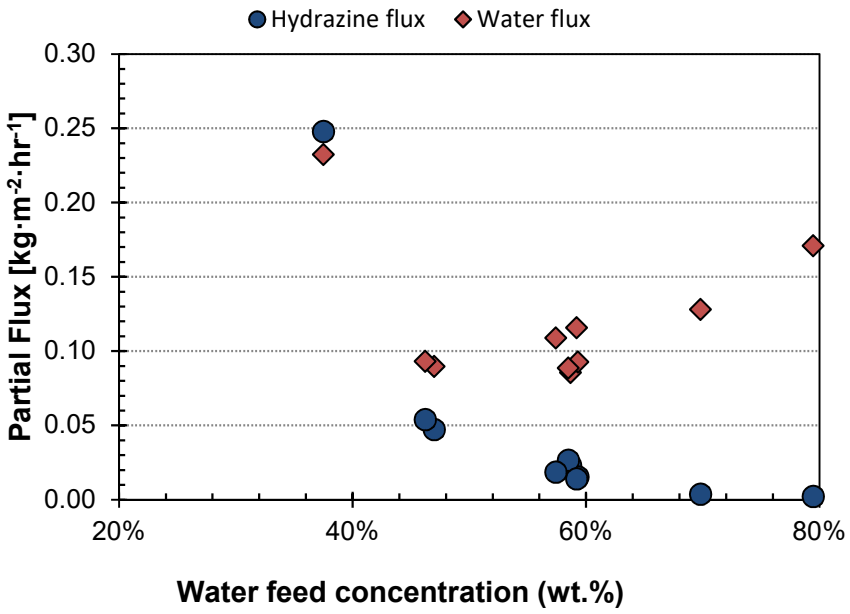

Figure 5.12: Influence of feed composition on membrane partial fluxes at a constant temperature of 50 °C Pervap™ 4101

From Figure 5.12 it can be seen that the Pervap™4101 membrane is more selective towards water than hydrazine throughout the concentration range, except at the azeotropic point (36 wt. % water) where the hydrazine partial flux is slightly higher than the water flux. The hydrazine partial flux decreases from around 0.25 $kg \cdot m^{-2} \cdot h^{-1}$ to almost zero as the water feed concentration increases. The hydrazine partial flux also decreases sharply as the feed water content increases away from the azeotropic point to around 0.9 $kg \cdot m^{-2} \cdot h^{-1}$ and then increases again 0.17 $kg \cdot m^{-2} \cdot h^{-1}$.

This phenomena in Figure 5.12 where the water partial flux increase, while the hydrazine partial flux decrease as the feed water concentration increase can be explained by polarity of the solution. At higher water concentrations the polar interactions with the hydrophilic membrane selectively removes water as opposed to lower water concentrations and where the polar interactions between water and hydrazine increases and thereby increasing the difficulty of permeation causing a reduction in flux.

5.2.2.2. Influence of feed temperature

The effect of feed temperature on pervaporation performance of the Pervap™ 4101 membrane was investigated by varying the feed temperature from 30 to 60 ± 1 °C at a constant feed composition and absolute vacuum pressure of less than 100 Pa. This procedure was done for three different hydrazine hydrate feed compositions.

The total membrane flux for the various temperatures are given in Figure 5.13, while the membrane water selectivity over the same temperature range are given in Figure 5.14 with details of the calculations supplied in Appendix D.

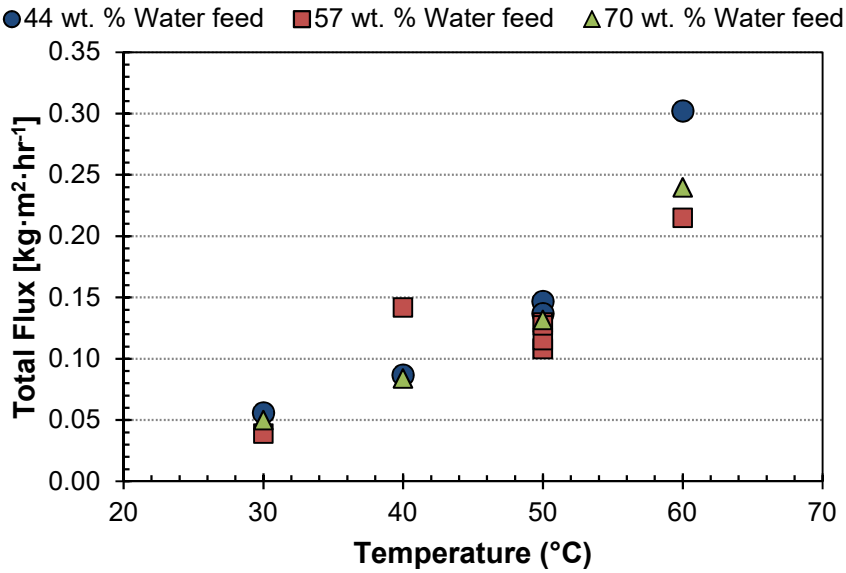

Figure 5.13: Influence of operating temperature on total membrane flux for Pervap™ 4100 at various feed concentrations

From Figure 5.13 it is evident that the total flux through the membrane increases in an exponential fashion with an increase in feed temperature from 30 to 60 °C for all three feed compositions. The direct proportionality of pervaporation flux to temperatures as described above can be attributed to an increase in activity of the feed molecules and therefore the diffusion rate through the membrane (Mohanty and Purkait, 2011).

Various other researchers using a variety of binary feed components observed the same temperature dependence as found in this study (Cao and Henson, 2002, Mulder, 2012, Sunitha et al., 2011). The effect of temperature on pervaporation using hydrazine hydrate as feed has not been reported in the open literature and Hoda et al.

(2005) even neglected the effect of temperature on diffusion in their attempt to model a spiral wound pervaporation model.

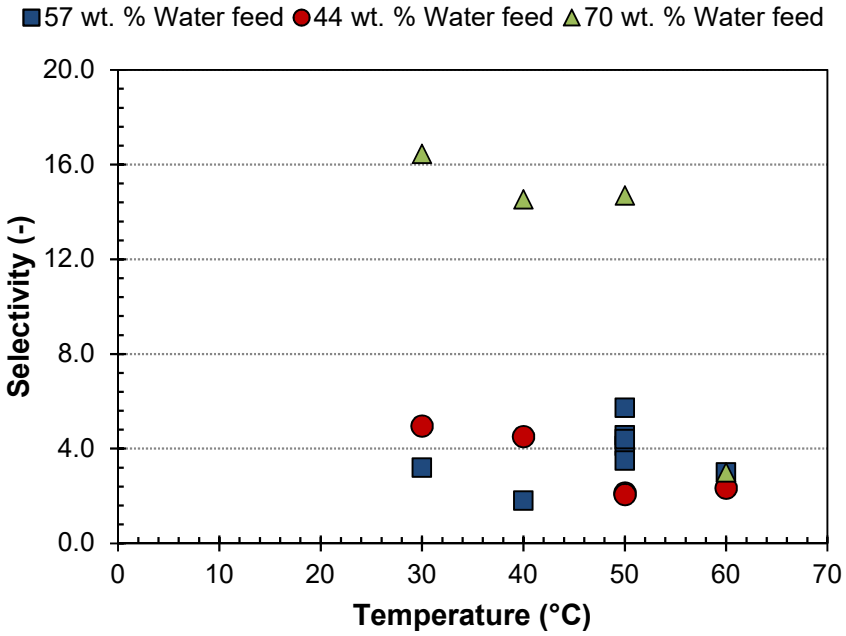

Figure 5.14: Influence of operating temperature on the membrane selectivity for Pervap™ 4101 at various feed concentrations

From Figure 5.14 it can be seen that for all three feed water concentrations tested the water selectivity decreased with an increase in temperature. An increase in flux due to temperature as shown in Figure 5.13 will result in a decrease in membrane selectivity, as selectivity is inversely proportional to flux (Mohanty and Purkait, 2011). A decrease in selectivity with increase in temperature was observed by various researcher for a variety of systems for example (Luo et al. (1997), Burshe et al. (1999), Van der Gryp (2003)).

The temperature dependence of the permeation flux can be empirically represented by the semi-logarithmic plot as given in Figure 5.15. The water flux at four temperatures is plotted in logarithmic form as a function of reciprocal absolute temperature for three different feed water concentrations.

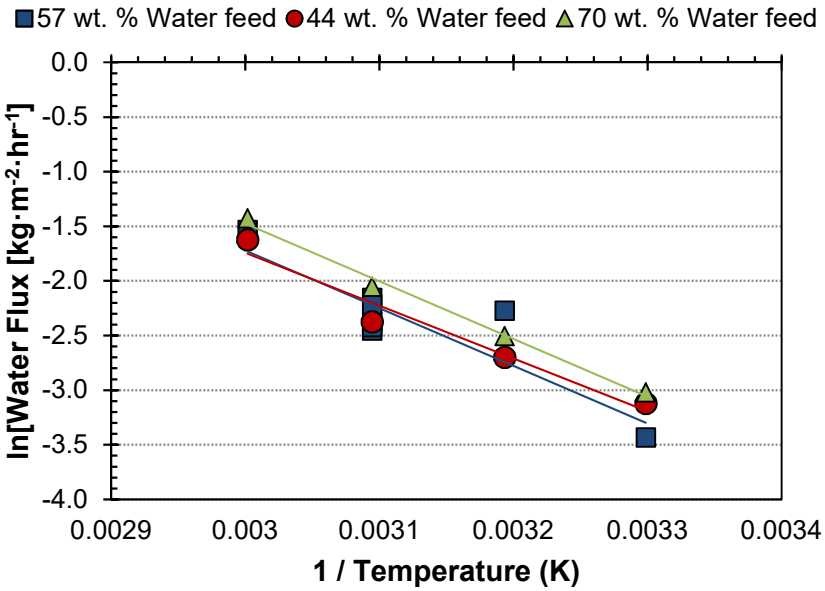

Figure 5.15: Arrhenius plot of hydrazine flux versus reciprocal temperature for various feed mass concentration

From Figure 5.15 it can be seen that the water flux increases with an increase in feed water concentration and increases with increase in temperature as expected from the Arrhenius relationship in Equation (2-6).

$$J = J_0 \exp\left(\frac{E}{RT}\right) \tag{5-1}$$

It can further be seen that all three concentrations had a very similar negative slope from which the activation energy can be calculated, making use of the method as described by Feng and Huang (1994). The activation energy for water was calculated between 40.2 to 43.9 kJ·mol^{-1} for the three feed concentrations. No literature data is available on hydrazine-water systems and literature values for other solvents and membranes varied from as low as 6.2 kJ·mol^{-1} reported by Park et al. (1994) and as high as 52.5 kJ·mol^{-1} as reported by Van der Gryp (2003).

5.2.3. Separation capabilities of pervaporation

Basile et al. (2015) stated that an additional way to evaluate the effect of the membrane on the separation process is to compare pervaporation with distillation using a vapour liquid McCabe-Thiele diagram. Such a separation diagram is shown in Figure 5.16 for the separation of water from a hydrazine hydrate mixture using Pervap™ 4101 at 50 °C and literature data from Ravindra et al. (1999c) and Sunitha et al. (2011). The VLE data was calculated by ChemCad® using a NRTL activity coefficient model at 101 kPa.

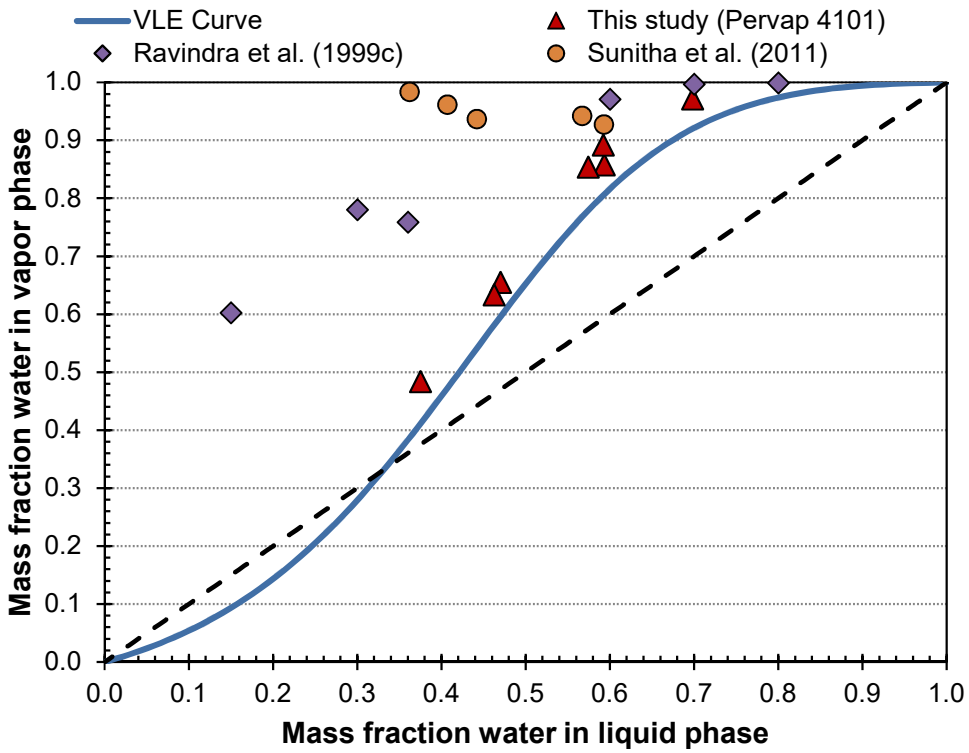

Figure 5.16: Separation diagram for hydrazine hydrate at 50 °C using Pervap™ 4101

Although the VLE data in Figure 5.16 does not directly compare the performance between distillation and pervaporation, experimental results that has a liquid-vapour data point far away from the VLE are enhancing the water-hydrazine separation with respects to the thermodynamic limit of distillation.

It is important to note that all data points from this study and literature data from Ravindra et al. (1999c) and Sunitha et al. (2011) are located above the VLE line. Water is therefore preferentially removed by pervaporation in all three cases.

The experimental results from this study follows the general trend of the VLE line, but is distinctly above for all points. At high water feed concentrations the performance of Ravindra et al. (1999c) and Sunitha et al. (2011) are very similar, but at lower feed water concentrations the data points from Sunitha et al. (2011) moves further away from the VLE curve.

It can therefore be concluded that hydrazine hydrate can theoretically be dehydrated past the azeotropic points using membranes like: Pervap™ 4101 from this study, ethyl cellulose like Ravindra et al. (1999c) and PEBAX®-2533 like Sunitha et al. (2011).

The variance between the theoretical VLE curve and the pervaporation curve found in this study is so small, especially compared to literature data like Ravindra et al. (1999c) and Sunitha et al. (2011), that pervaporation using commercial membranes is not as promising as using the ethyl cellulose membranes as used by Ravindra et al. (1999c) or PEBAX®-2533 membranes as used by Sunitha et al. (2011).

5.3. Concluding remarks

After a detailed literature review and consultation with various international manufactures, eight commercially available polymer membranes (Pervap™ 4060, 4100, 4101, 4102, POL-AL-M2, POL-OL-M1 and PEBA and PDMS) were procured. Visual and mechanical stability tests indicated that PEBA and PDMS membranes from Pervatech BV showed severe interaction and are therefore not suitable for operation in hydrazine-water systems. Pervap™ 4060, 4101 and 4102 showed the highest visual and mechanical stability, but Pervap™ 4100, POL-AL-M2 and POL-OL-M1 were also included in the pervaporation screening as it only showed minor interaction in the active layer.

Based on the contact angle characterisation results, all tested membranes had a water contact angle smaller than 90 ° and were therefore characterised as hydrophilic membranes. It was also observed that the hydrazine hydrate contact angles were smaller that the water contact angles, thereby indicating that the hydrazine is strongly held by the membranes when compared to water. FTIR studies with EC membranes performed by Ravindra et al. (1997) also led to the same conclusions.

membrane has a higher water selectivity towards hydrazine when compared to water.

The membrane contact angle generally increased with an increase in water concentration in the hydrazine-water solution.

During the pervaporation screening tests it was found that all four Pervap™ membranes (4060, 4100, 4101 and 4102) as well as the POL-OL-M1 and POL-AL-M2 were water selective at concentration below the azeotropic point. Only Pervap™ 4101 and 4102 had a water selectivity high enough to dehydrate hydrazine monohydrate past the required azeotrope, with Pervap™ 4101 achieving it with the highest total flux.

Sorption studies on Pervap™ 4101 membranes at 50 °C and feed concentrations between 36 and 100 wt. % water revealed that membrane swelling is as high as 80 %. This high membrane swelling could be part of the reason the Pervap™ 4101 has lower water selectivity when compared to the laboratory synthesised membranes used by Ravindra et al. (1999c) and Sunitha et al. (2011). It was further observed that as the feed water concentration increases the membrane swelling, water sorption selectivity and total sorption decreases. The sorption selectivity tests differs from the hypothesis from Mandal et al. (2008) and Satyanarayana and Bhattacharya (2004) and confirms that the sorption selectivity of hydrophilic membranes are more water than hydrazine selective and that the presence of hydrazine potentially only enhances the water sorption.

Both sorption and pervaporation studies shows that the Pervap™ 4101 membrane is water selective. Using the solution diffusion model as proposed by Baker (2000) the diffusion selectivity can be calculated. The calculated diffusion selectivity is much larger than the sorption selectivity and the pervaporation process is therefore diffusion dominated.

Based on the performance characterisation of Pervap™ 4101 membrane it can be concluded that temperature has no effect on sorption selectivity or swelling, while it increases the transmembrane flux in pervaporation leading to a reduced selectivity.

The feed concentration had a minor effect on the membrane swelling and led to an increase in water selectivity with an increase in water wt. %. At the azeotropic concentration (36 wt. % water), pervaporation on Pervap™ 4101 has the highest transmembrane flux which then rapidly decreases as the water content increases. It then becomes concentration independent.

Plotting the sorption and pervaporation results on a McCabe-Thiele VLE diagram showed that Pervap™ 4101 has the potential to separate a hydrazine-water mixture past the azeotropic point, where after ordinary distillation can dehydrate the mixture to the required purity. Commercial Pervap™ 4101 does, however, not compare to literature results obtained by Ravindra et al. (1999c) and Sunitha et al. (2011) on laboratory synthesised membranes.

CHAPTER SIX - MODELLING

Overview

The main aim of this chapter is to develop a sorption and diffusion model that is able to accurately predict experimental pervaporation values based on input feed conditions. The model is based on the solution-diffusion theory that separately describes the sorption step (based on the Flory Huggins theory) and diffusion step (based on Fick's first law of diffusion).

This chapter is subdivided into five sections that start with a general introduction to the chapter (Section 6.1). Section 6.2 describes the statistical method that was used to evaluate the deviation from theoretically predicted results found in the experiments. All work pertaining to the sorption and pervaporation models is discussed in Section 6.3 and Section 6.4 respectively. The chapter is concluded in Section 6.5 with a brief overview of major results.

6.1. Introduction

The modelling of selective permeation of water and hydrazine through flat sheet polymeric membranes was performed in this chapter. The modelling is based on the well-known solution-diffusion model, where the sorption step is described by making use of the Flory-Huggins equations, and the diffusion transport step described by making use of Fick's first law of diffusion as described in Section 3.2. The modelling will be based on experimental results obtained from this study using a Pervap™ 4101 membrane. The pervaporation modelling results will be compared to experimental data obtained from two related studies by Ravindra et al. (1999c) and Sunitha et al. (2011) using ethyl cellulose and PEBAX®-2533 membranes respectively. All detail calculations pertaining to this chapter are supplied in Appendix H.

6.2. Statistical evaluation of modelling parameters

The accuracy of the sorption model in Section 6.3 and pervaporation model in Section 6.4 will be evaluated by making use of three statistical performance parameters, namely: coefficient of determination (R^2), mean absolute percentage error (MAPE) and root mean square error (RMSE).

The coefficient of determination (R^2) can be used to statistically evaluate how accurately the theoretical regression line approximates the experimental results and ranges between 0 and 1, with a value higher than 0.8 generally accepted to indicate a good experimental fit (Taylor, 1990, Nagelkerke, 1991).

The mean absolute percentage error (MAPE) was calculated using Equation (6-1), where a smaller value indicate a better experimental fit. The MAPE method has known drawbacks that include being biased to underestimation of experimental results and reporting lower values compared to overestimation of experimental results (Hoyt, 1979, Armstrong and Overton, 1977).

$$MAPE = \frac{100}{N}\sum_{i=1}^{N}\frac{\left|\left(J_{i,exp} - J_{i,theory}\right)\right|}{J_{i,exp}} \qquad (6\text{-}1)$$

The root mean square error (RMSE) was calculated using Equation (6-2), where a smaller value as per MAPE method also indicated a better experimental fit (Willmott, 1982).

$$RMSE = \sqrt{\frac{1}{N}\sum_{i=1}^{N}\left(J_{i,exp} - J_{i,theory}\right)^2} \tag{6-2}$$

6.3. Sorption modelling

6.3.1. Solution methodology

The sorption modelling step is based on the Flory-Huggins theory that makes use of a combination of concentration dependent and concentration independent interaction parameters. The theoretical solution is reliant on solving Equation (3-7) in terms of partial volume fractions within the membrane.

$$\begin{aligned} ln\left(\frac{\Phi_i}{\Phi_j}\right) - ln\left(\frac{v_i}{v_j}\right) &= (r-1)ln\left(\frac{\Phi_i}{v_j}\right) - g_{ij}(u_j)(\Phi_j - \Phi_i) - g_{ij}(v_j)(v_i - v_j) \\ -\Phi_p(g_{ip} - rg_{jp}) + u_i\Phi_p\frac{\partial g_{ip}}{\partial u_j} - v_i v_j\frac{\partial y g_{ij}}{\partial v_j} &+ \Phi_p u_i\frac{\partial g_{ip}}{\partial u_j} - \frac{v_i}{v_j}u_j\Phi_p\frac{\partial g_{jp}}{\partial u_i} \end{aligned} \tag{3-7}$$

Where

Φ_i / Φ_j	are the volume fractions of water and hydrazine in a ternary system, when a polymer is exposed to a binary liquid mixture.
v_i / v_j	are the volume fractions of either water or hydrazine in the binary feed.
V_i / V_j	are the molar volumes of water or hydrazine respectively.
r	is the ratio of the hydrazine to water molar volumes.
g_{ij}	is the concentration dependent interaction parameter between water and hydrazine.
u_i / u_j	are the volume fractions of water and hydrazine in the polymer on a polymer free basis.
g_{ip} / g_{jp}	are the concentration dependent interaction parameters between water or hydrazine and the polymer.
Φ_p	is the polymer fraction in the ternary system.

Before Equation (3-7) can be solved in terms of volume fractions of water (Φ_i) and hydrazine (Φ_j), the volume fraction of the swollen polymer (Φ_p) needs to be calculated as well as the various interaction parameters.

The volume fraction of the swollen polymer (Φ_p) can be approximated by using Equation (6-3) as proposed by Mandal et al. (2008).

$$\Phi_p = \left[1 + \frac{\rho_m}{\rho_S}\left(\frac{M_s}{M_d}\right) - \left(\frac{\rho_P}{\rho_S}\right)\right]^{-1} \tag{6-3}$$

where ρ_m and ρ_S are the densities (g·cm^{-3}) of the polymer and solvent respectively; M_d and M_s are the membrane masses before and after swelling.

The calculation of the concentration dependent interaction parameters between water and hydrazine (g_{ij}) is done in Section 6.3.2 and the concentration independent interaction parameter between the water or hydrazine and polymer ,g_{ip} and g_{jp}, is done in Section 6.3.3. The estimation of the solution model parameters and statistical evaluation of the results are done in Section 6.3.4.

6.3.2. Evaluation of the concentration dependent binary interaction parameter between two solvents (g_{ij})

The binary interaction parameters between the two solvents (g_{ij}) as given in Equation (3-11) were calculated by combining the excess Gibbs free energy as proposed by Prausnitz et al. (1998) with the Flory-Huggins theory proposed by Flory (1953) and as used by authors Cao and Henson (2002) and Hoda et al. (2005).

$$g_{ij} = \frac{1}{x_i v_j}\left[x_i ln\frac{x_i}{v_i} + x_j ln\frac{x_j}{v_j} + \frac{\Delta G^E}{RT}\right] \tag{3-11}$$

where x_i and x_j are the molar feed fractions of water and hydrazine respectively and ΔG^E is the Gibbs free energy of the water-hydrazine solution. In order to solve the water-hydrazine interaction parameter, the Gibbs free energy was calculated by using activity coefficient data obtained from ChemCad® 7.1.1 using a NTRL thermodynamic

model and solving by use of the Redlich-Kister two constant Margules methods. The Margules constants (A_{ij} and A_{ji}) are calculated by making use of a minimisation in Matlab®, using a non-linear unconstrained optimization routine.

The binary interaction parameters between water and hydrazine (g_{ij}) were found to be highly concentration dependent as suggested by Mulder and Smolders (1984) and only slightly temperature dependent with the results shown in the Figure 6.1 surface plot.

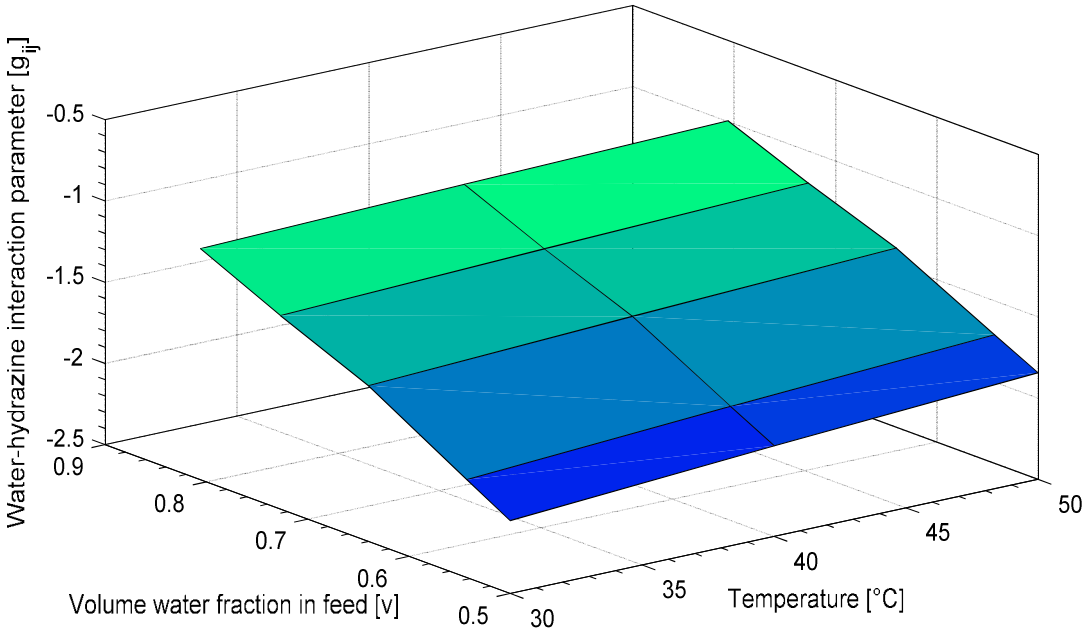

Figure 6.1: Surface plot showing the fourth-order polynomial relationship between χ_{ij} and v_i at temperatures between 30 °C and 50 °C

The fourth order polynomial coefficients for the concentration dependent interaction parameters (g_{ij}) was calculated using the polynomial curve fitting module Polyfit in Matlab® with the results for temperatures of 50 °C given in Equation (6-4).

$$g_{ij} = 157.5{v_i}^4 - 403.4{v_i}^3 + 381.3{v_i}^2 + 154.78v_i + 20.8 \quad (6\text{-}4)$$

Using hydrazine monohydrate (36 wt. % water), the water-hydrazine interaction parameter (g_{ij}) was calculated with the result shown in Table 6.1, along with literature data by Hoda et al. (2005) and Mandal et al. (2008).

Table 6.1: Concentration dependent interaction parameters (g_{ij}) results

Interaction parameter (g_{ij})	Concentration [wt. % water]	Temperature [°C]	Reference
-2.05	36	30	This study
-1.84	36	50	This study
-2.33	36	unspecified	(Hoda et al., 2005)
-2.58	36	unspecified	(Mandal et al., 2008)

The interaction parameter (g_{ij}) in this study shown in Table 6.1 relates well to the literature sources. The highly negative value of the water-hydrazine interaction coefficient suggests a strong affinity between water and hydrazine.

6.3.3. Evaluation of the binary interaction parameter between individual solvents and polymer (χ_{ip}) and (χ_{jp})

The binary interaction parameters can be considered either concentration independent (χ_{ip} and χ_{jp}), when small amount of non-solvent sorbes into the polymer, or concentration dependent (g_{ip} and g_{jp}) in the majority of other cases (Krigbaum and Carpenter, 1954). Ravindra et al. (1999c) and Mandal et al. (2008) both used concentration independent interaction parameters in water-hydrazine systems due to the simplicity and accuracy and this study will therefore start off with a concentration independent interaction parameter approach.

The polymer-solvent concentration independent interaction parameter (χ_{ip}) as given in Equation (6-5) was calculated by making use of the Flory-Huggins theory.

$$\chi_{ip} = \frac{V_i(\delta_p - \delta_i)^2}{RT} \qquad \chi_{jp} = \frac{V_j(\delta_p - \delta_j)^2}{RT} \tag{6-5}$$

where δ_p and $\delta_{i/j}$ are the solubility parameters of either the polymer and water/hydrazine respectively; $V_{i/j}$ is the molar volume of water / hydrazine. The Hildebrand solubility parameters were obtained from Barton (1991). The results

obtained for the concentration independent interaction parameters are given in Table 6.2, along with various literature references.

Table 6.2: Concentration independent solvent polymer interaction parameters

Membrane	Temperature [°C]	χ_{ip}	χ_{jp}	Reference
Pervap™ 4101	50	5.47	3.68	This study
Ethyl cellulose	50	2.50	1.80	Ravindra et al. (1999c)
Ethyl cellulose	50	5.41	3.59	Mandal et al. (2008)
BM20	50	5.41	2.60	Mandal et al. (2008)
BM30	50	5.41	3.60	Mandal et al. (2008)
BM40	50	5.41	3.60	Mandal et al. (2008)
BM70	50	5.42	3.61	Mandal et al. (2008)
BM80	50	5.43	3.61	Mandal et al. (2008)
ABS	50	5.43	3.62	Mandal et al. (2008)

The calculated concentration independent solvent polymer interaction in Table 6.2 compares well to literature values from Mandal et al. (2008) and Ravindra et al. (1999c) that investigated hydrazine monohydrate interaction with various ethyl cellulose and acrylonitrile butadiene styrene laboratory synthesised membranes.

The solvent-polymer interaction parameters can be described from standard thermodynamic principles, therefore as the value of the interaction parameters decreases, the sorption increases. From the sorption results in Section 5.2, it can be seen than the percentage sorption is higher in hydrazine hydrate compared to pure water. As the interaction parameter decreases, the sorption theoretically increases.

6.3.4. Estimation of the solution model parameters

The predicted water sorption in the membrane on a polymer free basis (u_i) was calculated by substituting the interaction parameters and experimental sorption results into Equation (3-7) and solving the equation in terms of volume fraction of water in the ternary system (Φ_i).

$$ln\left(\frac{\Phi_i}{\Phi_j}\right) - ln\left(\frac{v_i}{v_j}\right) = (r-1)ln\left(\frac{\Phi_i}{v_j}\right) - g_{ij}(u_j)(\Phi_j - \Phi_i) - g_{ij}(v_j)(u_i - v_j)$$
$$-\Phi_p(g_{ip} - rg_{jp}) + u_i\Phi_p\frac{\partial g_{ip}}{\partial u_j} - v_i v_j\frac{\partial y g_{ij}}{\partial v_j} + \Phi_p u_i\frac{\partial g_{ip}}{\partial u_j} - \frac{v_i}{v_j}u_j\Phi_p\frac{\partial g_{jp}}{\partial u_i} \quad (3\text{-}7)$$

The predicted volume fraction of water on a polymer free basis (u_i) along with the experimental sorption results are plotted in Figure 6.2 as a function of water volume fraction in the feed (v_i).

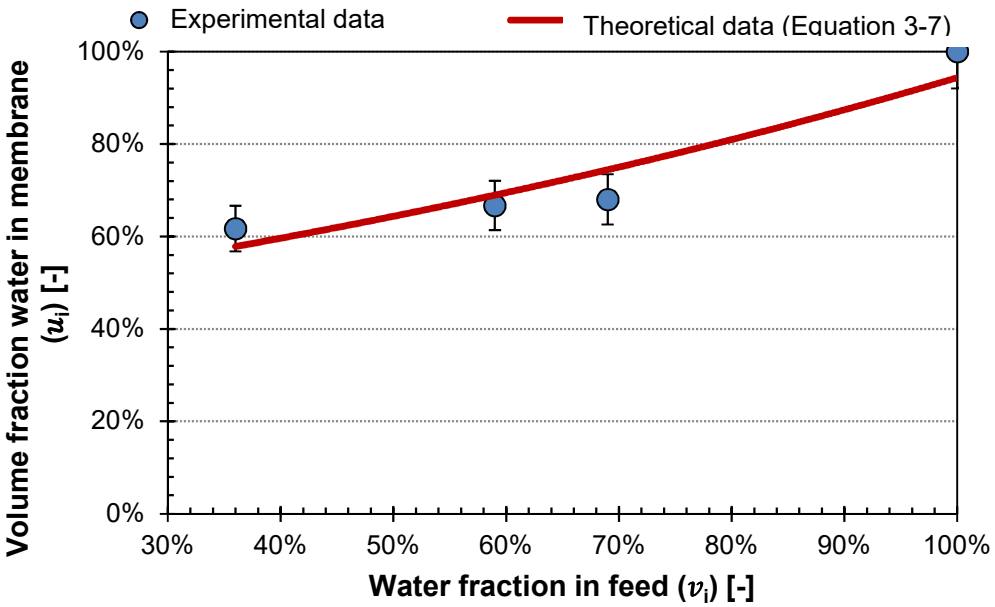

Figure 6.2: Comparison between experimental sorption values and predicted values making use of concentration independent interaction parameters at 50 °C

From Figure 6.2 it can be seen that the predicted sorption values using a concentration independent solvent-polymer interaction coefficient describes the sorption process with an acceptable level of accuracy. The accuracy of the sorption fit between experimental and predicted values are quantified with a R^2 value of 0.8806, MAPE value of 6.19 and RMSE value of 0.048.

Numerous researchers opted for the same simplified approach that make use of concentration independent interactions due to relatively accuracy with limited input requirements (Mandal et al., 2008, Yang et al., 1998). A potential drawback of the simplified approach is that it does not take any non-ideality into account.

6.4. Pervaporation modelling

6.4.1. Solution methodology

Fick's first law as described in Section 3.3.2 was used to describe the mass transport step in the solution-diffusion model and the partial fluxes can be calculated from Equation (3-20):

$$J_i = -D_i \frac{dc_i}{dz} \tag{3-20}$$

where the partial component flux (J_i) can be calculated by making use of a concentration dependent diffusion coefficient (D_i) for a specified concentration gradient over the membrane ($\frac{dc_i}{dz}$).

6.4.2. Diffusion coefficients

The solution technique to model the partial fluxes assumes that hydrazine hydrate and the PVA polymer solution form an ideal mixture. The partial component fluxes for either water or hydrazine can therefore be written in terms of individual solvent concentration and can be solved by making use of concentration dependent diffusion coefficients.

The diffusion coefficient of low molecular weight components within the polymer membrane is concentration dependent (Hoda et al., 2005) and therefore the concentration dependence of the diffusion coefficient needs to be taken into account with a hydrazine hydrate system. The diffusion coefficients, as described in Section 3.3, are given in Table 6.3 in terms of mass fraction.

Table 6.3: Diffusion coefficients used for ideal system

Reference model	Diffusion equation	Equation number	Reference
Greenlaw	$D_i = \rho_m . {D_i}^0 (x_i + \beta_{ji} x_j)$	(3-24)	(Greenlaw et al., 1977b)
	$D_j = \rho_m . {D_j}^0 (x_j + \beta_{ij} x_i)$	(3-25)	
Long	$D_i = \rho_m . {D_i}^0 exp(\beta_i x_i)$	(3-30)	(Long, 1965)
	$D_j = \rho_m . {D_j}^0 exp(\beta_j x_j)$	(3-31)	
Brun	$D_i = \rho_m . {D_i}^0 exp(\beta_{ii} x_i + \beta_{ij} x_j)$	(3-32)	(Brun et al., 1985)
	$D_j = \rho_m . {D_j}^0 exp(\beta_{ji} x_i + \beta_{jj} x_j)$	(3-33)	

The theoretical values of the water and hydrazine partial fluxes for specified mass fractions were calculated by substituting the expressions for the diffusion coefficients (Table 6.3) in Fick's first law of diffusion (Equation (3-23)). The partial flux equations for both water and hydrazine are given in Table 6.4, with the detail derivations shown in Appendix H.

Table 6.4: Partial flux equations for various diffusion coefficient models

Model	Partial flux equations for water
Greenlaw	$J_i = \frac{-\rho_m . {D_i}^0}{z} \left[\frac{{x_i}^2}{2} + \beta_{ji} x_i (1 - x_i)\right]$
	$J_j = \frac{-\rho_m . {D_j}^0}{z} \left[\frac{{x_j}^2}{2} + \beta_{ij} x_j (1 - x_j)\right]$
Long	$J_i = \frac{-\rho_m . {D_i}^0}{z} \left(\frac{exp(\beta_i x_i)}{\beta_i} + Ci\right)$
	$J_j = \frac{-\rho_m . {D_j}^0}{z} \left(\frac{exp(\beta_j x_j)}{\beta_j} + Cj\right)$
Brun	$J_i = \frac{-\rho_m . D_i}{z} \frac{C_i(\beta_{ii} - \beta_{ij}) + exp^{\beta_{ii} x_i + \beta_{ij}(1 - x_i)}}{\beta_{ii} - \beta_{ij}}$
	$J_j = \frac{-\rho_m . D_j}{z} \frac{C_j(\beta_{jj} - \beta_{ji}) + exp^{\beta_{jj} x_j + \beta_{ji}(1 - x_j)}}{\beta_{jj} - \beta_{ji}}$

6.4.3. Modelling data used

Three sets of pervaporation data were selected for diffusion modelling of hydrazine hydrate. The experimental data from this study using a Pervap™ 4101 membrane together with data obtained using ethyl cellulose polymeric membrane by Ravindra et al. (1999c), as well as data obtained using PEBAX®-2533 by Sunitha et al. (2011) is given in Table 6.5.

Table 6.5: Experimental data of flux and selectivity at 50 °C obtained during this study as well as data from Ravindra et al. (1999c) and Sunitha et al. (2011)

This study						
Wt. % water	0.47	0.57	0.70	0.79	-	-
J [kg·m^{-2}·h^{-1}]	0.14	0.12	0.13	0.17	-	-
α	2.07	4.57	14.71	19.47	-	-
Ravindra et al. (1999c)						
Wt. % water	0.15	0.30	0.36	0.60	0.70	0.8
J [kg·m^{-2}·h^{-1}]	1.305	0.833	0.833	1.111	4.162	4.721
α	8.6	8.3	5.6	22.2	127.8	250.0
Sunitha et al. (2011)						
Wt. % water	0.362	0.407	0.442	0.567	0.593	-
J [kg·m^{-2}·h^{-1}]	0.052	0.0545	0.0589	0.061	0.063	-
α	105	36.25	18.75	12.5	8.75	-

The literature data obtained from both Ravindra et al. (1999c) and Sunitha et al. (2011) was limited to testing at 50 °C, therefore temperature effect on diffusivity was neglected. The same assumption was made by Hoda et al. (2005) in the modelling of data through a hollow fibre module.

6.4.4. Modelling of the partial fluxes

This section of the study aims to directly compare the theoretical partial flux equations for both water and hydrazine as derived in Section 6.4.2 and given in Table 6.4 with the three sets of experimental data (this study, Ravindra et al. (1999c) and Sunitha et al. (2011)), from Table 6.5.

The results obtained from the modelling of the theoretical partial flux equations for the concentration dependent diffusion coefficients (see Table 6.3) along with all three sets of experimental results from Table 6.5 are plotted for a range of water mass feed fractions. The comparative plots between the experimental results and the diffusion coefficient as proposed by Long (1965) are given in Figure 6.3, Greenlaw et al. (1977a) in Figure 6.4 and Brun et al. (1985) in Figure 6.5.

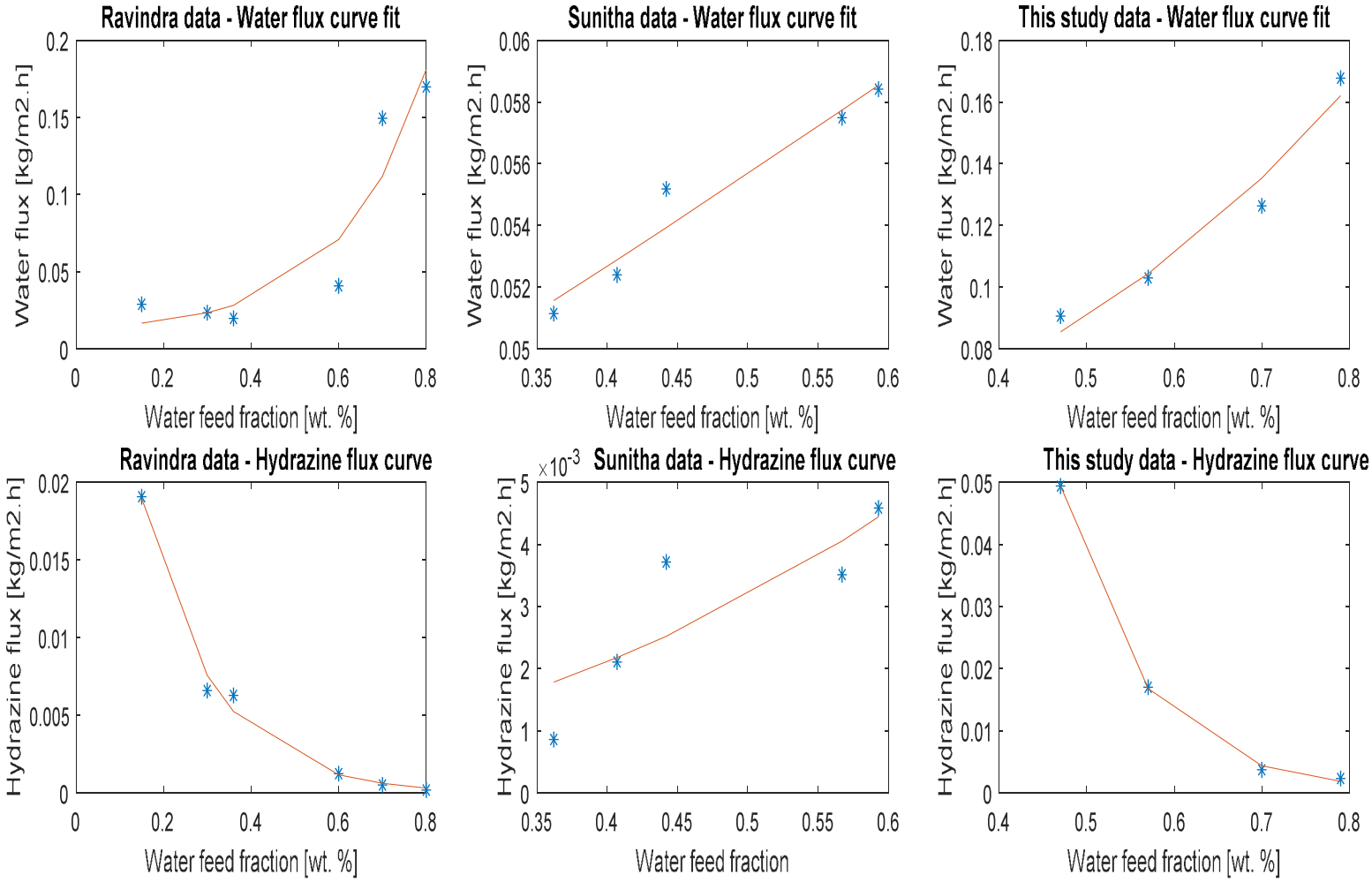

Figure 6.3: Comparison between water and hydrazine partial flux experimental results with Long's model

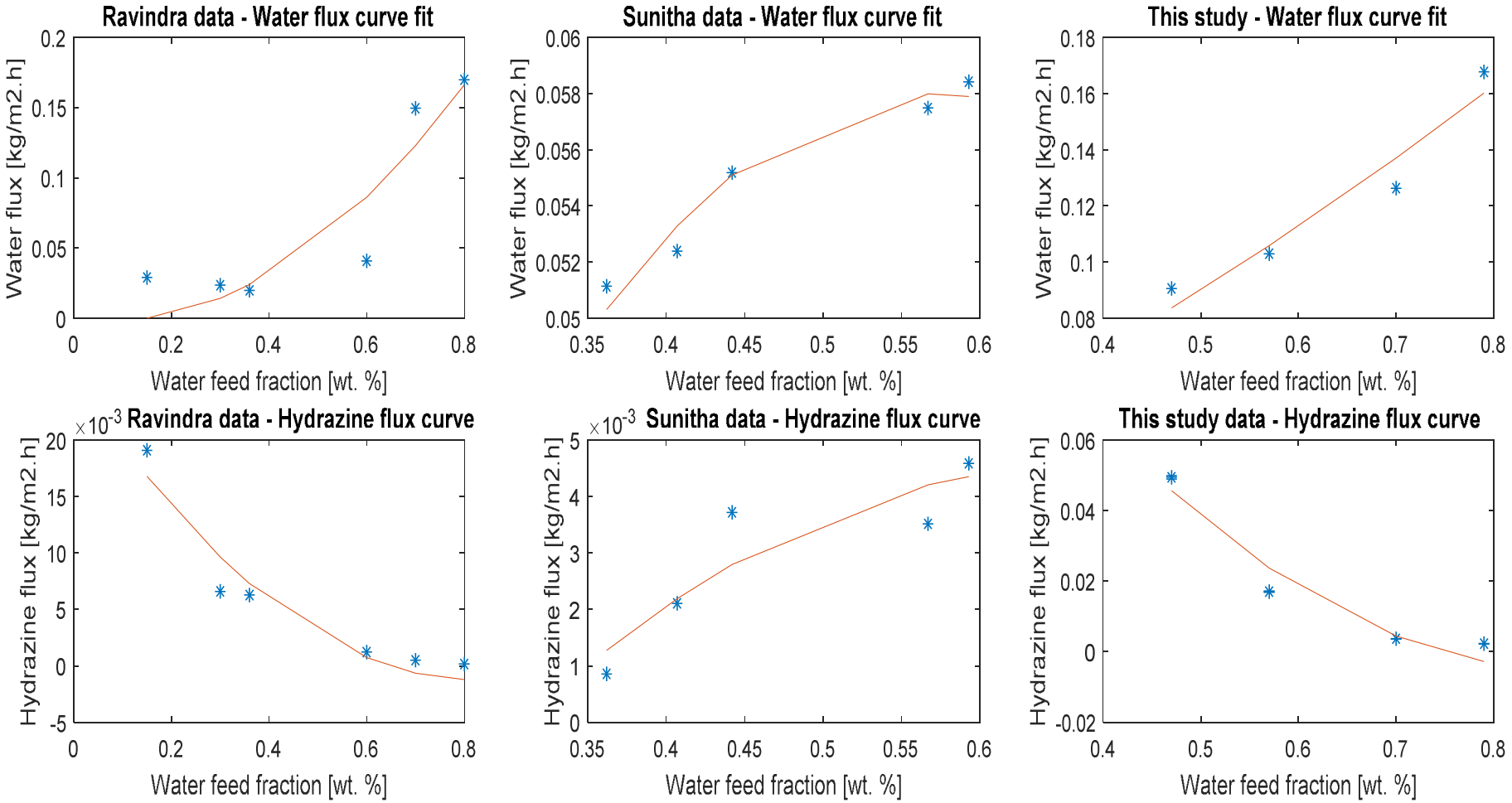

Figure 6.4: Comparison between water and hydrazine partial flux experimental results with Greenlaw's model

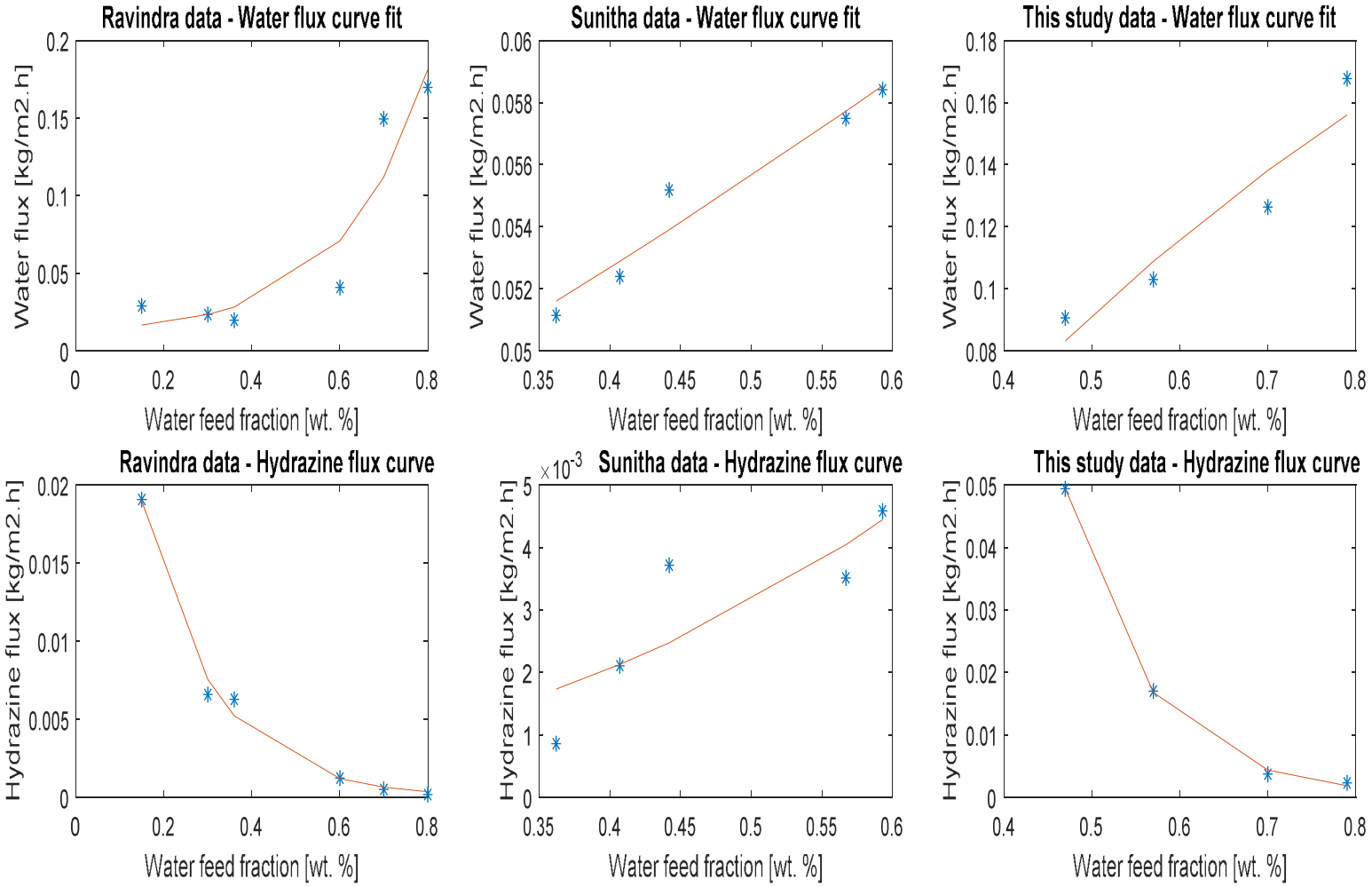

Figure 6.5: Comparison between water and hydrazine partial flux experimental results with Brun's model

The accuracy of each diffusion coefficient model given in Table 6.4 was calculated. The accuracy of all three experimental datasets (as per Table 6.5) was calculated in terms of R^2, MAPE and RMSE statistical methods with the results supplied in Table 6.6.

Table 6.6: Accuracy of water and hydrazine partial fluxes for testing results of this study (R-values) using various diffusion models

Dataset	Model	Water flux			Hydrazine flux		
		R^2	MAPE	RMSE	R^2	MAPE	RMSE
This study	Long	0.9896	4.4	0.0052	0.9999	9.6	0.0004
	Greenlaw	0.9832	5.9	0.0066	0.9851	71.8	0.0046
	Brun	0.9723	7.6	0.0076	0.9723	9.6	0.0004
Ravindra	Long	0.9704	31.8	0.0211	0.998	22.0	0.0006
	Greenlaw	0.9595	48.7	0.0249	0.9814	193.2	0.0018
	Brun	0.9704	31.8	0.0211	0.998	29.0	0.0006
Sunitha	Long	0.9866	0.9	0.0006	0.915	32.3	0.0007
	Greenlaw	0.9878	1.1	0.0006	0.9515	20.4	0.0006
	Brun	0.9860	1.0	0.0007	0.9146	30.8	0.0007

It can be seen from Figure 6.3 that the exponential diffusion coefficient as derived by Long (1965) yielded a good approximation on the majority of the experimental partial flux data. However on the experimental data obtained from Ravindra et al. (1999c), the water flux was under-estimated, especially in the low water feed fraction region. The Long model also had greater variation in accuracy to predict, the hydrazine partial flux on the experimental data obtained form Sunitha et al. (2011). The statistical data in Table 6.6 supports this argument as it can be seen that the Long model has the highest overall R^2 value and lowest MAPE and RMSE values, indicating the best fit between the three correlations.

The Long model was developed to simulate the pure component fluxes as a function of only its own concentration in the membrane, and therefore does not take any interaction between water and hydrazine within the membrane into account.

The Greenlaw model was used to investigate the possibility of further improving the experimental fit found by the Long model as the Greenlaw diffusion coefficient incorporates the coupling effect for water and hydrazine inside the membrane.

From Figure 6.4 and Table 6.6 it can clearly be seen that that the Greenlaw model offered no improvement and, in fact, increased the deviation between the experimental results and theoretical prediction. This is a strong indication that the interaction between the hydrazine and water within the membrane does not play an important role in the selective diffusion of either component through the membrane. From the sorption experimental results discussed in Section 5.2.1 (as illustrated in Figure 5.8) that the water content in the membrane remains relatively concentration independent for feed water concentrations ranging from 36 to 70 wt. % water. A further indication in support of this conclusion is that the water-polymer and hydrazine-polymer interaction parameters calculated in Section 6.3.3 are very close to each other (5.47 and 3.68 respectively) showing very similar interactions between individual solvents and the membrane.

Both the Long and Greenlaw models were initially developed for ideal mixtures. The deviation noted between the experimental and theoretical results, especially in the results by Sunitha et al. (2011), might be attributed to the polar-polar water-hydrazine mixture. The more complex six-coefficient exponential diffusion coefficient proposed by Brun et al. (1985) in Figure 6.5 was developed to predict the transport behaviour of non-ideal systems. The eight experimental data points used from this study allow for a single degree of freedom for optimisation of each of the partial flux equations. The theoretical model predicted the partial fluxes for both water and hydrazine with good accuracy, but does not offer any improvements on the results from the Long model. The Brun diffusion coefficient accounts for the non-ideality of the water-hydrazine system by making use of an exponential model which depends separately on the local component concentrations. The modelling accuracy obtained from the diffusion coefficients were sufficient not to warrant any further investigation into chemical potential equations as proposed by Yang et al. (1998) for modelling non-ideal systems.

The model parameters, i.e. diffusion coefficients at infinite dilution and plasticisation coefficients for the theoretical comparisons graphs in Figure 6.3 to Figure 6.5 are given in Table 6.8. Calculation details are supplied in Appendix H.

It is difficult to make a direct comparison between the limiting diffusion coefficients ($D_i{}^0$ and $D_i{}^0$) and plasticisation coefficients (β) found in this study for water and hydrazine partial fluxes with data found in literature because each individual system (solvent and membranes) is unique in this regard.

It is clear from Table 6.8 and Table 6.7 that the order of magnitude of the limiting diffusion coefficients and plasticisation coefficients reported in this study compare well with the literature values reported for similar systems.

Table 6.7: Literature limiting coefficients and plasticisation coefficients for various systems

System **Membrane**	$D_i{}^0$ **[m²·s⁻¹]**	$D_j{}^0$ **[m²·s⁻¹]**	β	**Reference**
water-hydrazine ethyl cellulose	2.57 x 10^{-8}	0.28 x 10^{-8}	-	Ravindra et al. (2000)
water-hydrazine ethyl cellulose	3.05 x 10^{-13}	1.36 x 10^{-12}	0.37-11.67 0.55-36.76	Hoda et al. (2005)
styrene-ethylbenzene polyurethane	8.78 x 10^{-12}	8.13 x 10^{-12}	19.9–58.5 -0.06- -13.7	Cao and Henson (2002)

Table 6.8: Results limiting coefficients and plasticisation coefficients for various systems (this study)

Water flux data	**Model**	D_i^0 **(m²·s⁻¹)**	β_i	β_{ii}	β_{ij}
This study	Greenlaw	1.16×10^{-09}	-	-	0.323
Ravindra	Greenlaw	5.44×10^{-09}	-	-	-0.090
Sunitha	Greenlaw	4.95×10^{-10}	-	-	4.116
This study	Long	1.77×10^{-10}	2.000	-	-
Ravindra	Long	1.37×10^{-10}	5.213	-	-
Sunitha	Long	2.63×10^{-10}	0.288	-	-
This study	Brun	2.56×10^{-07}	-	-6.479	-5.330
Ravindra	Brun	5.67×10^{-09}	-	1.490	-3.722
Sunitha	Brun	7.90×10^{-10}	-	-0.658	-1.248
Hydrazine flux data	**Model**	D_j^0 **(m²·s⁻¹)**	β_j	β_{jj}	β_{ji}
This study	Greenlaw	1.22×10^{-09}	-	-	-0.168
Ravindra	Greenlaw	5.13×10^{-10}	-	-	-0.273
Sunitha	Greenlaw	-2.32×10^{-10}	-	-	-1.118
This study	Long	4.30×10^{-12}	10.944	-	-
Ravindra	Long	6.53×10^{-12}	6.091	-	-
Sunitha	Long	-4.92×10^{-10}	-2.812	-	-
This study	Brun	4.24×10^{-8}	-	1.747	-9.196
Ravindra	Brun	3.23×10^{-11}	-	4.512	-1.650
Sunitha	Brun	-4.68×10^{-11}	-	-0.481	2.412

6.4.5. General conclusion

The permeation of water and hydrazine through the Pervap™ 4101 membrane, as well as experimental literature data from Ravindra et al. (1999c) and Sunitha et al. (2011) was modelled based on the solution-diffusion model. The sorption step was described by the Flory-Huggins equations, while the diffusion transport step was described by making use of Fick's first law of diffusion.

In Section 6.3 it was shown that the Flory-Huggins equations using a concentration dependent water-hydrazine interaction parameter and concentration independent solvent (water / hydrazine) – polymer interaction parameter describes the preferred sorption of water with a R^2 of 0.8806. A water-hydrazine interaction parameter of -2.05 was calculated for hydrazine monohydrate (36 wt. % water) and 50 °C, that suggests a strong affinity between water and hydrazine.

A concentration independent interaction parameter between hydrazine-polymer that is lower than water-polymer confirms the preferential sorption with an increase in hydrazine concentration in the feed results supplied in Section 5.2.

It was shown in Section 6.4 that Fick's first law of diffusion operating under the assumption of an ideal liquid and by making use of various diffusion coefficients correlations like Long (1965), Greenlaw et al. (1977a) and Brun et al. (1985) can be used to describe the diffusions transport step with a high level of accuracy (as high as an $R^2 > 0.99$) for a wide range of pervaporation membrane (Pervap™ 4101, ethyl cellulose and PEBAX®-2533). It was found that the relative simplified Long model that does not take solvent-solvent interaction into account, yielded the most accurate results.

CHAPTER SEVEN - CONCLUSIONS, RECOMMENDATIONS AND FUTURE WORK

OVERVIEW

The study is concluded with an overview of the main aim (Section 7.1.1), followed by the conclusions of each of the three study objectives (Section 7.1.2 to 7.1.4). All recommendations and future work is discussed in Section 7.2.

7.1. Conclusions

7.1.1. Main aim

From this study it can be concluded that commercially available polymeric membranes, specifically Pervap™ 4101, have the potential to dehydrate azeotropic mixtures of hydrazine hydrate. Laboratory synthesised membranes tested by authors like Ravindra et al. (1999c) and Sunitha et al. (2011) did however outperformed the Pevap™ 4101 in terms of pervaporation water selectivity.

7.1.2. Objective 1: Membrane selection and screening

Various international polymeric membrane suppliers were consulted and eight commercial polymers were procured for this study. Membrane screening and characterisation tests indicated that both membranes supplied by Pervatech BV are unsuitable for operation with hydrazine hydrate. Pervap™ 4060, 4101 and 4102 showed no visible interactions, while Pervap™ 4100 and POL-AL-M2 and POL-OL-M1 showed slight interaction on the active layer.

Pervaporation screening tests performed at 50 °C showed that all membranes as water selective over hydrazine and only the Pervap™ 4101 and Pervap™ 4102 membranes outperformed the theoretical water selectivity of 1.4 obtained by conventional distillation. The Pervap™ 4101 membrane measured a higher experimental flux when compared to the Pervap™ 4102 which also translates into a higher overall PSI value. Pervap™ 4101 membrane was selected from the screening test as the commercial polymeric membrane that shows the most promise to break the azeotropic point of hydrazine monohydrate.

7.1.3. Objective 2: Characterisation Pervap™ 4101 membrane

Sorption studies on Pervap™ 4101 membranes at 50 °C and feed concentrations between 36 and 100 wt. % water revealed that membrane swelling is as high as 80 %. Both sorption and pervaporation is water selective, but higher diffusion water selectivity's indicate that the separation process is diffusion controlled.

Based on the performance characterisation of Pervap™ 4101 membrane it can be concluded that temperature has no effect on sorption selectivity or swelling, while it increases the transmembrane flux in pervaporation leading to a reduced selectivity.

Plotting the sorption and pervaporation results on a McCabe-Thiele VLE diagram showed that Pervap™ 4101 has the potential to separate a hydrazine-water mixture past the azeotropic point, where after ordinary distillation can dehydrate the mixture to the required purity. Commercial Pervap™ 4101 does, however, not compare to literature results obtained by Ravindra et al. (1999c) and Sunitha et al. (2011).

7.1.4. Objective 3: Process mass transfer modelling

A water-hydrazine interaction parameter of -2.05 was calculated for hydrazine monohydrate (36 wt. % water) and 50 °C that suggests a strong affinity between water and hydrazine. A concentration independent interaction parameter between hydrazine-polymer (3.68) that is lower than water-polymer (5.47) confirms the preferential sorption with added hydrazine in the feed.

It was found that the relative simplified Long model that does not take solvent-solvent interaction into account, yielded the most accurate results ($R^2 > 0.999$) for the diffusion modelling step.

7.2. Recommendations and future work

Future experimental work should include investigating the performance of inorganic or mixed-matrix membranes to address the lack of stability and low water selectivities observed with the laboratory synthesised membranes tested in this study.

All membrane interaction with hydrazine monohydrate was shown to be with the support layer and studies should be carried out to find a more chemically resistant support for the active layer.

REFERENCES

ALTENA, F. W. & SMOLDERS, C. 1982. Calculation of liquid-liquid phase separation in a ternary system of a polymer in a mixture of a solvent and a nonsolvent. *Macromolecules,* 15**,** 1491-1497.

AMINABHAVI, T. M., HARLAPUR, S. F., BALUNDGI, R. H. & DALE ORTEGO, J. 1998. Theoretical and experimental investigations of molecular migration and diffusion kinetics of organic esters into tetrafluoroethylene/propylene copolymer membranes. *The Canadian Journal of Chemical Engineering,* 76**,** 104-112.

AMINABHAVI, T. M. & MUNK, P. 1979. Preferential adsorption onto polystyrene in mixed solvent systems. *Macromolecules,* 12**,** 607-613.

ARMSTRONG, J. S. & OVERTON, T. S. 1977. Estimating nonresponse bias in mail surveys. *Journal of marketing research***,** 396-402.

AUDRIETH, L. F. & OGG, B. A. 1951. *The chemistry of hydrazine*, Wiley.

BACHMANN, J., SPIELMANN, T., VENETZ, A. & KÖNIG, U. C. 2010. Pervaporative Trennung von MeOH/Toluol-Gemischen mit einer hydrophilen Polymerflachmembran. *Chemie Ingenieur Technik,* 82**,** 309-315.

BAKER, R. W. 2000. *Membrane technology*, Wiley Online Library.

BARTON, A. F. 1991. *CRC handbook of solubility parameters and other cohesion parameters*, CRC press.

BASILE, A., FIGOLI, A. & KHAYET, M. 2015. *Pervaporation, Vapour Permeation and Membrane Distillation: Principles and Applications*, Elsevier.

BINNING, R., LEE, R., JENNINGS, J. & MARTIN, E. 1961. Separation of liquid mixtures by permeation. *Industrial & Engineering Chemistry,* 53**,** 45-50.

BIRCHER JR JOHN, R. 1954. Dehydration of hydrazine solutions. Google Patents.

BOCK, H. 1958. On a Simple Method for Preparation of Anhydrous Hydrazine. *Z. Anorg.Allg.Chemical,* 293**,** 264-273.

BOWEN, T. C., NOBLE, R. D. & FALCONER, J. L. 2004. Fundamentals and applications of pervaporation through zeolite membranes. *Journal of Membrane Science,* 245**,** 1-33.

BRUN, J., LARCHET, C., MELET, R. & BULVESTRE, G. 1985. Modelling of the pervaporation of binary mixtures through moderately swelling, non-reacting membranes. *Journal of membrane science,* 23**,** 257-283.

BUCKLEY-SMITH, M. 2006. *The Use of Solubility Parameters to select membrane materials for Pervaporation of organic mixtures.* The University of Waikato.

BURSHE, M., SAWANT, S. & PANGARKAR, V. 1999. Dehydration of glycerine-water mixtures by pervaporation. *Journal of the American Oil Chemists' Society,* 76**,** 209-214.

BUSH, L. & SIMS, J. 1974. Morphological and physiological effects of maleic hydrazide on tobacco. *Physiologia Plantarum,* 32**,** 157-160.

CABASSO, I. 1983. Organic liquid mixtures separation by permselective polymer membranes. 1. Selection and characteristics of dense isotropic membranes employed in the pervaporation process. *Industrial & Engineering Chemistry Product Research and Development,* 22**,** 313-319.

CAO, B. & HENSON, M. A. 2002. Modeling of spiral wound pervaporation modules with application to the separation of styrene/ethylbenzene mixtures. *Journal of membrane science,* 197**,** 117-146.

CHADEHUMBE, C. 2008. *Tensile properties of thermoplastic starch and its blends with polyvinyl butyral and polyamides.* University of Pretoria.

References

CUNHA, V., PAREDES, M., BORGES, C., HABERT, A. & NOBREGA, R. 2002. Removal of aromatics from multicomponent organic mixtures by pervaporation using polyurethane membranes: experimental and modeling. *Journal of membrane science,* 206**,** 277-290.

DEE, L. 1971. Gas chromatographic determination of aqueous trace hydrazine and methylhydrazine as corresponding pyrazoles. *Analytical Chemistry,* 43**,** 1416-1419.

DEL POZO GOMEZ, M. T., REPKE, J.-U., KIM, D.-Y., YANG, D. R. & WOZNY, G. N. 2009. Reduction of energy consumption in the process industry using a heat-integrated hybrid distillation pervaporation process. *Industrial & Engineering Chemistry Research,* 48**,** 4484-4494.

DONDOS, A., REMPP, P. & BENOIT, H. Effet des proprietes thermodynamiques des melanges de solvants sur les dimensions de chaines macromoleculaires. Journal of Polymer Science: Polymer Symposia, 1970. Wiley Online Library, 9-16.

DUNLOP, A. 1967. *Extraction of hydrazine from aqueous solution using a fluorinated alcohol*.

DUTTA, B. K., JI, W. & SIKDAR, S. K. 1996. Pervaporation: principles and applications. *Separation and Purification Methods,* 25**,** 131-224.

DUTTA, S. 2004. *Dehydration of Hydrazine by Pervaporation: Blending of polymers, modification and Characterization of membranes.*

FAVRE, E. 2003. Temperature polarization in pervaporation. *Desalination,* 154**,** 129-138.

FEHER, F. & LINKE, K. H. 1966. Beiträge zur Chemie des Hydrazins und seiner Derivate. VII. Über die Umsetzung von absolutem Hydrazin mit Hydroxylamido-O-schwefelsäure. *Zeitschrift für anorganische und allgemeine Chemie,* 344**,** 18-22.

FENG, X. & HUANG, R. Y. 1994. Concentration polarization in pervaporation separation processes. *Journal of Membrane science,* 92**,** 201-208.

FENG, X. & HUANG, R. Y. 1997. Liquid separation by membrane pervaporation: a review. *Industrial & Engineering Chemistry Research,* 36**,** 1048-1066.

FLEMMING, H. & SLATER, C. 1992. Pervaporation-definition and background. *Membrane Handbook, VaNostrandReinhold***,** 113.

FLORY, P. J. 1953. *Principles of polymer chemistry*, Cornell University Press.

FONTALVO, J., CUELLAR, P., TIMMER, J., VORSTMAN, M., WIJERS, J. & KEURENTJES, J. 2005. Comparing pervaporation and vapor permeation hybrid distillation processes. *Industrial & engineering chemistry research,* 44**,** 5259-5266.

FRIESEN, D. T., NEWBOLD, D. D., MCCRAY, S. B. & RAY, R. J. 1995. Pervaporation by countercurrent condensable sweep. Google Patents.

GEORGE, S. C., PRASAD, K., MISRA, J. & THOMAS, S. 1999. Separation of alkane–acetone mixtures using styrene–butadiene rubber/natural rubber blend membranes. *Journal of applied polymer science,* 74**,** 3059-3068.

GEORGE, S. C. & THOMAS, S. 2001. Transport phenomena through polymeric systems. *Progress in Polymer Science,* 26**,** 985-1017.

GRAY, A. & FOCHTMAN, E. 1978. Amine Fuels via the Urea Process. DTIC Document.

GREENLAW, F., PRINCE, W., SHELDEN, R. & THOMPSON, E. 1977a. Dependence of diffusive permeation rates on upstream and downstream pressures: I. Single component permeant. *Journal of Membrane Science,* 2**,** 141-151.

GREENLAW, F., SHELDEN, R. & THOMPSON, E. 1977b. Dependence of diffusive permeation rates on upstream and downstream pressures: II. Two component permeant. *Journal of Membrane Science,* 2**,** 333-348.

HALE, C. & SHETTERLY, F. F. 1911. ANHYDROUS HYDRAZINE. I. A CONVENIENT APPARATUS FOR THE PREPARATION OF ANHYDROUS HYDRAZINE. *Journal of the American Chemical Society,* 33**,** 1071-1076.

HICKEY, P., JURICIC, F. & SLATER, C. 1992. The effect of process parameters on the pervaporation of alcohols through organophilic membranes. *Separation science and technology,* 27**,** 843-861.

HODA, N., SUGGALA, S. V. & BHATTACHARYA, P. K. 2005. Pervaporation of hydrazine–water through hollow fiber module: Modeling and simulation. *Computers & chemical engineering,* 30**,** 202-214.

HOYT, D. F. 1979. Practical methods of estimating volume and fresh weight of bird eggs. *The Auk***,** 73-77.

HUANG, R. Y. 1991. *Pervaporation membrane separation processes*, Elsevier Science Ltd.

IMAM, S. 2016. Minimizing the Pollution by Green Approach. *Imperial Journal of Interdisciplinary Research,* 2.

IZÁK, P., HOVORKA, Š., BARTOVSKÝ, T., BARTOVSKA, L. & CRESPO, J. 2007. Swelling of polymeric membranes in room temperature ionic liquids. *Journal of membrane science,* 296**,** 131-138.

JIANG, L. Y., WANG, Y., CHUNG, T.-S., QIAO, X. Y. & LAI, J.-Y. 2009. Polyimides membranes for pervaporation and biofuels separation. *Progress in Polymer Science,* 34**,** 1135-1160.

JONQUIERES, A., CLE, R., ROIZARD, D. & LOCHON, P. 1996. Pervaporative transport modelling in a ternary system: ethyltertiarybutylether/ethanol/polyurethaneimide. *Journal of membrane science,* 109**,** 65-76.

KOBER, P. A. 1917. Pervaporation, perstillation and percrystallization. *Proceedings of the Society for Experimental Biology and Medicine,* 14**,** 87-88.

KOCZKA, K., MANCZINGER, J., MIZSEY, P. & FONYO, Z. 2007. Novel hybrid separation processes based on pervaporation for THF recovery. *Chemical Engineering and Processing: Process Intensification,* 46**,** 239-246.

KRIGBAUM, W. & CARPENTER, D. 1954. Phase equilibria in polymer–liquid 1–liquid 2 systems. *Journal of Polymer Science Part A: Polymer Chemistry,* 14**,** 241-259.

KUJAWSKI, W. 2000. Application of pervaporation and vapor permeation in environmental protection. *Polish Journal of Environmental Studies,* 9**,** 13-26.

LARCHET, C., BRUN, J. & GUILLOU, M. 1983. Separation of benzene—n-heptane mixtures by pervaporation with elastomeric membranes. I. Performance of membranes. *Journal of Membrane Science,* 15**,** 81-96.

LEE, C. H. 1975. Theory of reverse osmosis and some other membrane permeation operations. *Journal of Applied Polymer Science,* 19**,** 83-95.

LEWIS 1957. Hydrazine recovery. Google Patents.

LI, Z.-L., ZHANG, Y.-Z., WANG, X.-J. & LI, H.-B. 2009. Pervaporation and its Applications in Dehydration of Hydrazine Fuels [J]. *Chinese Journal of Energetic Materials,* 1**,** 030.

LIPNIZKI, F. & TRÄGÅRDH, G. 2001. Modelling of pervaporation: models to analyze and predict the mass transport in pervaporation. *Separation and Purification Methods,* 30**,** 49-125.

References

LONE, S., AHMAD, S. A. & KUMAR, V. 2015. Modeling and Simulation of a Hybrid Process (Pervaporation+ Distillation) using MATLAB. *J Chem Eng Proces s Technol,* 6**,** 234.

LONG, R. 1965. Liquid permeation through plastic films. *Industrial & Engineering Chemistry Fundamentals,* 4**,** 445-451.

LUO, G., NIANG, M. & SCHAETZEL, P. 1997. Pervaporation separation of ethyl tert-butyl ether and ethanol mixtures with a blended membrane. *Journal of membrane science,* 125**,** 237-244.

LUYBEN, W. L. & CHIEN, I.-L. 2011. *Design and control of distillation systems for separating azeotropes*, John Wiley & Sons.

MANDAL, M. K., DUTTA, S. & BHATTACHARYA, P. 2008. Characterization of blended polymeric membranes for pervaporation of hydrazine hydrate. *Chemical Engineering Journal,* 138**,** 10-19.

MEINTJES, M. M. 2011. *Fermentation coupled with pervaporation: a kinetic study.* North-West University.

MELIN, T. & RAUTENBACH, R. 2007. *Membranverfahren: Grundlagen der Modul- und Anlagenauslegung*, Springer-Verlag.

MEULEMAN, E., WILLEMSEN, J., MULDER, M. & STRATHMANN, H. 2001. EPDM as a selective membrane material in pervaporation. *Journal of membrane science,* 188**,** 235-249.

MOHANTY, K. & PURKAIT, M. K. 2011. *Membrane technologies and applications*, CRC Press.

MULDER, J. 2012. *Basic principles of membrane technology*, Springer Science & Business Media.

MULDER, M. 1991. Thermodynamic principles of pervaporation. *Pervaporation Membrane Separation Processes, Elsevier, Amsterdam***,** 225-250.

MULDER, M., FRANKEN, T. & SMOLDERS, C. 1985. Preferential sorption versus preferential permeability in pervaporation. *Journal of membrane science,* 22**,** 155-173.

MULDER, M. & SMOLDERS, C. 1984. On the mechanism of separation of ethanol/water mixtures by pervaporation I. Calculations of concentration profiles. *Journal of Membrane Science,* 17**,** 289-307.

NACHBAUR, E. & LEISEDER, G. 1971. SIMPLE AND HARMLESS PREPARATION OF ANHYDROUS HYDRAZINE. *MONATSHEFTE FUR CHEMIE,* 102**,** 1718-&.

NAGELKERKE, N. J. 1991. A note on a general definition of the coefficient of determination. *Biometrika,* 78**,** 691-692.

NICOLAISEN 1956. Extraction of aniline from hydrazine in the dehydration of hydrazine by azeotropic distillation. Google Patents.

NICOLAISEN. 1957. *Process for the production of hydrazine*.

NICOLAISEN, B. H. & SMITH, J. C. J. 1958. Distillation of unsymmetrical dimethylhydrazine. Google Patents.

NUNES, S. P. & PEINEMANN, K.-V. 2001. *Membrane technology*, Wiley Online Library.

PARK, H., MEERTENS, R., MULDER, M. & SMOLDERS, C. 1994. Pervaporation of alcohol-toluene mixtures through polymer blend membranes of poly (acrylic acid) and poly (vinyl alcohol). *Journal of membrane science,* 90**,** 265-274.

PAUL, D. 1976. The solution-diffusion model for swollen membranes. *Separation and Purification Methods,* 5**,** 33-50.

References

PENNEMAN, R. & AUDRIETH, L. 1948. Quantitative determination of hydrazine. *Analytical chemistry,* 20**,** 1058-1061.

PENNEMAN, R. & AUDRIETH, L. 1949. The Ternary System: Hydrazine--Water--Sodium Hydroxide. *Journal of the American Chemical Society,* 71**,** 1644-1647.

PORTER, M. C. 1989. Handbook of industrial membrane technology.

PRAUSNITZ, J. M., LICHTENTHALER, R. N. & DE AZEVEDO, E. G. 1998. *Molecular thermodynamics of fluid-phase equilibria*, Pearson Education.

RAUTENBACH, R. & ALBRECHT, R. 1980. Separation of organic binary mixtures by pervaporation. *Journal of Membrane Science,* 7**,** 203-223.

RAVINDRA, R., KAMESWARA RAO, A. & KHAN, A. 1999a. Processing of liquid propellant reaction liquors by pervaporation. *Journal of applied polymer science,* 72**,** 141-149.

RAVINDRA, R., KROVVIDI, K. R., KHAN, A. & RAO, A. K. 1997. FTIR, diffusivity, selectivity, and aging studies of interactions of hydrazine, water, and hydrazine hydrate with the ethylcellulose membrane. *Macromolecules,* 30**,** 3288-3292.

RAVINDRA, R., KROVVIDI, K. R., KHAN, A. & RAO, A. K. 1999b. Dsc studies of states of water, hydrazine and hydrazine hydrate in ethylcellulose membrane. *Polymer,* 40**,** 1159-1165.

RAVINDRA, R., SRIDHAR, S. & KHAN, A. 1999c. Separation studies of hydrazine from aqueous solutions by pervaporation. *Journal of Polymer Science Part B: Polymer Physics,* 37**,** 1969-1980.

RAVINDRA, R., SRIDHAR, S., KHAN, A. & RAO, A. 2000. Pervaporation of water, hydrazine and monomethylhydrazine using ethylcellulose membranes. *Polymer,* 41**,** 2795-2806.

ROBERTSON, A. E. 1949. Separation of hydrocarbons. Google Patents.

SATYANARAYANA, S. & BHATTACHARYA, P. 2004. Pervaporation of hydrazine hydrate: separation characteristics of membranes with hydrophilic to hydrophobic behaviour. *Journal of membrane science,* 238**,** 103-115.

SATYANARAYANA, S., SUBRAHMANYAM, V., VERMA, H., SHARMA, A. & BHATTACHARYA, P. 2006. Application of positron annihilation: study of pervaporation dense membranes. *Polymer,* 47**,** 1300-1307.

SCHLIEBS, R. 1985. Hydrazine and its Derivatives. Preparation, Properties, Applications. Von EW Schmidt. Wiley, Chichester 1984. XXV, 1059 S., geb.£ 87.00.–ISBN 0-471-89170-3. *Angewandte Chemie,* 97**,** 360-360.

SCOTT, R. L. 1949. The thermodynamics of high polymer solutions. IV. Phase equilibria in the ternary system: Polymer—Liquid 1—Liquid 2. *The journal of chemical physics,* 17**,** 268-279.

SHAO, P. & HUANG, R. 2007. Polymeric membrane pervaporation. *Journal of Membrane Science,* 287**,** 162-179.

SHELDEN, R. & THOMPSON, E. 1984. Dependence of diffusive permeation rates and selectivities on upstream and downstream pressures: IV. Computer simulation of nonideal systems. *Journal of membrane science,* 19**,** 39-49.

SHIEH, J.-J. & HUANG, R. Y. 1998a. A pseudophase-change solution-diffusion model for pervaporation. I. Single component permeation.

SHIEH, J.-J. & HUANG, R. Y. 1998b. A pseudophase-change solution-diffusion model for pervaporation. II. Binary mixture permeation. *Separation science and technology,* 33**,** 933-957.

SMITHA, B., SUHANYA, D., SRIDHAR, S. & RAMAKRISHNA, M. 2004. Separation of organic–organic mixtures by pervaporation—a review. *Journal of membrane science,* 241**,** 1-21.

References

SOMMER, S. & MELIN, T. 2004. Design and optimization of hybrid separation processes for the dehydration of 2-propanol and other organics. *Industrial & engineering chemistry research,* 43**,** 5248-5259.

STEPHAN, W., NOBLE, R. D. & KOVAL, C. A. 1995. Design methodology for a membrane/distillation column hybrid process. *Journal of Membrane Science,* 99**,** 259-272.

STOLLE, R. & HOFMANN, K. 1904. 697. Ueber Hydrazincarbonsäure. *European Journal of Inorganic Chemistry,* 37**,** 4523-4524.

SUNITHA, K., NIKHITHA, P., SATYANARAYANA, S. & SRIDHAR, S. 2011. Recovery of hydrazine and glycerol from aqueous solutions by membrane separation techniques. *Separation Science and Technology,* 46**,** 2418-2426.

TAYLOR, R. 1990. Interpretation of the correlation coefficient: a basic review. *Journal of diagnostic medical sonography,* 6**,** 35-39.

TORRES-ALVAREZ, M. & WOLF-MACIEL, M. SIMULATION OF THE PERVAPORATION PROCESS FOR SEPARATING ORGANIC MIXTURES USING SOLUTION-DIFFUSION MODEL.

TRONG, Q. N. 1987. Modelling of the influence of downstream pressure for highly selective pervaporation. *Journal of membrane science,* 34**,** 165-183.

TYLKOWSKI, B. & TSIBRANSKA, I. 2015. Overview of main techniques used for membrane characterization. *J. Chem. Technol. Metall,* 50**,** 3-12.

VAN DER GRYP, P. 2003. *Separation by pervaporation of methanol from tertiary amyl methyl ether using a polymeric membrane.* Potchefstroom University for Christian Higher Education.

VAN DER GRYP, P. 2008. *Separation of Grubbs-based catalysts with nanofiltration.* North-West University.

VAN HOOF, V., VAN DEN ABEELE, L., BUEKENHOUDT, A., DOTREMONT, C. & LEYSEN, R. 2004. Economic comparison between azeotropic distillation and different hybrid systems combining distillation with pervaporation for the dehydration of isopropanol. *Separation and Purification Technology,* 37**,** 33-49.

VANE, L. M., ALVAREZ, F. R., MAIRAL, A. P. & BAKER, R. W. 2004. Separation of vapor-phase alcohol/water mixtures via fractional condensation using a pilot-scale dephlegmator: enhancement of the pervaporation process separation factor. *Industrial & engineering chemistry research,* 43**,** 173-183.

VASSE, F. 1974. *CONTRIBUTION A L'ETUDE DE L'EXTRACTION DU 1, 3-BUTADIENE DES COUPES PETROLIERES PAR PERVAPORATION A TRAVERS DES MEMBRANES PERMESELECTIVES.*

VILLALUENGA, J. G. & TABE-MOHAMMADI, A. 2000. A review on the separation of benzene/cyclohexane mixtures by pervaporation processes. *Journal of Membrane Science,* 169**,** 159-174.

WATT, G. W. & CHRISP, J. D. 1955. Hydrazine from Semicarbazide Solvolysis. *Industrial & Engineering Chemistry,* 47**,** 1206-1208.

WIJMANS, J. & BAKER, R. 1995. The solution-diffusion model: a review. *Journal of membrane science,* 107**,** 1-21.

WILLMOTT, C. J. 1982. Some comments on the evaluation of model performance. *Bulletin of the American Meteorological Society,* 63**,** 1309-1313.

WILSON, R., MINK, W., MUNGER, H. & CLEGG, J. 1955. Dehydration of hydrazine by azeotropic distillation. *AIChE Journal,* 1**,** 220-224.

WYNN, N. 2001. Pervaporation comes of age. *Chem. Eng. Prog,* 97**,** 66-72.

XIE, Z. 2012. *Hybrid organic-inorganic pervaporation membranes for desalination.* Citeseer.

References

XU, W. 2001. *Design and development of a pervaporation membrane separation module.* University of Toronto.

YANG, J. S., KIM, H. J., JO, W. H. & KANG, Y. S. 1998. Analysis of pervaporation of methanol-MTBE mixtures through cellulose acetate and cellulose triacetate membranes. *Polymer,* 39**,** 1381-1385.

YOSHIKAWA, M., KUNO, S. I. & KITAO, T. 1994. Specialty polymeric membranes 3. Pervaporation separation of acetic acid/water mixtures through polymeric membranes having a pyridine moiety as a side group. *Journal of applied polymer science,* 51**,** 1021-1027.

YUAN, S. & SCHWARTZBERG, H. Mass transfer resistance in cross membrane evaporation into air. AI Ch. E. Symp. Ser, 1972. 41.

APPENDIX A - ADDITIONAL MEMBRANE PROPERTIES

OVERVIEW

In this Appendix additional membrane information and properties are supplied for the various commercially available polymeric membranes.

A.1. Supplier datasheets

Additional supplier information for each of the commercial membranes are given in Table A.1 to Table A.6. No additional information was available for POL-OL-M1 and POL-AL-M2 from PolyAn GmbH.

Table A.1: Membrane Datasheet: Pervap™ 4100

Membrane	**Pervap™ 4100**
Main application	Standard PVA membrane used for dehydration of volatile organic mixtures
Maximum temperature – Short Term	105 °C
Maximum temperature – Long Term	100 °C
Maximum water content	Up to 30 wt. %
pH	Typical 5 - 8

Table A.2: Membrane Datasheet: Pervap™ 4101

Membrane	**Pervap™ 4101**
Main application	Highly cross-linked PVA membrane for dehydration of reaction mixtures
Maximum temperature – Short Term	105 °C
Maximum temperature – Long Term	100 °C
Maximum water content	up to 50 wt. %
pH	Typical 5 - 8

Table A.3: Membrane Datasheet: Pervap™ 4102

Membrane	**Pervap™ 4102**
Main application	Modified and highly cross-linked membrane used for the dehydration of volatile organic mixtures
Maximum temperature – Short Term	105 °C
Maximum temperature – Long Term	100 °C
Maximum water content	Up to 30 wt. %
pH	Typical 5 - 8

Table A.4: Membrane Datasheet: Pervap™ 4060

Membrane	**Pervap™ 4060**
Main application	Organophilic PDMS membrane to remove trace organics from aqueous solutions
Maximum temperature – Short Term	90 °C
Maximum temperature – Long Term	80 °C
Maximum water content	up to 100 wt.%
pH	Typical 5 - 8

Appendix A – Additional membrane properties

Table A.5: Membrane Datasheet: PEBA

Membrane	**PEBA**
Main application	Recovery of organics from natural feeds or removal of VOC
Maximum temperature – Short Term	80 °C
Maximum temperature – Long Term	70 °C
Maximum water content	Not specified
pH	3-8

Table A.6: Membrane Datasheet: PDMS

Membrane	**PDMS**
Main application	Recovery of organics from natural feeds or removal of VOC
Substrate	PET
Maximum temperature – Short Term	80 °C
Maximum temperature – Long Term	70 °C
Maximum water content	Not specified
pH	1-12

APPENDIX B – ADDITIONAL LITERATURE INFORMATION

OVERVIEW

This Appendix provides additional information that may falls outside the scope of understanding the aim and objectives of this study, which will add to the general understanding of the field. The Appendix is divided into three sub-sections starting with additional membrane properties (Appendix B.1), followed by various pervaporation modules (Appendix B.2) and integrated systems using pervaporation in Appendix B.3.

B.1. Membrane properties

B.1.1. Membrane fouling

Membrane fouling is described as a deposition of impermeable substances in the feed that accumulate on the membrane surface (Buckley-Smith, 2006). Membrane fouling reduces the membrane efficiency by reducing the flux but can itself be reduced by filtering the incoming feed, periodically cleaning the membrane or by creating a turbulent flow regime (Smitha et al., 2004). Baker (2000) states that membrane fouling and concentration polarisation are the two most important factors in general membrane separation. However, it is less of a problem in pervaporation.

B.1.2. Concentration polarisation

Baker (2000) defines concentration polarisation as feed mixture components permeating at different rates and therefore forming concentration gradients in the fluids on both sides of the membrane.

The most common methods to reduce concentration polarisation involve an alteration of the feed flow pattern over the membrane. Some of the mitigation options for either turbulent or laminar flow include feed flow through tubes or fibres, circulatory flow between plates or flow along a spiral cylinder (Matthiasson & Sivik, 1980).

Concentration polarization reduces the rate of separation in the pervaporation processes because of a decreased flux of the more permeable substance and an increased flux of the less permeable substance (Feng and Huang, 1997).

Some researchers in pervaporation (Ravindra, Sridhar, Khan & Rao, 1999; Moulik, Kumar, Bohra & Sridhar, 2015) assumed the effects of concentration polarization to be negligible. In other cases, the feed was continuously stirred to prevent any resulting decrease in flux. Ravindra et al. (1999c) observed an increase in selectivity and flux which they attributed to a reduced degree of concentration polarization.

B.2. Pervaporation modules

One of the criteria for industrial pervaporation operations is to have a large surface area. These membranes need to be installed in an appropriate membrane module with various potential configurations. Some of the main factors in module selection according to (Basile et al., 2015) are membrane packing density, reduced energy consumption and access for membrane cleaning and replacement.

B.2.1. Plate and frame modules

One of the earliest modules developed for pervaporation was the plate-and-frame membrane module with the advantage of ease of construction, operation under harsh conditions and a membrane packing density of between 100-400 m^2/m^3 (Smitha et al., 2004). Basile et al. (2015) reports that this configuration is the most widely used in pervaporation applications. (Shao and Huang, 2007) reported a low transport resistance in these modules that aids the evaporation of permeate through the dense phase membrane. Plate and frame modules are normally more expensive for small scale applications (Xu, 2001).

B.2.2. Spiral wound modules

A spiral wound module makes use of flat sheet membranes with, feed and permeate spacers and wrapped around a perforated tube that creates a flow path for the permeate. Spiral wound modules offer a compact solution (with a packing density of around 900 m^2/m^3) that is easily replaceable and can be scaled up simply by adding additional modules (Mohanty and Purkait, 2011).

B.2.3. Hollow fibre modules

Hollow fibre modules consist of thousands of hollow fibres within a limited space. The feed solution can either flow in radial or parallel mode with respect to the fibre direction. Two main types of geometries are followed in hollow fibre module; (i) a closed-in design mainly used for the separation of gasses into single components; (ii) a second design type that is open at both ends and is normally used for ultrafiltration pervaporation (Xu, 2001). Mohanty and Purkait (2011) report that theoretical packing density could be as high as 10 000 m^2/m^3.

B.2.4. Tubular modules

Tubular membranes are normally associated with inorganic membranes located inside a tube, as they are not self-supporting. The feed is normally from the inside of the membrane, Tubular modules suffer from a low packing density and therefore an increase in capital costs (Mohanty and Purkait, 2011).

B.3. Integrated systems involving pervaporation

The low pressure required by pervaporation is usually provided by a vacuum pump for laboratory applications. For an industrial-scale plant the energy requirements for a vacuum pump would become excessively high.

The phase change from liquid to vapour requires an additional input (enthalpy of vaporisation), leading to a reduction of feed temperature. The effect becomes more prominent in thin and highly permeable membranes (Favre, 2003). On industrial-scale, thermo-driven pervaporation is often used by adding heat exchangers to the feed stream.

In industrial applications were the permeate has no value and can be discarded, using a sweep gas is the preferred (Yuan and Schwartzberg, 1972).

Less frequently used methods like pervaporation with a condensable and both miscible and immiscible carrier as proposed and patented by Robertson (1949) and Friesen et al. (1995) have not been implemented on an industrial-scale and are therefore not discussed in further detail.

A simple improvement to the single stage liquid permeate condensate system is to use either (i) a fractional condensation of permeate; this design adds to the complexity of the system and is therefore not widely used (Baker, 2000) (ii) using a vertical type heat exchanger called a dephlegmator to achieve the required separation (Vane et al., 2004).

Integrated membrane and distillation systems (hybrid systems) have been investigated in literature for numerous years with the main application being to

separate azeotropic- and close boiling point mixtures (Luyben and Chien, 2011). Industrial applications normally require higher flux demands that can be achieved solely by pervaporation. For this reason integrated systems with pervaporation and distillation are preferred in industrial applications (Kujawski, 2000).

Numerous literature studies claim that hybrid systems are beneficial when compared to azeotropic distillation. These studies include: Van Hoof et al. (2004); Sommer and Melin (2004); Fontalvo et al. (2005); Koczka et al. (2007) and Del Pozo Gomez et al. (2009). Various configurations have been proposed, with the majority of the authors selecting to place the pervaporation unit after the distillation column for additional dehydration of the product.

In organic / organic separations hybrid distillation-pervaporation systems are used, especially when trying to break the azeotrope due to increased efficiency (Stephan et al., 1995).

APPENDIX C - MEMBRANE STABILITY TESTING AND CHARACTERISATION

Overview

Detailed results for the membrane stability tests and contact angle characterisation is discussed in this Appendix. This appendix is sub-divided into three main sections that start with the visual stability tests (Section C.1), followed by the mechanical stability tests (Section C.2) and contact angle results in Section C.3.

C.1. Membrane visual stability screening tests

The visual membrane stability testing was performed on all eight polymer membranes. The membranes were soaked in a hydrazine hydrate solution for a period of seven days. The membrane was classified as stable if the active layer did not show any interaction over the period. Typical observations for the eight polymer membranes is shown in Figure C.1 to Figure C.8.

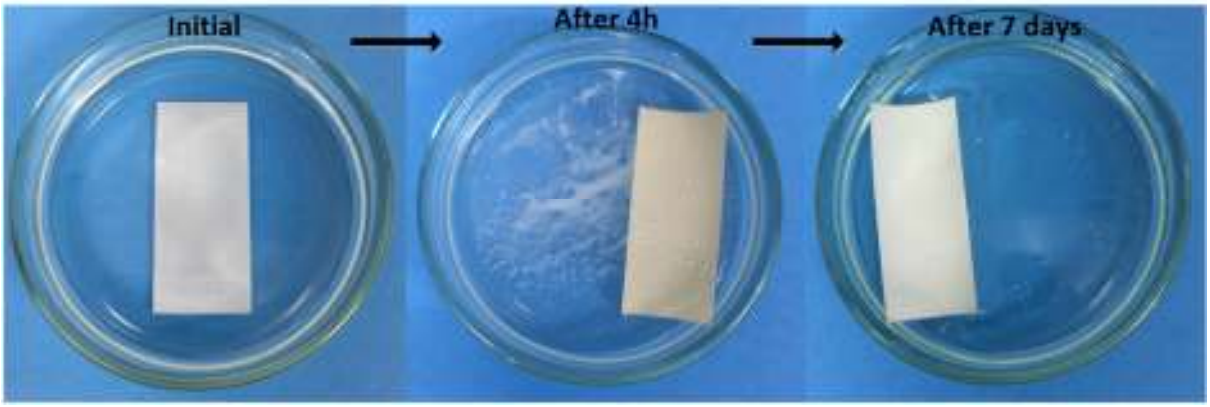

Figure C.1: Visual stability on the Pervap™ 4060 membrane in hydrazine hydrate

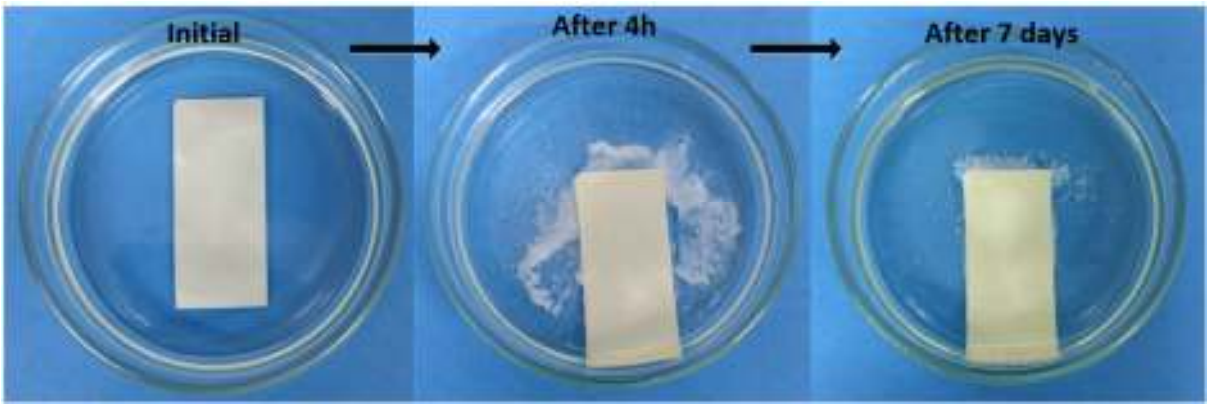

Figure C.2: Visual stability on the Pervap™ 4100 membrane in hydrazine hydrate

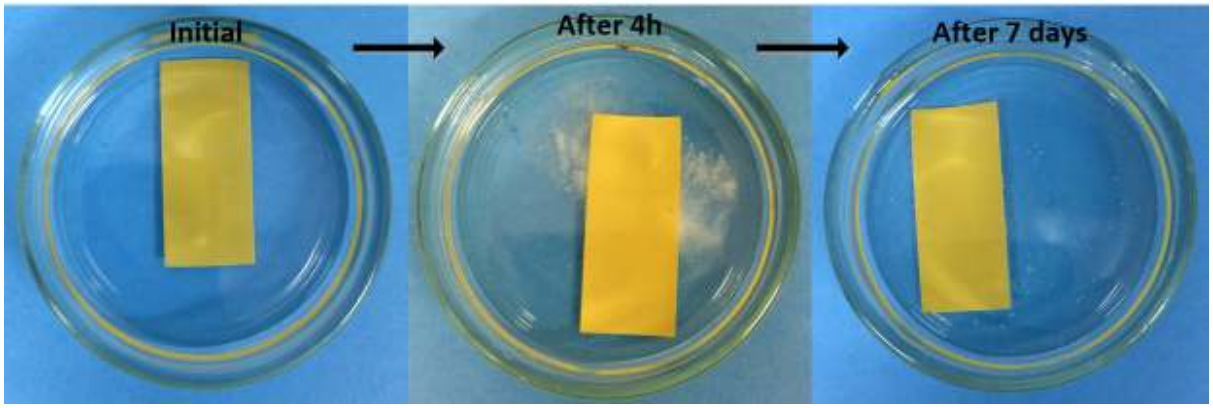

Figure C.3: Visual stability on the Pervap™ 4101 membrane in hydrazine hydrate

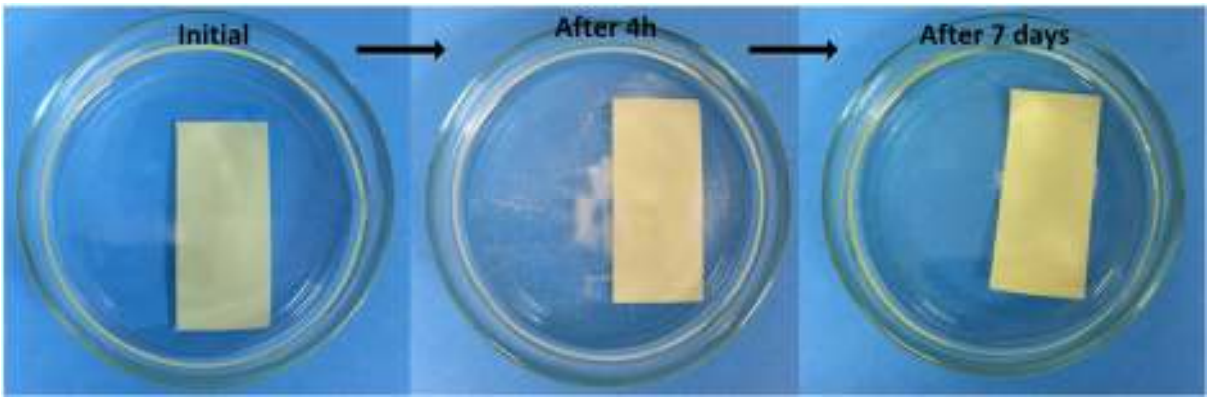

Figure C.4: Visual stability on the Pervap™ 4102 membrane in hydrazine hydrate

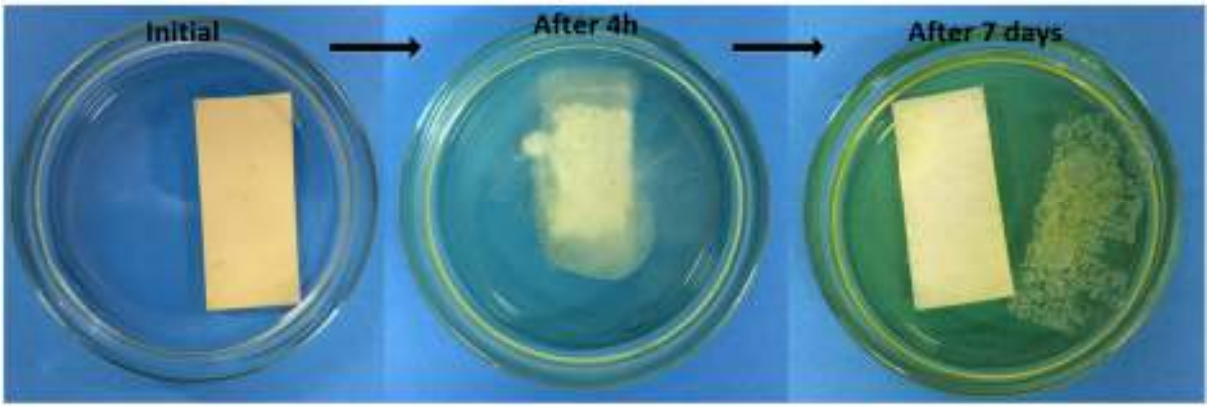

Figure C.5: Visual stability on the Pervatech PEBA membrane in hydrazine hydrate

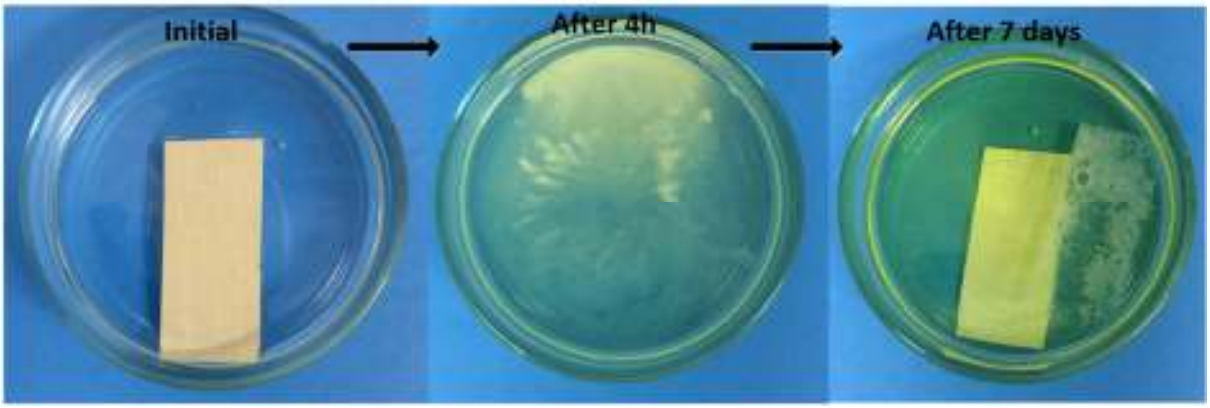

Figure C.6: Visual stability on the Pervatech PDMS membrane in hydrazine hydrate

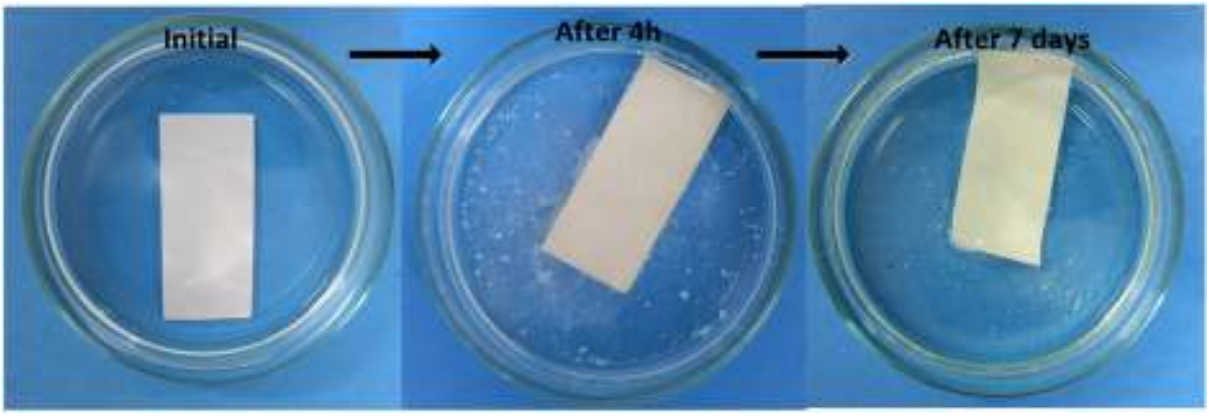

Figure C.7: Visual stability on the POL-Al-M2 membrane in hydrazine hydrate

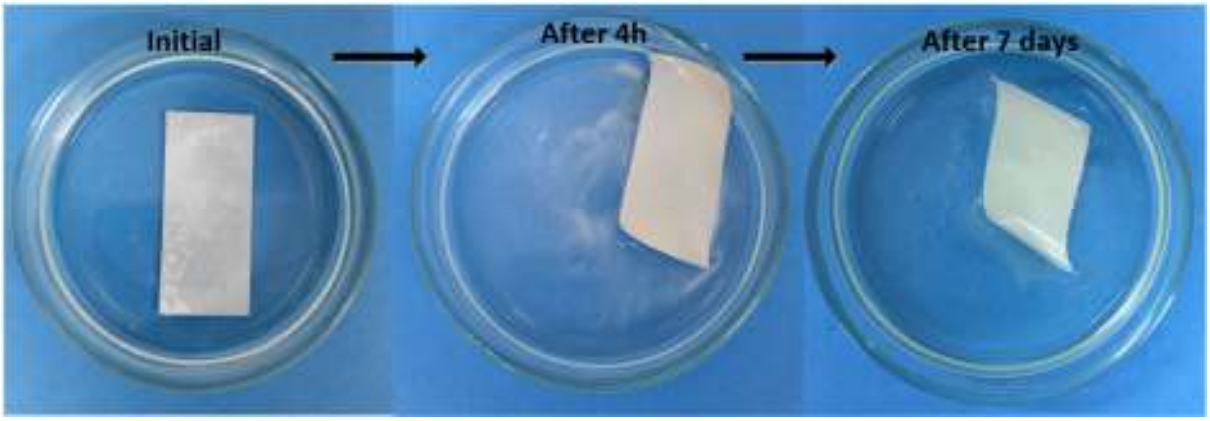

Figure C.8: Visual stability on the POL-OL-M1 membrane in hydrazine hydrate

C.2. Membrane mechanical stability testing

The membrane tensile strength was measured before and after exposing the various membranes to hydrazine monohydrate for a period of seven days using the experimental setup as described in Section 4.2.2 with the detail results given in Table C.1.

Table C.1: Membrane tensile strength testing results

Membrane name	Test number	Initial tensile strength [MPa]	Final tensile strength [MPa]	Variance in tensile strength [%]
Pervap™ 4060	**Ave**	**30.1**	**26.5**	**88%**
	Test 1	30.3	26.7	
	Test 2	26.7	26.3	
	Test 3	33.4	26.5	
Pervap™ 4100	**Ave**	**27.9**	**23.7**	**85%**
	Test 1	27.5	23.9	
	Test 2	28.5	23.8	
	Test 3	27.7	23.4	
Pervap™ 4101	**Ave**	**39.3**	**37.3**	**95%**
	Test 1	37.6	39.8	
	Test 2	40.6	37.80	
	Test 3	39.8	34.3	
Pervap™ 4102	**Ave**	**27.5**	**26.2**	**95%**
	Test 1	27.4	27.5	
	Test 2	28.0	24.5	
	Test 3	27.0	26.5	
POL-AL-M2	**Ave**	**49.7**	**38.1**	**77%**
	Test 1	50.1	40.2	
	Test 2	48.5	38.8	
	Test 3	50.4	35.4	
POL-OL-M1	**Ave**	**31.6**	**22.9**	**72%**
	Test 1	36.0	23.0	
	Test 2	29.4	22.9	
	Test 3	29.4	22.8	

C.3. Membrane contact angle characterisation testing

The contact angle was measured for various concentrations (36, 59, 69 80 and 100 wt. % water at ambient temperature (25°C) according to the experimental procedure described in Section 4.4. The results are shown in Table C.2 and Table C.3.

Table C.2: Contact angle results for 100, 80 and 69 wt. % water

Membrane	100 wt. % water					80 wt. % water					69 wt. % water				
	Nr.	Theta Left	Theta Right	Ave Theta	Contact Angle	Nr.	Theta Left	Theta Right	Ave Theta	Contact Angle	Nr.	Theta Left	Theta Right	Ave Theta	Contact Angle
Pervap™ 4060	**Ave**	**107**	**106**	**107**	**73**	**Ave**	**113**	**110**	**112**	**68**	**Ave**	**133**	**138**	**135**	**45**
Pervap™ 4060	1	100	107	104	76	1	107	105	106	74	1	135	133	134	46
Pervap™ 4060	2	110	107	108	72	2	119	116	117	63	2	131	143	137	43
Pervap™ 4060	3	111	104	108	72	3	110	108	109	71	-	-	-	-	-
Pervap™ 4100	**Ave**	**129**	**128**	**129**	**51**	**Ave**	**146**	**137**	**142**	**38**	**Ave**	**142**	**142**	**142**	**38**
Pervap™ 4100	1	123	135	129	51	1	146	135	140	40	1	144	144	144	36
Pervap™ 4100	2	135	133	134	46	2	142	146	144	36	2	143	141	142	38
Pervap™ 4100	3	124	127	125	55	3	150	130	140	40	3	141	142	141	39
Pervap™ 4101	**Ave**	**105**	**112**	**108**	**72**	**Ave**	**123**	**121**	**122**	**58**	**Ave**	**139**	**134**	**140**	**40**
Pervap™ 4101	1	105	116	111	70	1	137	122	129	51	1	138	138	138	42
Pervap™ 4101	2	104	109	106	74	2	123	125	124	56	2	140	122	140	40
Pervap™ 4101	3	109	118	113	67	3	112	120	116	64	3	140	143	141	39
Pervap™ 4102	**Ave**	**122**	**116**	**119**	**61**	**Ave**	**147**	**149**	**148**	**32**	**Ave**	**131**	**132**	**132**	**48**
Pervap™ 4102	1	122	119	120	60	1	147	148	148	32	1	145	143	144	36
Pervap™ 4102	2	128	119	124	56	2	148	150	149	31	2	123	126	125	55
Pervap™ 4102	3	122	118	120	60	3	146	148	147	33	3	127	127	127	53
Pervap™ 4102	4	115	110	113	67	4	146	150	148	32	-	-	-	-	-
Pol-AL-M2	**Ave**	**107**	**110**	**109**	**71**	**Ave**	**134**	**139**	**136**	**44**	**Ave**	**138**	**129**	**134**	**46**
Pol-AL-M2	1	103	105	104	76	1	130	146	138	42	1	126	118	122	58
Pol-AL-M2	2	115	114	114	66	2	138	132	135	45	2	151	141	146	34
Pol-AL-M2	3	114	115	114	66	-	-	-	-	-	-	-	-	-	-
Pol-OL-M1	**Ave**	**126**	**130**	**128**	**52**	**Ave**	**136**	**129**	**133**	**47**	**Ave**	**143**	**137**	**140**	**40**
Pol-OL-M1	1	121	127	124	56	1	140	126	133	47	1	139	139	139	41
Pol-OL-M1	2	119	127	123	57	2	132	132	132	48	2	147	134	141	39
Pol-OL-M1	3	138	138	138	42										

Table C.3: Contact angle results for 59 and 36 wt. % water

Membrane	59 wt. % water					36 wt. % water				
	Nr.	Theta Left	Theta Right	Ave Theta	Contact Angle	Nr.	Theta Left	Theta Right	Ave Theta	Contact Angle
Pervap™ 4060	**Ave**	**135**	**125**	**130**	**50**	**Ave**	**154**	**131**	**142**	**38**
Pervap™ 4060	1	142	111	126	54	1	155	137	146	34
Pervap™ 4060	2	136	133	135	45	2	154	129	141	39
Pervap™ 4060	3	128	132	130	50	3	153	127	140	40
Pervap™ 4100	**Ave**	**126**	**126**	**130**	**50**	**Ave**	**159**	**143**	**151**	**29**
Pervap™ 4100	1	125	113	125	55	1	168	118	143	37
Pervap™ 4100	2	114	124	124	56	2	167	138	153	27
Pervap™ 4100	3	138	142	142	38	3	161	153	157	23
Pervap™ 4101	**Ave**	**122**	**109**	**116**	**64**	**Ave**	**155**	**155**	**155**	**25**
Pervap™ 4101	1	129	113	121	59	1	148	153	150	30
Pervap™ 4101	2	127	113	120	60	2	152	153	153	27
Pervap™ 4101	3	112	103	108	73	3	157	161	159	21
Pervap™ 4101	-	-	-	-	-	4	160	157	159	21
Pervap™ 4102	**Ave**	**131**	**134**	**132**	**48**	**Ave**	**131**	**154**	**143**	**37**
Pervap™ 4102	1	125	143	134	46	1	142	147	145	35
Pervap™ 4102	2	137	122	129	51	2	115	166	141	39
Pervap™ 4102	3	130	137	134	46	3	136	150	143	37
Pol-AL-M2	**Ave**	**142**	**123**	**133**	**47**	**Ave**	**158**	**86**	**122**	**58**
Pol-AL-M2	1	131	112	131	49	1	163	40	102	78
Pol-AL-M2	2	153	134	134	46	2	154	131	142	38
Pol-OL-M1	**Ave**	**128**	**125**	**127**	**53**	**Ave**	**143**	**132**	**137**	**43**
Pol-OL-M1	1	130	124	127	53	1	146	139	143	37
Pol-OL-M1	2	123	119	121	59	2	137	122	129	51
Pol-OL-M1	3	132	133	133	47	3	145	135	140	40

APPENDIX D - PERVAPORATION RESULTS

OVERVIEW

This Appendix provides the detail results obtained from the pervaporation experiments. Appendix D is subdivided into three subsections starting with the measure pervaporation results (Section D.1), followed by the pervaporation sample calculations for membrane flux and selectivity (Section D.2). The calculated pervaporation are supplied in Section D.3.

D.1. Pervaporation measured results

D.1.1. Pervaporation measured results for screening tests

The raw data for the pervaporation screening tests performed at 50 °C on all stable membranes are shown in Table D.1. The sample cumulative time in minutes, sample mass collected that permeated through each membrane (g/h) and permeate water fraction was reported for each test.

Table D.1: Measured pervaporation results for screening tests at 50 °C

POL-OL-M1[1]			POL-AL-M2			Pervap™ 4060		
Time [min]	Sample mass [g/h]	Permeate water fraction	Time [min]	Sample mass [g/h]	Permeate water fraction	Time [min]	Sample mass [g/h]	Permeate water fraction
30	7.12	-	30	11.75	0.479	60	1.89	0.428
57	16.40	-	60	14.94	0.454	120	2.01	0.417
87	15.90	-	90	10.71	0.490	180	1.96	0.433
117	12.92	-	120	12.13	-	240	1.78	0.440
147	16.07	-	150	10.61	-	270	2.14	0.414
177	12.10	0.456	-	-	-	300	1.94	-
207	13.69	0.431	-	-	-	-	-	-
237	11.57	-	-	-	-	-	-	-

[1] Screening tests done at 30 °C

Table D.1 (cont.): Measured pervaporation results for screening tests at 50 °C

Pervap™ 4100			Pervap™ 4101			Pervap™ 4102		
Time [min]	Sample mass [g/h]	Permeate water fraction	Time [min]	Sample mass [g/h]	Permeate water fraction	Time [min]	Sample mass [g/h]	Permeate water fraction
20	3.26	-	30	5.02	-	160	1.57	0.570
60	3.06	-	60	2.80	-	220	1.69	0.518
80	3.55	-	90	2.43	-	280	1.89	0.511
100	2.68	0.194	120	2.30	0.480	340	1.97	0.506
120	3.01	0.167	150	2.34	-	370	1.86	0.490
140	3.02	-	180	2.62	-	-	-	-
160	3.02	-	210	2.62	0.500	-	-	-
-	-	-	240	2.57	0.471	-	-	-
-	-	-	270	2.59	-	-	-	-

D.1.2. Pervaporation measured results for Pervap™ 4101

The raw data for the pervaporation characterisation tests on Pervap™ 4101 membrane with constant temperature in each test are shown in Table D.2 (30 °C), Table D.3 (40 °C), Table D.4 (50 °C) and Table D.6 (60 °C). The sample cumulative time in minutes, sample mass collected that permeated through each membrane (g/h) and permeate water fraction was reported for each test.

Table D.2: Measured pervaporation results for Pervap™ 4101 at 30 °C

70 wt. % water			59 wt. % water			44 wt. % water		
Time [Min]	Mass permeated [g/h]	Permeate water fraction	Time [Min]	Mass permeated [g/h]	Permeate water fraction	Time [Min]	Mass permeated [g/h]	Permeate water fraction
60	0.30	0.95	60	0.25	0.82	60	0.27	0.78
120	0.22	0.97	120	0.21	0.82	120	0.26	0.78
240	0.27	0.97	180	0.22	0.82	180	0.29	0.79
300	0.27	0.98	300	0.21	0.84	240	0.33	0.81
-	-		-	-	-	300	0.30	0.79

Table D.3: Measured pervaporation results for Pervap™ 4101 at 40 °C

69 wt. % water			57 wt. % water			62 wt. % water		
Time [Min]	Mass permeated [g/h]	Permeate water fraction	Time [Min]	Mass permeated [g/h]	Permeate water fraction	Time [Min]	Mass permeated [g/h]	Permeate water fraction
60	0.46	0.96	45	0.92	0.71	60	0.43	0.77
120	0.43	0.97	90	0.83	0.74	120	0.46	0.77
180	0.46	0.97	135	0.79	0.72	180	0.48	0.79
223	0.45	0.98	180	0.77	0.78	240	0.48	0.69

Table D.4: Measured pervaporation results for Pervap™ 4101 at 50 °C

79 wt. % water			70 wt. % water			59 wt. % water			59 wt. % water		
Time [Min]	Mass permeated [g/h]	Permeate water fraction	Time [Min]	Mass permeated [g/h]	Permeate water fraction	Time [Min]	Mass permeated [g/h]	Permeate water fraction	Time [Min]	Mass permeated [g/h]	Permeate water fraction
60	0.94	0.97	60	0.64	0.93	40	5.40		150	0.60	0.85
120	0.94	0.98	120	0.71	0.97	80	4.58		210	0.59	0.89
177	0.93	0.99	180	0.71	0.97	140	2.82	0.55	270	0.56	0.83
237	0.94	-	240	0.70	0.97	180	0.81	0.66	330	0.58	0.87
-	-	-	300	0.72	0.97	220	0.62	0.77	390	0.60	0.86
-	-	-	-	-	-	280	0.58	0.80	450	0.59	0.88
-	-	-	-	-	-	340	0.58	0.86	-	-	-
-	-		-	-	-	395	0.57	0.86	-	-	-

Table D.4 (cont.): Measured pervaporation results for Pervap™ 4101 at 50 °C

59 wt. % water			57 wt. % water			47 wt. % water			38 wt. % water		
Time [Min	Mass permeated [g/h]	Permeate water fraction	Time [Min]	Mass permeated [g/h]	Permeate water fraction	Time [Min]	Mass permeated [g/h]	Permeate water fraction	Time [Min]	Mass permeated [g/h]	Permeate water fraction
150	0.72	0.89	150	0.83	0.86	150	0.65	0.67	30	5.02	-
210	0.71	0.89	210	0.78	0.85	210	0.79	0.65	60	2.80	-
270	0.68	0.90	270	0.75	0.83	270	0.97	-	90	2.43	-
330	0.71	0.89	330	0.69	0.88	330	0.74	0.65	120	2.30	0.48
390	0.70	0.89	-	-	-	390	0.74	0.67	150	2.34	-
-	-	-	-	-	-	-	-	-	180	2.62	-
-	-	-	-	-	-	-	-	-	210	2.62	0.50
-	-	-	-	-	-	-	-	-	240	2.57	0.47

Table D.5: Measured pervaporation results for Pervap™ 4101 at 60 °C

70 wt. % water			55 wt. % water			45 wt. % water		
Time [Min]	Mass permeated [g/h]	Permeate water fraction	Time [Min]	Mass permeated [g/h]	Permeate water fraction	Time [Min]	Mass permeated [g/h]	Permeate water fraction
20	1.36	0.88	20	1.36	0.76	20	1.36	0.67
40	1.61	0.88	40	1.61	0.76	40	1.61	0.64
60	1.66	0.87	60	1.66	0.76	60	1.66	0.67
80	1.64	-	80	1.64	-	70	1.64	-

D.2. Pervaporation sample calculations

One complete pervaporation calculation is given in the following section. The section is subdivided into calculating the total membrane flux (Section D.2.1) and secondly calculating the membrane selectivity (α). The sample data in Table D.6 for the calculation was obtained from the raw experimental data with the feed temperature of 50 °C and 59 wt. % water.

Table D.6: Sample data for pervaporation sample calculations at 50 °C and 59 wt. % water

Time (min)	Cumulative time (min)	Mass permeated (g)	Permeate water fraction
60	150	0.72	0.89
60	210	0.71	0.89
60	270	0.68	0.90
60	330	0.71	0.89
60	390	0.70	0.89

D.2.1. Sample calculation for total membrane flux

The permeation flux denotes the rate of a specific compound permeating per unit surface area for a given membrane as:

$$J = \frac{Q}{A_m . t} \tag{D-1}$$

where J ($kg \cdot m^{-2} \cdot h^{-1}$) is the membrane flux, Q (kg) the mass of permeate collected, A_m (m^2) the membrane effective area and t (h) the time:

$$J_T = \frac{0.72\text{g x } \frac{1\text{ kg}}{1000\text{g}}}{0.00541\text{ x}60\text{ min x } \frac{1\text{h}}{60\text{min}}} = 0.133\ \frac{\text{kg}}{\text{m}^2.\text{h}}$$

The water and hydrazine partial fluxes are the product of the total flux (J_T) and the component mass fraction ($\gamma_{\text{hydrazine}}$ or γ_{water}) with the following calculation:

$$J_{water} = J_T \cdot y_{water} \tag{D-2}$$

$$J_{hydrazine} = J_T \cdot y_{hydrazine} \tag{D-3}$$

The sample calculation for the partial hydrazine flux is:

$$J_{water} = J_T \cdot y_{water} = 0.133 \text{ x } 0.89 = 0.118$$

The hydrazine flux can then be calculated either from Equation D-3 or flow subtracting the hydrazine partial flux from the total flux ($J_{hydrazine} = J_T - J_{hydrazine}$).

D.2.2. Sample calculation for membrane selectivity

The membrane selectivity (α) is calculated using the feed and permeate concentrations as shown below:

$$\alpha = \frac{X_i \,.\, Y_j}{X_j \,.\, Y_i} = \frac{Y_i \,/\, (1 - Y_i)}{X_i \,/\, (1 - X_i)} \tag{D-4}$$

$$\alpha = \frac{0.109/\,(1 - 0.109)}{0.64/\,(1 - 0.64)} = 5.63$$

D.3. Pervaporation calculated results

D.3.1 Pervaporation calculated results for screening tests

The calculated pervaporation results obtained by using the raw screening data for membranes (POL-OL-M1, POL-AL-M2, Pervap™ 4060, 4100, 4101 and 4102) at 50 °C and 36 wt. % water from Table D.1 are shown in Table D.7.

Table D.7: Calculated pervaporation total flux and selection results for screening tests at 50 °C

POL-OL-M1[1]			POL-AL-M2			Pervap™ 4060		
Time [min]	Total Flux [kg·m^{-2}·h^{-1}]	Select. [-]	Time [min]	Total Flux [kg·m^{-2}·h^{-1}]	Select. [-]	Time [min]	Total Flux [kg·m^{-2}·h^{-1}]	Select. [-]
30	1.32	-	30	2.17	1.16	60	0.35	1.32
57	3.03	-	60	2.76	1.04	120	0.37	1.26
87	2.94	-	90	1.98	1.21	180	0.36	1.35
117	2.39	-	120	2.24	-	240	0.33	1.38
147	2.97	-	150	1.96	-	270	0.39	1.24
177	2.24	1.19	-	-	-	300	0.36	-
207	2.53	1.08	-	-	-	-	-	-
237	2.14	-	-	-	-	-	-	-
SS	**2.30**	**1.14**		**2.06**	**1.14**		**0.36**	**1.33**

Table D.7 (cont.): Calculated pervaporation total flux and selection results for screening tests at 50 °C

Pervap™ 4100			Pervap™ 4101			Pervap™ 4102		
Time [min]	Total Flux [kg·m^{-2}·h^{-1}]	Selectivity [-]	Time [min]	Total Flux [kg·m^{-2}·h^{-1}]	Selectivity [-]	Time [min]	Total Flux [kg·m^{-2}·h^{-1}]	Selectivity [-]
20	0.60	-	30	0.93	-	160	0.29	2.06
60	0.56	-	60	0.52	-	220	0.31	1.67
80	0.66	-	90	0.45	-	280	0.35	1.62
100	0.49	0.81	120	0.43	1.54	340	0.36	1.59
120	0.56	0.83	150	0.43	-	370	0.34	1.49
140	0.56	-	180	0.48	-	-	-	-
160	0.56	-	210	0.48	1.67	-	-	-
-	-	-	240	0.47	1.48	-	-	-
SS	**0.56**	**0.82**		**0.48**	**1.58**		**0.35**	**1.57**

A summary of the steady state results from Table D.7 are shown in Table D.8.

Table D.8: Calculated pervaporation results for PSI and partial component fluxes for screening tests at 50 °C

Membrane	PSI	Water Flux [kg·m^{-2}·h^{-1}]	Hydrazine Flux [kg·m^{-2}·h^{-1}]
POL-OL-M1	2.62	1.02	1.28
POL-AL-M2	2.34	0.98	1.08
Pervap™ 4060	0.48	0.15	0.21
Pervap™ 4100	0.46	0.10	0.46
Pervap™ 4101	0.76	0.23	0.25
Pervap™ 4102	0.55	0.18	0.18

D.3.2 Pervaporation calculated results for Pervap™ 4101

The calculated pervaporation results obtained by using the raw data for Pervap™ 4101 membrane at 30, 40, 50 and 60 °C and various water feed concentrations from Table D.2 to Table D.5 are shown in Table G.9 to Table D.18.

Table D.9: Calculated pervaporation total flux and selection results for Pervap™ 4101 at 30 °C

70 wt. % water			59 wt. % water			44 wt. % water		
Time [Min]	Total flux [kg/m^2.h]	Selectivity α [-]	Time [Min]	Total flux [kg/m^2.h]	Selectivity α [-]	Time [Min]	Total flux [kg/m^2.h]	Selectivity α [-]
60	0.05	8.08	60	0.05	3.25	60	0.05	4.59
120	0.04	16.05	120	0.04	3.11	120	0.05	4.41
240	0.05	13.78	180	0.04	3.26	180	0.05	4.62
300	0.05	19.54	300	0.04	3.61	240	0.06	5.41
-	-	-	-	-	-	300	0.05	4.86
SS	**0.05**	**16.46**	**SS**	**0.04**	**3.32**	**SS**	**0.06**	**4.96**

Table D.10: Calculated pervaporation results for PSI and partial component fluxes for Pervap™ 4101 at 30 °C

Feed water	70 wt. %	41 wt. %	44 wt. %
PSI	0.78	0.13	0.28
Water flux [kg/m2.h]	0.0459	0.0324	0.0448
Hydrazine flux [kg/m2.h]	0.0012	0.0068	0.0114

Table D.11: Calculated pervaporation total flux and selection results for Pervap™ 4101 at 40 °C

69 wt. % water			57 wt. % water			62 wt. % water		
Time [Min]	**Total flux [kg/m².h]**	**Selectivity α [-]**	**Time [Min]**	**Total flux [kg/m².h]**	**Selectivity α [-]**	**Time [Min]**	**Total flux [kg/m².h]**	**Selectivity α [-]**
60	0.09	12.17	45	0.17	1.71	60	0.08	4.52
120	0.08	14.64	90	0.15	1.92	120	0.08	4.52
180	0.08	14.43	135	0.15	1.82	180	0.09	5.12
223	0.08	27.59	180	0.14	2.50	240	0.09	3.05
SS	**0.08**	**13.75**	**SS**	**0.15**	**2.08**	**SS**	**0.09**	**4.23**

Table D.12: Calculated pervaporation results for PSI and partial component fluxes for Pervap™ 4101 at 40 °C

Feed water	**69 wt. %**	**69 wt. %**	**69 wt. %**
PSI	1.13	0.31	0.37
Water flux [kg/m2.h]	0.0802	0.1099	0.0651
Hydrazine flux [kg/m2.h]	0.0021	0.0372	0.0219

Table D.13: Calculated pervaporation total flux and selection results for Pervap™ 4101 at 60 °C

70 wt. % water			55 wt. % water			47 wt. % water		
Time [Min]	**Total flux [kg/m².h]**	**Selectivity α [-]**	**Time [Min]**	**Total flux [kg/m².h]**	**Selectivity α [-]**	**Time [Min]**	**Total flux [kg/m².h]**	**Selectivity α [-]**
20	0.28		20	0.26		20	0.25	2.55
40	0.25		40	0.22		40	0.30	2.20
60	0.24	3.05	60	0.22	2.95	60	0.31	2.48
80	0.24	3.00	80	0.22	2.90	70	0.30	-
SS	**0.2433**	**3.05**	**SS**	**0.2200**	**2.95**	**SS**	**0.3024**	**2.41**

Table D.14: Calculated pervaporation results for PSI and partial component fluxes for Pervap™ 4101 at 60 °C

Feed water	**70 wt. %**	**55 wt. %**	**47 wt. %**
PSI	0.74	0.65	0.73
Water flux [kg/m2.h]	0.1217	0.1320	0.1992
Hydrazine flux [kg/m2.h]	0.1217	0.0880	0.1032

Table D.15: Calculated pervaporation total flux and selection results for Pervap™ 4101 at 50 °C

79 wt. % water			70 wt. % water			59 wt. % water			58 wt. % water		
Time [Min]	**Total flux [kg/m².h]**	**Selectivity α [-]**	**Time [Min]**	**Total flux [kg/m².h]**	**Selectivity α [-]**	**Time [Min]**	**Total flux [kg/m².h]**	**Selectivity α [-]**	**Time [Min]**	**Total flux [kg/m².h]**	**Selectivity α [-]**
60	0.17	8.80	60	0.07	0.12	40	-	-	143	-	-
120	0.17	12.22	120	0.03	0.13	80	-	-	203	0.18	3.14
177	0.17	19.47	180	0.03	0.13	140	0.45	0.86	263	0.40	1.06
237	0.17	-	240	0.03	0.13	180	0.34	1.35	323	0.17	3.44
5	-	-	300	0.03	0.13	220	0.23	2.34	383	0.17	3.57
6	-	-	-	-	-	280	0.20	2.70	443	0.19	3.11
7	-	-	-	-	-	340	0.14	4.14	-	-	-
8	-	-	-	-	-	395	0.14	4.12	-	-	-
SS	**0.1733**	**15.84**	SS	**0.0285**	**0.13**	**SS**	**0.1920**	**3.65**	**SS**	**0.1742**	**3.37**

Table D.16: Calculated pervaporation results for PSI and partial component fluxes for Pervap™ 4101 at 50 °C

Feed water	79 wt. %	70 wt. %	59 wt. %	58 wt. %
PSI	2.75	0.00	0.70	0.59
Water flux [kg/m2.h]	0.1697	0.0079	0.0779	0.0661
Hydrazine flux [kg/m2.h]	0.0036	0.0207	0.1141	0.1081

Table D.17: Calculated pervaporation total flux and selection results for Pervap™ 4101 at 50 °C - continued

59 wt. % water			57 wt. % water			47 wt. % water			38 wt. % water		
Time [Min]	**Total flux [kg/m².h]**	**Selectivity α [-]**	**Time [Min]**	**Total flux [kg/m².h]**	**Selectivity α [-]**	**Time [Min]**	**Total flux [kg/m².h]**	**Selectivity α [-]**	**Time [Min]**	**Total flux [kg/m².h]**	**Selectivity α [-]**
150	0.13	5.63	150	0.15	4.68	150	0.12	2.29	30	0.93	-
210	0.13	5.59	210	0.14	4.19	210	0.15	2.08	60	0.52	-
270	0.13	6.26	270	0.14	3.55	270	0.18	-	90	0.45	-
330	0.13	5.49	330	0.13	5.22	330	0.14	2.11	120	0.43	1.54
390	0.13	5.61	-	-	-	390	0.14	2.24	150	0.43	-
-	-	-	-	-	-	-	-	-	180	0.48	-
-	-	-	-	-	-	-	-	-	210	0.48	1.67
-	-	-	-	-	-	-	-	-	240	0.47	1.48
SS	**0.1284**	**5.79**	**SS**	**0.1369**	**4.32**	**SS**	**0.1368**	**2.14**	**SS**	**0.4813**	**1.58**

Table D.18: Calculated pervaporation results for PSI and partial component fluxes for Pervap™ 4101 at 50 °C - continued

Feed water	59 wt. %	57 wt. %	47 wt. %	38 wt. %
PSI	0.74	0.59	0.29	0.75
Water flux [kg/m2.h]	0.1147	0.1165	0.0896	0.23
Hydrazine flux [kg/m2.h]	0.0137	0.0204	0.0472	0.24

APPENDIX E - SORPTION RESULTS

OVERVIEW

This Appendix provides the detail results obtained from the sorption experiments during this study. This Appendix is sub-divided into three sections with the raw sorption results in Section E.1 given first, followed by a sample sorption calculation in Section E.2 for both membrane swelling ration and sorption selectivity. The last sub-section is the detailed sorption calculation results (Section E.3).

E.1. Sorption measured results

The sorption experiments were conducted using a feed water concentration between 36 and 100 wt. %., while the temperatures were varied between 30 and 50 °C. The detailed experimental results for 36 wt. % water is given in Table E.1, while the results for 59 wt. % water is given in Table E.2, 69 wt.% water in Table E.3 and 100 wt.% water in Table E.4.

Table E.1: Sorption experiment measured results for 36 wt. % water

Mass fraction water in feed [wt. %]	Temp [°C]	Membrane mass dry [g]	Membrane mass swollen [g]	Mass fraction water in membrane [wt. %]
36	50	0.1258 0.1220	0.2192 0.2340	71
36	50	0.1222 0.1149	0.2292 0.2079	59
36	50	0.1048 0.1219	0.1989 0.2183	62
36	50	0.1163 0.1161	0.1161 0.2132	52
36	50	0.1165 0.1155	0.2044 0.2050	62
36	50	0.1225 0.1223	0.2166 0.2276	65
36	40	0.1147 0.1132 0.1170	0.1888 0.1918 0.1986	63
36	40	0.1181 0.1643	0.1885 0.2758	66
36	40	0.1578 -	0.2910 -	63
36	30	0.1201 -	0.2001 -	-
36	30	0.1201 0.1197 0.1221	0.2036 0.2012 0.2056	66
36	30	0.1207 0.1151	0.2157 0.1932	59
36	30	0.1142 0.1142	0.1931 0.1852	61

Table E.2: Sorption experiment measured results for 59 wt. % water

Mass fraction water in feed [wt. %]	Temp [°C]	Membrane mass dry [g]	Membrane mass swollen [g]	Mass fraction water in membrane [wt. %]
59	50	0.1705 -	0.275 -	-
59	50	0.2100 -	0.3308 -	-
59	50	0.1627 0.1627	0.2677 0.2708	67
59	50	0.2130 -	0.3325 -	68
59	50	0.2242 -	0.356 -	68
59	50	0.1624 -	0.2635 -	64

Table E.3: Sorption experiment measured results for 69 wt. % water

Mass fraction water in feed [wt. %]	Temp [°C]	Membrane mass dry [g]	Membrane mass swollen [g]	Mass fraction water in membrane [wt. %]
69	50	0.1574 -	0.2602 -	73
69	50	0.1988 -	0.2784 -	63
69	50	0.1511 -	0.2512 -	67
69	50	0.2038 -	0.3027 -	69

Table E.4: Sorption experiment measured results for 100 wt. % water

Mass fraction water in feed [wt. %]	Temp [°C]	Membrane mass dry [g]	Membrane mass swollen [g]	Mass fraction water in membrane [wt. %]
100	30	0.0275	0.0453	100
100	40	0.0314	0.0476	100
100	50	0.0307	0.0469	100

E.2. Sample sorption sample calculations

One complete sorption calculation will be demonstrated in the following section. The section is subdivided into calculating the membrane swelling ratio as well as the sorption selectivity. The sample data for the calculation was obtained from the raw

experimental data in Table E.1 with a summary of the calculated results summarised in Section E.3.

E.2.1. Sorption sample calculation of the swelling ratio

The percentage sorption can be calculated by the equation:

$$\% \text{ Sorption} = \frac{M_s - M_d}{M_d} \text{ x } 100\ \% \tag{4-2}$$

where M_s and M_d are the mass of the swollen and dry membrane strips respectively. The first data point from TableE.1 is used for the sample calculation:

$$\% \text{ Sorption} = \frac{0.2192 - 0.1258}{0.1258} \text{ x } 100\ \% = 74.2\ \%$$

E.2.2. Sample calculations of the sorption selectivity

The sorption water selectivity (α_s) for a binary mixture can be calculated using:

$$\alpha_s = \frac{X_i \,.\, Y_j}{X_j \,.\, Y_i} = \frac{Y_{water} \,/\, (1 - Y_{water})}{X_{water} \,/\, (1 - X_{water})} \tag{4-3}$$

where Y_{water} and X_{water} is the mass fraction water in the membrane and feed respectively. The sample calculations of the sorption selectivity again using the first data point from Table E.1.

$$\alpha_s = \frac{0.71/(1 - 0.71)}{0.36/(1 - 0.36)} = 4.35$$

E.3. Sorption calculated results

Each experiment in this section has been repeated several times at the same experimental conditions to increase the reliability of the results. This chapter only contains the average value for each experimental condition. The calculated results from the raw experimental data in Table E.1 to Table E.4 are summarised in Table E.5

Table E.5: Sorption experiment calculated results

Mass fraction hydrazine feed	Temp (°C)	Membrane mass dry (g)	Membrane mass swollen (g)	Mass fraction hydrazine in membrane	% Sorption	Degree of swelling	Water selectivity
64%	30	0.1183	0.1997	38%	69%	1.69	2.89
64%	40	0.1309	0.2224	36%	70%	1.70	3.18
64%	50	0.1184	0.2075	38%	75%	1.75	2.86
41%	50	0.1905	0.3055	33%	60%	1.60	1.39
31%	50	0.1778	0.2731	32%	54%	1.54	0.96
0%	50	0.0299	0.0466	0%	56%	1.56	-

APPENDIX F - GAS CHROMATOGRAPH (GC) DATA

Overview

This Appendix consists of a discussion on the concentration determination and analyses of samples with a gas chromatograph (GC). Appendix F is subdivided into three subsections starting with general background information on hydrazine analysis (Section F.1), followed by the calibration curve (Section F.2). This appendix is concluded with the calculation procedure for the composition of hydrazine in Section F.3.

F.1. Background

Hydrazine is a hygroscopic chemical that readily oxidises in ambient air and absorbs carbon dioxide from the air (Schliebs, 1985). Penneman and Audrieth (1948) employed titration to determine hydrazine concentrations with potassium iodate as the titrant. However, Satyanarayana and Bhattacharya (2004) reported that the Penneman method is prone to errors and suggested the use of a gas chromatogram (GC). Several authors such as Dee (1971), Villaluenga and Tabe-Mohammadi (2000) and others (Torres-Alvarez and Wolf-Maciel, Penneman and Audrieth, 1948), on hydrazine analysis confirm that the GC method works for hydrazine concentration determination. The GC method as reported by Gray and Fochtman (1978) was employed for the analysis in this work. In the selected procedure, excess acetone is added to a known volume of sample. The acetone reacts with the hydrazine to form a hydrazone derivative called acetone azine. The reaction is shown in the chemical formula in Figure F.1.

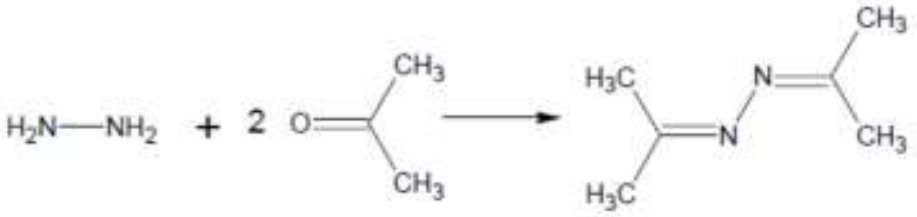

Figure F.1: Chemical formula of hydrazine and acetone to form acetone azine

The acetone serves as a diluent and derivatizing agent while it has a fast reaction rate without interference form the excess acetone (Gray and Fochtman, 1978). According to Gray and Fochtman (1978) the acetone azine is stable for up to 30 days. The stability further increases if the organics are subtracted from the water (Gray and Fochtman, 1978).

F.2. Calibration curve of the Derivative-Acetone

A Scion 436-GC with a flame ionizing detector (FID) was used to analysed samples' concentrations. The GC was fitted with a 30 m GsBP-5™ capillary column from GS-Tek. The column has an internal diameter of 0.32 mm and film thickness of 1 µm.

The injector, detector and oven temperatures were set at 200 °C, 300 °C and ramping from 75 °C to 220 °C for a total analysis time of 5 minutes. Hydrogen was used as carrier gas, synthetic air as the combustion gas and nitrogen as make-up gas. The hydrogen, combustion gas and nitrogen were fed at 3 mL/min, 300 mL/min and 25 mL/min respectively. The split ratio was set at 220. The observed retention times at these conditions was 1.6 minutes for the acetone peak and for 3.1 minutes for the acetone azine peak.

To be able to use the GC as an analytical tool, a calibration curve was required for the specific GC at the conditions mentioned above. The calibration curve was plotted with the y-axis as the area ratio of acetone azine and acetone while the x-axis represents the volume ratio of the hydrazine and acetone. Different mixtures where prepared by diluting hydrazine monohydrate with acetone as per the procedure from Gray and Fochtman (1978). The samples all contained 2 mL hydrazine monohydrate. The acetone volume of the different samples were varied from 8 mL up to 240 mL.

Each sample was injected five times to determine the accuracy of the calibration curve. The experimental error between the injections was below 10 % for each sample. Refer to Section G.2 for details on the calculation method. The average area ratios with the standard deviation and experimental error are shown along with the corresponding volume ratios in Table F.1. The same data are represented in Figure F.2.

Table F.1: Calibration curve data for gas chromatographic analysis

$V_{Hydrazine}/V_{Acetone}$	$A_{Derivative}/A_{Acetone}$	Standard Deviation	95 % Experimental Error
0.16	4.76	0.114	5.4 %
0.13	2.75	0.078	6.4 %
0.11	1.48	0.100	9.5 %
0.08	0.79	0.025	7.2 %
0.04	0.27	0.002	2.0 %
0.02	0.13	0.004	4.0 %
0.01	0.06	0.002	6.8 %
0.005	0.03	0.001	4.9 %
0.0027	0.02	0.0001	1.4 %

A third order polynomial fit (with an R^2 value of 0.9972) was used to determine the equation represented by the calibration curve. This equation was used to determine the concentration of the samples obtained during the pervaporation experiments.

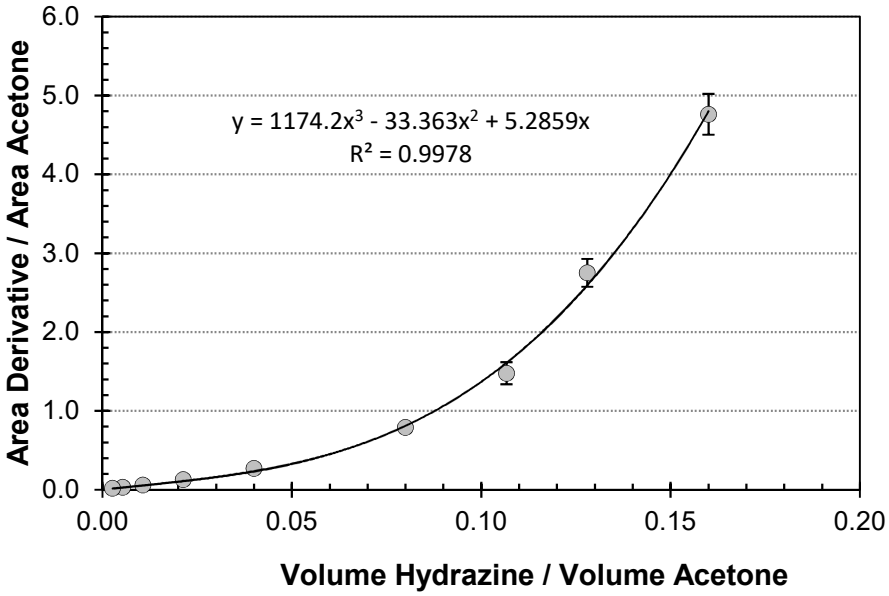

Figure F.2: Calibration curve for Acetone-Hydrazine Azine mixtures

In Figure F.2 the error bars indicate the effect of the 95 % experimental error. It should be noted that at higher concentrations hydrazine the experimental error results in larger values for the variance from the mean even though the experimental error as a percentage might be lower.

F.3. Determination of the composition of hydrazine

The composition of hydrazine was determined by converting the area ratios of the acetone and derivative peaks from a chromatograph in Figure F.3.

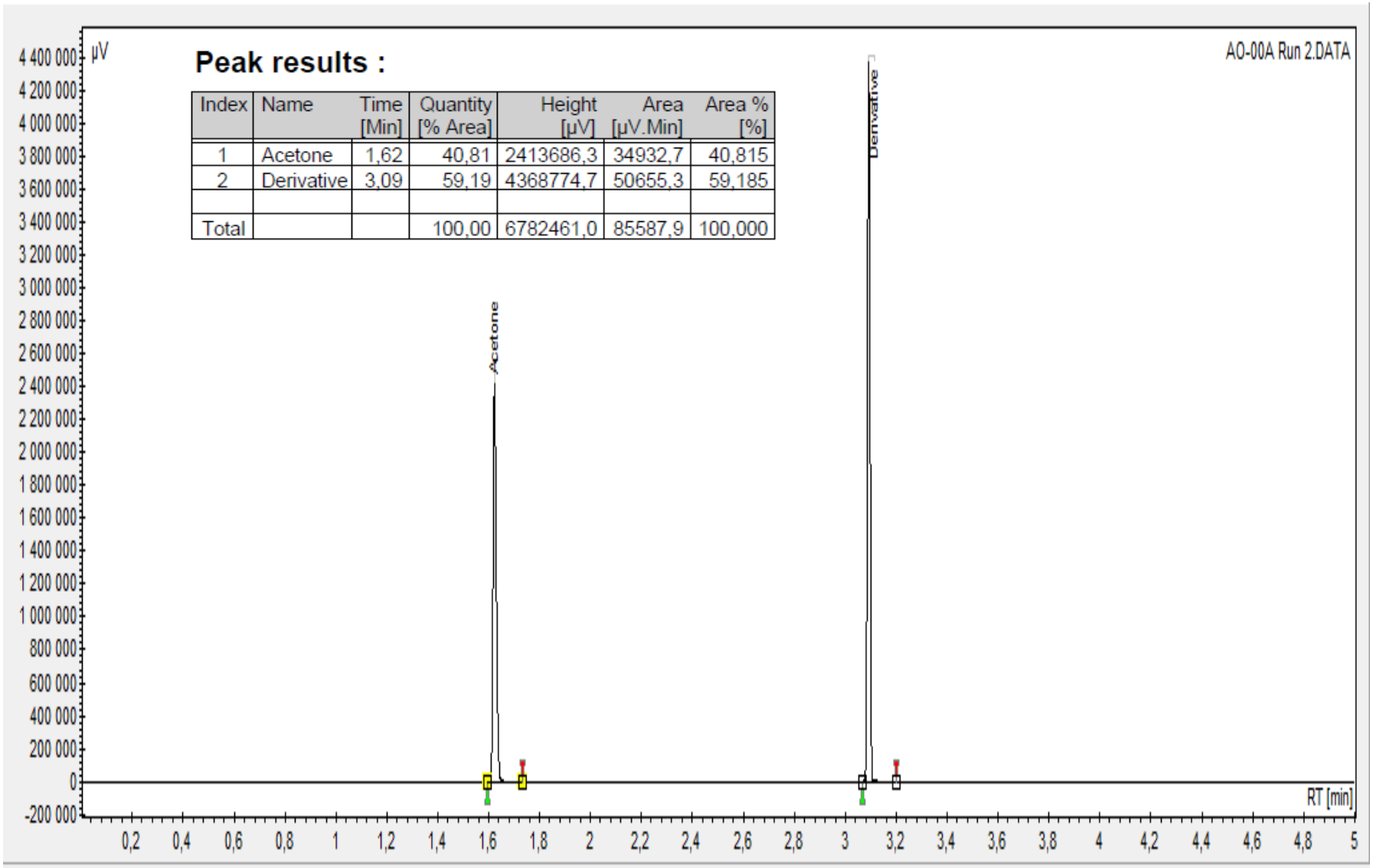

Index	Name	Time [Min]	Quantity [% Area]	Height [µV]	Area [µV.Min]	Area % [%]
1	Acetone	1,62	40,81	2413686,3	34932,7	40,815
2	Derivative	3,09	59,19	4368774,7	50655,3	59,185
Total			100,00	6782461,0	85587,9	100,000

Figure F.3: Typical result sheet for hydrazine and water from the Gas Chromatogram

Given the area of acetone is 34 932.7 and the area of the derivative is 50 655.3 the area ratio can be calculated as shown below:

$$\frac{A_{Derivative}}{A_{Acetone}} = \frac{50\,655.3}{34\,932.7} = 1.45$$

Using the third order polynomial fit ($y = 1174.2x^3 - 33.363x^2 + 5.2859x$) shown in Figure F.2 the volume fraction can be determined. In the equation y represents the area ration while x represents the volume ratio. The goal seek function in Excel was used to determine the volume ratio at each area ratio point. For this example calculation, the volume ratio was taken as 0.028.

$$\frac{V_{Hydrazine}}{V_{Acetone}} = 0.028$$

The volume fraction hydrazine in the sample was calculated by taking the product of the volume ratio above and the known amount of acetone that was used in the sample. Therefore:

$$\%\,Hydrazine = \frac{\left(V_{Acetone} \times \frac{V_{Hydrazine}}{V_{Acetone}}\right)}{Sample\ Volume} \times 100 = \frac{1.4 \times 0.028}{0.35} \times 100 = 11.3\,\%$$

APPENDIX G - STATISTICAL INFERENCE AND EXPERIMENTAL ERROR

Overview

This appendix contains more detailed information the statistical interference and experimental error calculation for the experimental work performed during this study. This Appendix is sub-divided into five sections, with the first Section (G.1) containing background theory to explain the basic statics that were used. The second section (G.2) is on the experimental error calculation for the gas chromatogram that was used for the analysis of the feed and permeate for both the sorption and pervaporation tests. The third Section (G.3) is on the experimental error calculations on pervaporation experiments with two different membranes, Pervap™ 4060 (G.3.1) and Pervap™ 4101 (G.3.2). This section is followed by the sorption experimental error calculations (G.4) and tensile strength experimental error in Section (G.5).

G.1. Confidence levels in experimental measurements

Every experimental measurement is subjected to an amount of uncertainty. This means that there will be a certain amount of variation in the results if an experimental measurement is done more than once. Another term that is often used to explain the experimental uncertainty is the experimental error. This section aims to quantify the experimental error expected in the gas chromatogram-, pervaporation- and sorption experiments.

The mean (μ) is often considered to be the best approximation of the "true" value that is being measured in a set of data points (George and Thomas, 2001). The standard deviation is a representation of the variability of the set of data (Van der Gryp, 2003). One of the most used statistical methods to estimate the variance of data from the mean is the central limit theorem (Van der Gryp, 2003). The central limit theorem was also used in this work to determine the variance and the confidence intervals.

The central limit theorem states that the mean of all the samples from the same population will be approximately the same as the population mean. It also states that all the samples will follow an approximate normal distribution pattern (Van der Gryp, 2003). The probability density distribution for the sample mean ($\bar{x}$) and sample size n will be statistically defined as (Lipnizki and Trägårdh, 2001):

$$z = \frac{\bar{x} - \mu}{\sigma/\sqrt{n}} \tag{G-1}$$

where z is the standard variable, μ is the population mean, σ the standard deviation and n the sample size (Lipnizki and Trägårdh, 2001).

The level of confidence that the sample mean is estimated to be the same to the population mean is defined by the inequalities shown in Equation (G-2) (Lipnizki and Trägårdh, 2001).

$$z_l \leq \frac{\bar{x} - \mu}{\sigma/\sqrt{n}} \leq z_h \tag{G-2}$$

with z_l the lower standard variable and z_h the upper standard variable (Lipnizki and Trägårdh, 2001). Rearranging Equation (G-2) results in Equation (G-3) which can be used to determine the minimum and maximum values for the population mean. (Lipnizki and Trägårdh, 2001)

$$\overline{x} - \frac{z_h \sigma}{\sqrt{n}} \leq \mu \leq \overline{x} - \frac{z_l \sigma}{\sqrt{n}} \tag{G-3}$$

The cumulative probability (α) can be determined from the desired confidence level by Equation (G-4) (Lipnizki and Trägårdh, 2001).

$$\text{Confidence } \% = 100(1 - \alpha) \tag{G-4}$$

The standard variable values shown in Table G.1 were extracted from Lipnizki and Trägårdh (2001).

Table G.1: Cumulative probability of the standard normal distribution as a function of the standard variable (Lipnizki and Trägårdh, 2001)

Desired Confidence %	Cumulative Probability (α)	Standard variable (z)
80%	0.89973	1.28
90%	0.94950	1.64
95%	0.97500	1.96
98%	0.99010	2.33
99%	0.99506	2.58

G.2. Calculation of Gas Chromatogram experimental error

The experimental error on the gas chromatogram was calculated by injecting a known concentration a total of ten times. A sample mixture of 59 wt. % water was used for this purpose. The peak area results from the various injections, as well as the calculated results from the calibration curve are given in Table G.2.

Table G.2: Data used for experimental error calculation of the gas chromatogram

Run nr.	$A_{Acetone}$	$A_{Derivative}$	$A_{Derivative} / A_{Acetone}$	$V_{Hydrazine} / V_{Acetone}$	% Hydrazine
Run 1	42 787	60 990	1.425	0.103	41.4%
Run 2	34 933	50 655	1.450	0.104	41.7%
Run 3	31 126	49 226	1.582	0.104	41.7%
Run 4	21 935	31 227	1.424	0.100	40.1%
Run 5	25 615	37 141	1.450	0.101	40.4%
Run 6	30 713	47 097	1.533	0.103	41.2%
Run 7	33 368	45 266	1.357	0.099	39.4%
Run 8	19 941	28 053	1.407	0.100	40.0%
Run 9	45 983	62 268	1.354	0.099	39.4%
Run 10	38 076	50 074	1.315	0.097	39.0%

The calculated statistic values of the data shown in Table G.2 are represented in Table G.3 for the 95 % confidence intervals.

Table G.3: Calculated statistic values

Parameter	Value
Mean value	0.40
Standard deviation	0.010
Upper limit	39.0%
Lower limit	41.7%
95 % Confidence interval	0.006
Experimental error	3%

G.3. Calculation of pervaporation experimental error

Two separate pervaporation experiments were performed with five runs each on Pervap™ 4060 and Pervap™ 4101 membranes to determine the reproducibility and experimental error for the pervaporation experiments. The results for the Pervap™ 4060 membrane are discussed in Section G.3.1, while the results for the Pervap™ 4101 membrane are discussed in Section G.3.2.

G.3.1. Water pervaporation with Pervap™4060 membrane

The first pervaporation test was performed using pure water and Pervap™ 4060 membrane operating at 30 °C with the total flux results given in Table G.4.

Table G.4: Reproducibility on pervaporation experiments using Pervap™ 4060

Cumulative time [min]	Mass permeate [g/h]	Total flux [kg·m^{-2}·h^{-1}]	Cumulative time [min]	Mass permeate [g/h]	Total flux [kg·m^{-2}·h^{-1}]	Cumulative time [min]	Mass permeate [g/h]	Total flux [kg·m^{-2}·h^{-1}]
	Run 1			**Run 2**			**Run 3**	
30	11.483	2.12	49	1.254	0.23	30	2.058	0.38
60	3.928	0.73	190	1.113	0.21	61	2.399	0.44
90	2.672	0.49	331	0.794	0.15	93	2.719	0.50
120	2.905	0.54	361	2.523	0.47	123	2.396	0.44
150	2.132	0.39	398	2.992	0.55	153	2.142	0.40
180	2.761	0.51	454	2.684	0.50	184	2.216	0.41
210	-	-	501	2.586	0.48	214	1.964	0.36
240	2.886	0.53	920	2.956	0.55	244	1.758	0.32
-	-	-	953	2.890	0.53	274	1.582	0.29
-	-	-	982	3.016	0.56	-	-	-

Table G.4 (cont.): Reproducibility on pervaporation experiments using Pervap™ 4060

Cumulative time [min]	Mass permeate [g/h]	Total flux [kg·m^{-2}·h^{-1}]	Cumulative time [min]	Mass permeate [g/h]	Total flux [kg·m^{-2}·h^{-1}]
	Run 4			**Run 5**	
31	19.161	3.54	30	6.260	1.16
61	9.707	1.79	60	2.616	0.48
91	4.085	0.76	90	2.554	0.47
121	2.480	0.46	120	2.519	0.47
152	2.605	0.48	150	2.463	0.46
182	2.587	0.48	180	2.521	0.47
213	2.589	0.48	-	-	-

The reproducibility of the results is important to maintain certainty and obtain scientifically acceptable experimental conclusion. The flux reproducibility of Pervap™ 4060 at 30 °C with pure water is shown as a flux response curve in Figure G.1.

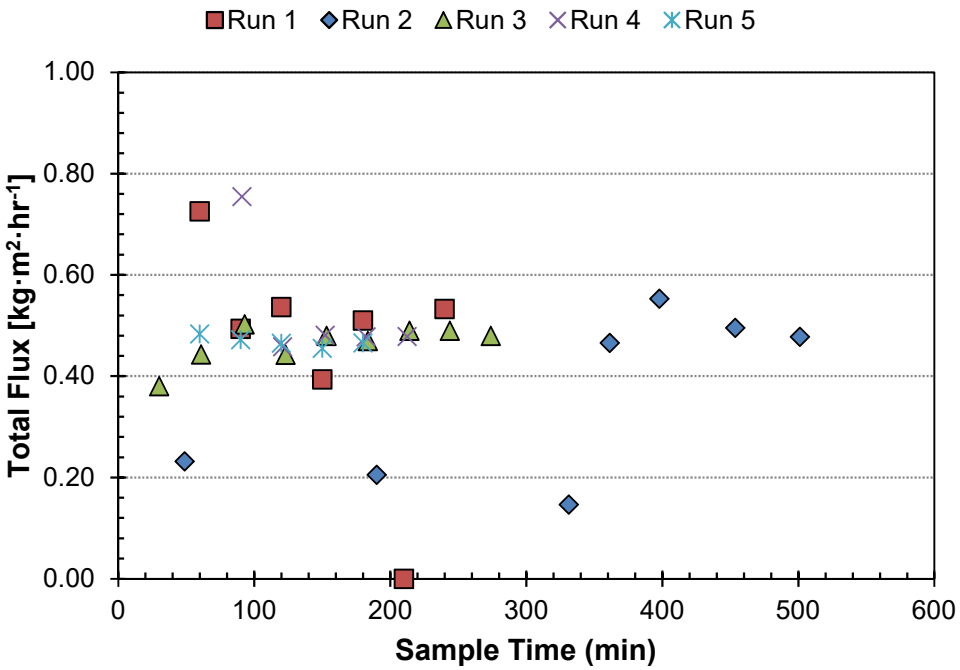

Figure G.1: Reproducibility curve of the flux obtained with Pervap™ 4060

From Figure G.1 it can be seen the average time until stable flux values were obtain was about 2 hours. The exception was with Run 2 which took 6 hours. It can however be noted from Figure G.1 that the flux values all stabilized around an average of about 0.5 $kg \cdot m^{-2} \cdot h^{-1}$. The steady-state values were calculated from the last few experimental points for each run. These values were used in the experimental error calculation. The steady-state results for Pervap™ 4060 are given in Table G.5.

Table G.5: Steady-state experimental results

Run number	Total flux [$kg \cdot m^{-2} \cdot h^{-1}$]
Run 1	0.52
Run 2	0.55
Run 3	0.50
Run 4	0.48
Run 5	0.46

The experimental error for the flux values using Pervap™ 4060 during the pervaporation experiments are given in Table G.6 for both the 95 % confidence intervals.

Table G.6: Statistic values for pervaporation with Pervap™ 4060 membrane

Parameter	Value
Mean value	0.50
Standard deviation	0.03
95% Confidence interval	0.026
Upper limit	0.528
Lower limit	0.476
Experimental error	11%

G.3.2. Pervaporation with Pervap™ 4101 membrane

A feed mixture of 59 wt. % water at 50 °C was used to determine the reproducibility for the pervaporation experiments with the results given in Table G.7.

Table G.7: Reproducibility on Pervap™ 4101 membrane

Time [min]	Permeate [g/h]	Total flux [kg·m^{-2}·h^{-1}]	Water wt. fraction	Time [min]	Permeate [g/h]	Total flux [kg·m^{-2}·h^{-1}]	Water wt. fraction	Time [min]	Permeate [g/h]	Total flux [kg·m^{-2}·h^{-1}]	Water wt. fraction
Run 1				Run 2				Run 3			
40	5.403	1.00	-	150	0.605	0.11	0.85	143	0.530	0.10	-
80	4.580	0.85	-	210	0.588	0.11	0.89	203	0.682	0.13	0.82
140	2.818	0.52	0.55	270	0.563	0.10	0.83	263	2.706	0.50	0.60
180	0.810	0.15	0.66	330	0.582	0.11	0.87	323	0.630	0.12	0.83
220	0.619	0.11	0.77	390	0.596	0.11	0.86	383	0.603	0.11	0.83
280	0.583	0.11	0.80	450	0.585	0.11	0.88	443	0.638	0.12	0.81
340	0.582	0.11	0.86	-	-	-	-	-	-	-	-
395	0.570	0.11	0.86	-	-	-	-	-	-	-	-

Table G.7 (cont.): Reproducibility on Pervap™ 4101 membrane

Time [min]	Permeate [g/h]	Total flux (kg/m^2.h)	Water wt. fraction	Time [min]	Permeate [g/h]	Total flux (kg/m^2.h)	Water wt. fraction
Run 4				Run 5			
150	0.83	0.154	0.86	150	0.720	0.133	0.89
210	0.78	0.144	0.85	210	0.711	0.131	0.89
270	0.75	0.139	0.83	270	0.680	0.126	0.90
330	0.69	0.127	0.88	330	0.706	0.131	0.89
				390	0.698	0.129	0.89

The flux reproducibility of Pervap™ 4101 (with a feed temperature of 50 °C and concentration of 59 wt. % water) is shown as a flux response curve in Figure G.2 while the reproducibility of the water content in the permeate of the same membrane, at the same conditions is shown in Figure G.3.

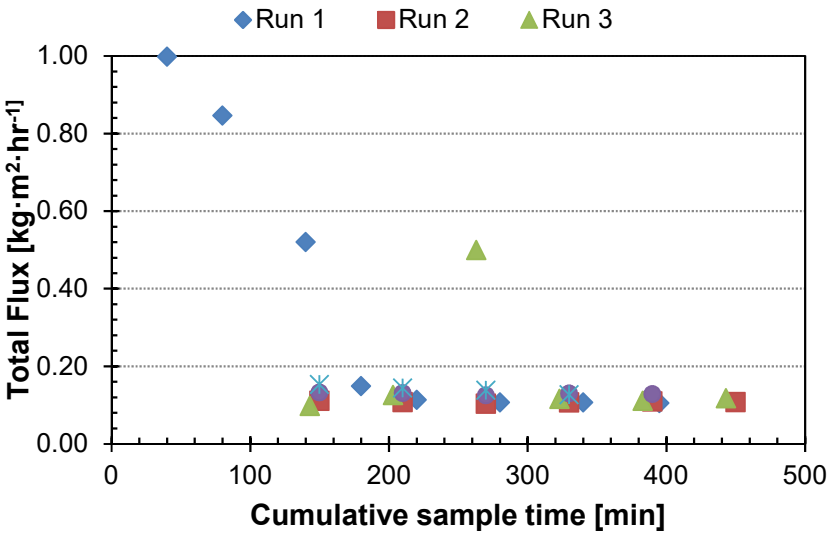

Figure G.2: Reproducibility curve of the flux obtained with Pervap™ 4101

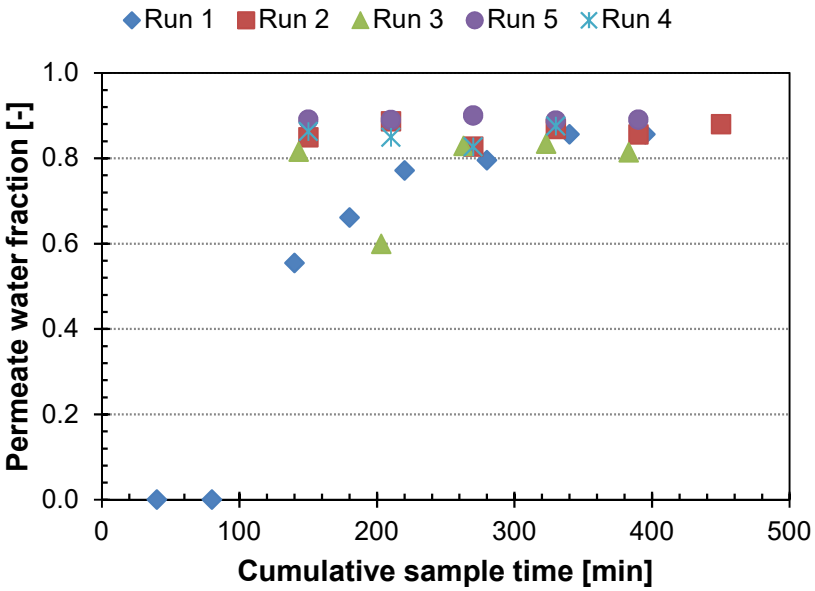

Figure G.3: Reproducibility curve of the fraction water in the permeate with Pervap™ 4101

From Figure G.2 it can be seen the average time until stable flux values were obtained was about two and a half hours. It can be noted from Figure G.2 that the flux values

all stabilised around an average of about 0.85 $kg \cdot m^{-2} \cdot h^{-1}$. The steady-state values were calculated from the last few experimental points for each run from which the experimental error was calculated. The steady-state results for Pervap™ 4101 are given in Table G.8.

Table G.8: Steady-state experimental results

Run number	Total flux [$kg \cdot m^{-2} \cdot h^{-1}$]	Selectivity
Run 1	0.107	0.836
Run 2	0.109	0.855
Run 3	0.115	0.826
Run 4	0.128	0.893
Run 5	0.127	0.863

The experimental errors for the flux and permeate water content that were obtained during pervaporation with Pervap™ 4101 using 59 wt. % water at 50 °C as feed are given in Table G.9.

Table G.9: Pervaporation flux experimental error using 59 wt. % water as feed

Parameter	Flux statistics	Selectivity
Mean value	0.50	0.85
Standard deviation	0.03	0.02
95% Confidence interval	0.026	0.020
Upper limit	0.528	0.88
Lower limit	0.476	0.83
Experimental error	11%	5%

G.4. Calculation of sorption experimental error

The experimental error for the sorption experiments was calculated in terms of percentage sorption as well as membrane water selectivity. The sample procedure as described in Section 4.6 was repeated twelve times for the swelling and a combined sample between two sorption experiments were analysed six time. The percentage sorption and membrane water selectivity for each run is given in Table G.10.

Table G.10: Reproducibility of sorption results at 50 °C using 36 wt. % water with Pervap™ 4101 membrane

M_d	M_s	% Sorption	Selectivity
0.1258	0.2192	74%	29%
0.1220	0.2340	92%	
0.1222	0.2292	88%	41%
0.1149	0.2079	81%	
0.1048	0.1989	90%	38%
0.1219	0.2183	79%	
0.1163	0.2127	83%	48%
0.1161	0.2132	84%	
0.1165	0.2044	75%	38%
0.1155	0.2050	77%	
0.1225	0.2166	77%	35%
0.1223	0.2276	86%	

The calculate statistic values of the data shown in Table G.10 are represented in Table G.10 for the 95 % confidence intervals.

Table G.11: Statistic values for sorption with Pervap™ 4101

Parameter	% Sorption	Selectivity
Mean value	0.82	0.38
Standard deviation	0.055	0.056
Upper limit	0.74	0.29
Lower limit	0.92	0.48
95 % Confidence interval	0.031	0.045
Experimental error	8 %	24 %

G.5. Calculation of tensile strength experimental error

The experimental error for mechanical strength tests was calculated in terms of tensile strength. The sample procedure as described in Section 4.2.2 was repeated eight times. The tensile strength for each run is given in Table G.12.

Table G.12: Reproducibility of tensile strength results using PEBA membrane

Run nr.	Tensile strength [Mpa]
1	28.7
2	28.7
3	31.5
4	29.4
5	31.7
6	31.4
7	27.9
8	27.9
9	31.7
10	31.5

The calculate statistic values of the data shown in Table G.12 are represented in Table G.13 for the 95 % confidence intervals.

Table G.13: Statistic values for tensile strength using PEBA membrane

Parameter	Tensile
Mean value	30.1
Standard deviation	1.603
Upper limit	27.90
Lower limit	31.70
95 % Confidence interval	0.993
Experimental error	7%

G.6. Calculation of contact angle experimental error

The experimental error for contact angle is calculated in this section. The sample procedure as described in Section 4.3 was repeated ten times. The contact angle for each run is given in Table G.14.

Table G.14: Reproducibility of contact angle results

Run nr.	Contact angle [°]
1	170
2	152.1
3	157.4
4	129
5	155
6	152.6
7	153.1
8	160.9
9	185
10	153

The calculate statistic values of the data shown in Table G.14 are represented in Table G.15 for the 95 % confidence intervals.

Table G.15: Statistic values for contact angle tests

Parameter	Tensile
Mean value	156.81
Standard deviation	13.530
Upper limit	129.00
Lower limit	185.00
95 % Confidence interval	8.386
Experimental error	11%

APPENDIX H - DETAILED MODELLING AND SIMULATION RESULTS

Overview

The work in this Appendix focusses on the mass transfer modelling relates to the solution-diffusion model. Appendix H is sub-divided into two subsections. The sorption modelling shown in Section H.1 and the pervaporation modelling in Section H.2.

H.1. Sorption modelling

H.1.1. Calculation inputs

The density (ρ) and specific volume (V) for both pure components water and hydrazine were obtained from ChemCad® 7.1.1 for three temperatures ranging from 30 ° to 50 °C in 10°C increments, with the data shown in Table H.1.

Table H.1: Density and specific volume data for hydrazine and water for temperatures between 30 °C and 50 °C

Parameter	Symbol	Unit	30 °C	40 °C	50 °C
Water density	ρ_i	$kg \cdot m^{-3}$	995.3	992.0	987.8
Hydrazine density	ρ_j	$kg \cdot m^{-3}$	999.2	990.5	981.7
Water specific volume	V_i	$cm^3 \cdot g^{-1}$	0.0181	0.0181	0.0182
Hydrazine specific volume	V_j	$cm^3 \cdot g^{-1}$	0.0320	0.0323	0.0326

Activity coefficient data for both hydrazine and water were obtained from ChemCad® 7.1.1 using a NTRL thermodynamic model. The activity coefficient data is reported for varying water mole fractions between 0.500 and 0.806 and for three temperatures ranging from 30 ° to 50 °C in 10°C increments, with the data shown in Table H.2.

Table H.2: Activity coefficient data for hydrazine and water for temperatures between 30 °C and 50 °C

Water fraction		Activity coefficient					
		Water			Hydrazine		
mol	volume	30 °C	40 °C	50 °C	30 °C	40 °C	50 °C
0.806	0.703	0.7490	0.7650	0.7792	0.1539	0.1680	0.1822
0.727	0.603	0.6220	0.6420	0.6606	0.2853	0.3003	0.3151
0.640	0.497	0.5030	0.5250	0.5460	0.4525	0.4652	0.4776
0.543	0.403	0.4010	0.4230	0.4430	0.6305	0.6392	0.6476
0.500	0.363	0.3650	0.3860	0.4060	0.6982	0.7051	0.7118

H.1.2. Sample calculation for concentration dependent interaction parameter between binary solvents (g_{ij})

Using the activity coefficient data for molar water and hydrazine fractions (Table H.2) the two parameter Margules activity model constants A_{ij} and A_{ji} can be calculated by using Equations (H-1) and (H-2) in a non-linear system solver fsolve in Matlab®, with sample results for 50 °C given in Table H.3.

$$ln\,(\gamma_i) = \left[A_{ij} + 2\left(A_{ji} - A_{ij}\right)x_i\right]{x_j}^2 \quad \text{(H-1)}$$

$$ln\,(\gamma_j) = \left[A_{ji} + 2\left(A_{ij} - A_{ji}\right)x_j\right]{x_i}^2 \quad \text{(H-2)}$$

Using the Margules constants and hydrazine and water mole fractions the excess Gibbs free energy ($\frac{\Delta G^E}{RT}$) term can be calculated using Equation (H-3) the sample results for 50 °C given in Table H.3.

$$\frac{\Delta G^E}{RT} = x_i x_j\left(A_{21}x_i + A_{12}x_j\right) \quad \text{(H-3)}$$

The concentration dependent interaction parameter (g_{ij}) between the water and hydrazine can then be calculated using Equation (3-11).

$$g_{ij} = \frac{1}{x_i v_j}\left[x_i ln\frac{x_i}{v_i} + x_j ln\frac{x_j}{v_j} + \frac{\Delta G^E}{RT}\right] \quad \text{(3-11)}$$

H.1.3. Calculation variables and equations

The list of variables required to solve the sorption model is shown in Table H.3 and the list of equations used in Table H.4.

Table H.3: List of required variables for solving the sorption model

Nr.	Variable	Nr.	Variable
1	Φ_i	9	${\chi_{ip}}^b$
2	Φ_j	10	${\chi_{jp}}^b$
3	${\Phi_p}^{bi}$	11	u_i
4	${\Phi_p}^{bj}$	12	u_j
5	$g_{ip}(v_j)$	13	$\frac{\partial g_{ij}}{\partial u_j}$
6	$g_{ip}(u_j)$	14	$\frac{\partial g_{ij}}{\partial v_j}$
7	g_{ip}	15	$\frac{\partial g_{ip}}{\partial u_j}$
8	g_{jp}	16	$\frac{\partial g_{jp}}{\partial u_i}$

Table H.4: List of input equations for solving the sorption model

Nr.	Equation	Nr.	Equation
1	$u_i = \frac{\Phi_i}{\Phi_i + \Phi_j}$	2	$u_j = \frac{\Phi_j}{\Phi_i + \Phi_j}$
3	$\Phi_i + \Phi_j + \Phi_p = 1$		
4	${\Phi_p}^{bi} = \frac{-1}{{S_i}^b/\rho_i + 1}$	5	${\Phi_p}^{bj} = \frac{-1}{{S_j}^b/\rho_j + 1}$
6	${\chi_{ip}}^b = \frac{-\left[ln\left(1 - {\Phi_p}^{bi}\right) + {\Phi_p}^{bi}\right]}{\left({\Phi_p}^{bi}\right)^2}$	7	${\chi_{jp}}^b = \frac{-\left[ln\left(1 - {\Phi_p}^{bj}\right) + {\Phi_p}^{bj}\right]}{\left({\Phi_p}^{bj}\right)^2}$
8	$g_{ip} = {\chi_{ip}}^b + a.u_j + b\left(\Phi_p - {\Phi_p}^{bj}\right)$	9	$g_{jp} = {\chi_{jp}}^b + c.u_i + d\left(\Phi_p - {\Phi_p}^{bi}\right)$
10	$\frac{\partial g_{ip}}{\partial u_j} = a$	11	$\frac{\partial g_{jp}}{\partial u_i} = c$
12	$g_{ij}(v_j) = k_1 + k_2 v_j + k_3 {v_j}^2 + k_4 {v_j}^3 + k_4 {v_j}^4$	13	$g_{ij}(u_j) = k_1 + k_2 u_j + k_3 {u_j}^2 + k_4 {u_j}^3 + k_4 {u_j}^4$
14	$\frac{\partial g_{ij}}{\partial u_j} = k_2 + 2.k_3.v_j + 3.k_4 {v_j}^2 + 4.k_4 {v_j}^3$	15	$\frac{\partial g_{ij}}{\partial v_j} = k_2 + 2.k_3.u_j + 3.k_4 {u_j}^2 + 4.k_4 {u_j}^3$

Table H.4 (cont.): List of input equations for solving the sorption model

Nr.	Equation
16	$ln\left(\frac{\Phi_i}{\Phi_j}\right) - ln\left(\frac{v_i}{v_j}\right) = (r-1)ln\left(\frac{\Phi_i}{v_j}\right) - g_{ij}(u_j)(\Phi_j - \Phi_i) - g_{ij}(v_j)(v_i - v_j) - \Phi_p(g_{ip} - r g_{jp}) + u_i\Phi_j\frac{\partial g_{ij}}{\partial u_j} - v_i v_j\frac{\partial g_{ij}}{\partial v_j} + \Phi_p u_i\frac{\partial g_{ip}}{\partial u_j} - \frac{V_i}{V_j}u_j\Phi_p\frac{\partial g_{jp}}{\partial u_i}$

H.2. Diffusion modelling

Equation (3.23) was used to calculate the partial fluxes for both water and hydrazine by substituting the diffusion coefficient correlations as given in Table 6.9. The partial flux equations with the diffusion coefficients are given in Table H.5.

$$J_i = -D_i\frac{dc_i}{dz} \qquad \text{(H-4)}$$

Table H.5: Diffusion coefficient for various reference models

Reference model	Diffusion equation	Equation number
Greenlaw	$D_i = \rho_m . {D_i}^0(x_i + \beta_{ji}x_j)$	(3-24)
	$D_j = \rho_m . {D_j}^0(x_j + \beta_{ij}x_i)$	(3-25)
Mulder	$D_i = D_{0,i}\, e^{\tau_i c x_i \rho_m}$	(3-28)
	$D_j = D_{0,j}\, e^{\tau_j x_j \rho_m}$	(3-29)
Long	$D_i = \rho_m . {D_i}^0 exp(\beta_i x_i)$	(3-30)
	$D_j = \rho_m . {D_j}^0 exp(\beta_j x_j)$	(3-31)
Brun	$D_i = \rho_m . {D_i}^0 exp(\beta_{ii}x_i + \beta_{ij}x_j)$	(3-32)
	$D_j = \rho_m . {D_j}^0 exp(\beta_{ji}x_i + \beta_{jj}x_j)$	(3-33)

The detailed derivations for each reference model is shown below.

Greenlaw

$$J_i = -\rho_m . D_i \frac{dx_i}{dz} \tag{H-5}$$

$$J_i = -\rho_m . {D_i}^0 \frac{(x_i + \beta_{ji} x_j) dx_i}{dz} \tag{H-6}$$

$$J_i = \frac{-\rho_m . {D_i}^0}{z} \left(\frac{{x_i}^2}{2} + \beta_{ji} x_j x_i \right) \tag{H-7}$$

$$J_i = \frac{-\rho_m . {D_i}^0}{z} \left[\frac{{x_i}^2}{2} + \beta_{ji} x_i (1 - x_i) \right] \tag{H-8}$$

Long

$$J_i = -\rho_m . D_i \frac{dx_i}{dz} \tag{H-9}$$

$$J_i = -\rho_m . {D_i}^0 \frac{exp(\beta_i x_i) dx_i}{dz} \tag{H-10}$$

$$J_i = \frac{-\rho_m . {D_i}^0}{z} \left(\frac{exp(\beta_i x_i)}{\beta_i} + Ci \right) \tag{H-11}$$

Brun

$$J_i = -\rho_m . D_i \frac{dx_i}{dz} \tag{H-12}$$

$$D_i = \rho_m . {D_i}^0 exp(\beta_{ii} x_i + \beta_{ij} x_j)$$

$$J_i = -\rho_m . D_i \frac{exp(\beta_{ii} x_i + \beta_{ij} x_j) dx_i}{dz} \tag{H-13}$$

$$J_i = \frac{-\rho_m . D_i}{z} \frac{C_j(\beta_{ii} - \beta_{ij}) + exp^{\beta_{ii} x_i + \beta_{ij}(1 - x_i)}}{\beta_{ii} - \beta_{ij}} \tag{H-14}$$